

**MICROSTRUCTURAL AND GEOCHEMICAL
CHARACTERISATION OF MYLONITES ALONG
THE BUKIT TINGGI FAULT ZONE,
PENINSULAR MALAYSIA**

NORSAFAWATI BT SAAID

**FACULTY OF SCIENCE
UNIVERSITY OF MALAYA
KUALA LUMPUR**

2017

**MICROSTRUCTURAL AND GEOCHEMICAL
CHARACTERISATION OF MYLONITES ALONG
THE BUKIT TINGGI FAULT ZONE,
PENINSULAR MALAYSIA**

NORSAFAWATI BT SAAID

**DISSERTATION SUBMITTED IN FULFILLMENT OF THE
REQUIREMENTS FOR THE DEGREE OF MASTER OF SCIENCE**

**DEPARTMENT OF GEOLOGY
FACULTY OF SCIENCE
UNIVERSITY OF MALAYA
KUALA LUMPUR**

2017

UNIVERSITI MALAYA

ORIGINAL LITERARY WORK DECLARATION

Name of Candidate: NORSАFAWATI BINTI SAAID

Registration/Matric No: SGR 110085

Name of Degree: MASTER OF SCIENCE

Title of Project Paper/Research Report/Dissertation/Thesis ("this Work"):

**MICROSTRUCTURAL AND GEOCHEMICAL CHARACTERISATION
OF MYLONITES ALONG THE BUKIT TINGGI FAULT ZONE,
PENINSULAR MALAYSIA.**

Field of Study: STRUCTURAL GEOLOGY AND GEOCHEMISTRY

I do solemnly and sincerely declare that:

- (1) I am the sole author/writer of this Work;
- (2) This Work is original;
- (3) Any use of any work in which copyright exists was done by way of fair dealing and for permitted purposes and any excerpt or extract from, or reference to or reproduction of any copyright work has been disclosed expressly and sufficiently and the title of the Work and its authorship have been acknowledged in this work;
- (4) I do not have any actual knowledge nor do I ought reasonably to know that the making of this Work constitutes an infringement of any copyright work;
- (5) I hereby assign all and every rights in the copyright to this Work to the University of Malaya ("UM"), who henceforth shall be owner of the cop or use in any form or by any means whatsoever is prohibited without the written consent of UM having been first had and obtained;
- (6) I am fully aware that if in the course of making this Work I have infringed any copyright whether intentionally or otherwise, I may be subject to legal action or any other action as may be determined by UM.

Candidate's Signature:

Date:

Subscribed and solemnly declared before,

Witness's Signature:

Date:

Name:

Designation:

ABSTRACT

Bukit Tinggi Fault Zone (BTFZ) is a major fault zone in the western flank of Main Range Granite, Peninsular Malaysia. It trends NW-SE with steep dips and a broad zone of granite mylonites occur along the fault zone. This study aims to determine the condition of fault deformation from the microstructures of the mylonites, to determine the sense of shear from mesoscopic and microscopic kinematic indicators, and to determine the chemical changes in the mylonites. The orientation of the foliation and lineation are measured in the field and samples are collected for petrographic and geochemical analyses. Microscopic kinematic studies were done on oriented thin sections. The protolith of the mylonites is a megacrystic biotite granite. Fault deformation has formed fault rocks consisting mainly of protomylonite, minor mesomylonite and rare ultramylonite. The microstructures indicate that quartz and mica behave in a ductile manner during deformation and feldspars are mainly brittle, suggesting that deformation occurred at the brittle-transition zone, which corresponds to about 300°C to 500°C. Kinematic indicators present are S-C foliation, σ -porphyroclast, oblique foliation, mica fish and offset fractured clasts. The BTFZ has oblique slip, with dextral strike-slip component. Mylonites with SW dipping foliation give reverse slip and lesser normal slip is recorded from those with NE dips. The vergence is generally towards the E. For the major elements, there is a slight increase of SiO₂ in the mylonites relative to the protolith. The MnO, TiO₂, P₂O₅, MgO, Fe₂O₃ and CaO are depleted. Na₂O, K₂O, Cr₂O₃ and LOI show no clear trend. For the trace elements, Th increased, Sr, Ba, Ga and Zn are depleted, while Nb, Zr, Rb, Y, U and Pb has irregular trends. The chemical changes may be related to silicification and the breakdown of feldspars and biotite during deformation. Late Cretaceous age (84 Ma and 92 Ma) of deformation is obtained from ⁴⁰Ar/³⁹Ar dating of recrystallized biotite of the mylonite.

ABSTRAK

Zon Sesar Bukit Tinggi adalah zon sesar utama di bahagian barat Banjaran Granit Utama, Semenanjung Malaysia. Ia berorientasi Barat Laut-Tenggara dengan kemiringan yang curam serta zon milonit granit yang luas yang terdapat di sepanjang zon sesar. Kajian ini bertujuan untuk menentukan keadaan deformasi sesar daripada mikrostruktur milonit, untuk menentukan arah pergerakan daripada petunjuk kinematik mesoskopik dan mikroskopik serta menentukan perubahan kimia di dalam milonit. Orientasi foliasi-foliasi dan lineasi-lineasi diukur di lapangan dan sampel dikumpulkan untuk tujuan analisis petrografi dan geokimia. Kajian kinematik mikroskopik dijalankan ke atas keratan nipis terorientasi. Batuan asal (protolit) milonit adalah granit megakris biotit. Deformasi sesar telah membentuk batuan-batuan sesar terutamanya protomilonit, sedikit mesomilonit dan sangat sedikit ultramilonit. Mikrostruktur menunjukkan bahawa kuarza dan mika berkelakuan mulur semasa deformasi dan feldspar berkelakuan rapuh, sekaligus mencadangkan bahawa deformasi berlaku di zon peralihan rapuh, sepadan dengan suhu kira-kira 300°C hingga 500°C. Petunjuk kinematik yang hadir adalah foliasi S-C, porfiroklas σ , foliasi sendeng, "mica fish" dan porfiroklas "fragmented book-shaped". Zon Sesar Bukit Tinggi mempunyai komponen gelinciran serong dan gelinciran jurus manganan. Milonit dengan foliasi mengiring ke barat daya merekodkan gelinciran terbalik dan sedikit gelinciran normal direkodkan bagi foliasi yang mengiring ke arah timur laut. Arah ricihan umumnya adalah ke arah timur. Bagi elemen utama, terdapat sedikit peningkatan pada SiO₂ dalam milonit relatif kepada protolit. MnO, TiO₂, P₂O₅, MgO, Fe₂O₃ dan CaO berkurangan. Na₂O, K₂O, Cr₂O₃ dan LOI tidak menunjukkan corak yang jelas. Untuk unsur-unsur surih, unsur Th meningkat. Sr, Ba, Ga dan Zn berkurangan, manakala Nb, Zr, Rb, Y, U dan Pb mempunyai corak yang tidak teratur. Perubahan kimia mungkin berkaitan dengan proses silisifikasi serta pecahan feldspar dan biotit semasa proses deformasi. Umur Lewat Kretas (84 Ma dan

92 Ma) daripada proses deformasi diperolehi daripada kaedah pentarikan $^{40}\text{Ar} / ^{39}\text{Ar}$ biotit yang terhablur semula di dalam milonit.

University of Malaya

ACKNOWLEDGEMENTS

First and foremost I would like to thank my supervisor, Assoc. Prof. Dr. Ng Tham Fatt and Prof. Dr. Azman A. Ghani for their constant effort in teaching me the techniques and methodologies I utilized for my thesis research, the patience, encouragement, fruitful discussions, thoughtful and careful reviews of the different copies of the thesis drafts. I would also love to thank my committee, Ahmad Faiz, Mohd Afiq and Jorien Van Der Wall for the fruitful discussions and support. I appreciate Assoc. Prof. Mustaffa Kamal for the valuable discussions, suggestions and comment. A massive appreciation to Dr. Jasmi Hafiz for his genuine appreciation of my work and encouragement. I would also thank En. Zamrud Daunar, Pn. Zaiton, En. Aizad and Mrs. Fan for their assistance in the lab.

Thank you to those exceptional geology lecturers, department and staff who have always been supportive, friendly and willing to help. Special thanks to Ahmad Hariz bin Abdullah for his willingness to help whenever I needed help, the encouragement will never be forgotten. As well as Nor Hidayah bt. Arshad and Noor Zuliana bt. Awang for their persistent friendly nature, support and encouragement.

I would like to thank my beloved UM postgraduate group mates, Shafifiyaz, Fauziah, Aisyah, Sakinah, Afiqah, Hotimah, Yati, Aimee, Intan, Eli, Hani, Syahirah, Yuliana and Ain for their day to day support and encouragement. Finally, I would like to extend a very special thanks to my parents and siblings for their support and encouragement to gather with me along this journey since the time I was born.

Thank you, Love you ☺

TABLE OF CONTENT

ORIGINAL LITERARY WORK DECLARATION	
ABSTRACT.....	iii
ABSTRAK.....	iv
ACKNOWLEDGEMENTS.....	vi
LIST OF FIGURES.....	ix
LIST OF PLATES.....	xii
LIST OF TABLES.....	xv
LIST OF ABBREVIATIONS.....	xvi
LIST OF APPENDICES	xvii
CHAPTER 1: INTRODUCTION	
1.1 General introduction.....	1
1.2 Objectives.....	2
1.3 Study area.....	2
1.4 Previous works.....	2
1.5 Research methodology.....	4
1.5.1 Literature review.....	4
1.5.2 Fieldwork.....	4
1.5.3 Laboratory works.....	5
CHAPTER 2: REGIONAL GEOLOGY AND TECTONIC SETTING	
2.1 Introduction.....	10
2.2 Regional geology and tectonic setting.....	10
2.3 Major faults in Peninsular Malaysia.....	12
2.4 Bukit Tinggi Fault Zone.....	13
2.4.1 Geology of BTFZ.....	13
2.4.2 Structures of BTFZ.....	16
2.5 Kuala Lumpur Fault Zone.....	16
CHAPTER 3: PETROGRAPHY AND DEFORMATION MICROSTRUCTURES	
3.1 Introduction.....	22
3.2 Petrography of rocks at the Bukit Tinggi Fault Zone vicinity.....	26
3.2.1 Bukit Tinggi Granite.....	26
3.2.2 Mica-Chlorite Schist.....	28
3.3 Petrography of Mylonites.....	31
3.3.1 Protomylonite.....	33
3.3.2 Mesomylonite.....	34
3.3.3 Ultramylonite.....	35
3.4 Magmatism age.....	40
3.5 ⁴⁰ Ar/ ³⁹ Ar thermochronology.....	41
3.6 Discussion.....	45
3.6.1 Mechanism of deformation.....	45

3.6.2 Deformation temperature.....	54
3.6.3 Grain size reduction.....	55
3.6.4 Strain softening.....	56
3.6.5 Influence of fluid.....	57
 CHAPTER 4: KINEMATIC ANALYSIS OF THE MYLONITES	
4.1 Introduction.....	61
4.2 Mesoscopic features.....	62
4.3 Microstructure features.....	65
4.3.1 S-C fabric.....	65
4.3.2 Oblique foliation.....	68
4.3.3 Mantled porphyroclast.....	70
4.3.4 Mica fish.....	73
4.3.5 Fragmented book-shaped porphyroclast.....	75
4.4 Foliation.....	78
4.5 Lineation.....	79
4.6 Discussion.....	82
 CHAPTER 5: GEOCHEMICAL CHARACTERISATION OF THE MYLONITES	
5.1 Introduction.....	85
5.2 XRF whole-rock element analysis.....	85
5.3 Major element composition of mylonites.....	86
5.4 Trace element composition of mylonites.....	89
5.5 Protolith-normalised major and trace element data.....	94
5.6 Discussion.....	98
 CHAPTER 6: SUMMARY AND CONCLUSION	
6.1 Summary.....	101
6.1.1 Characteristics of the Bukit Tinggi Fault Zone (BTFZ).....	101
6.1.2 Characteristics of the mylonites.....	101
6.1.3 Kinematic analysis of the mylonites.....	103
6.1.4 Deformation related chemical changes.....	104
6.2 Conclusion.....	105
REFERENCES.....	107
LIST OF PUBLICATION AND PAPER PRESENTED.....	118
APPENDICES.....	119

LIST OF FIGURES

Figure 1.1: Map of main faults in Peninsular Malaysia. Bukit Tinggi Fault Zone (study area) transects the Main Range Granites. 1) Bok-Bak fault, 2) Kerau-Karak fault, 3) Lebir fault, 4) Bukit Tinggi Fault Zone, 5) Kuala Lumpur Fault Zone, 6) Endau fault, and 7) Lepar fault. Modified after Ng (1992).....	9
Figure 2.1 Simplified geological map of the Peninsular Malaysia. After Tate <i>et al.</i> (2009) and Metcalfe (2013).....	11
Figure 2.2: The tectonic map of the western flank of Main Range. The red dots show the sample locations. The age of tectonic events in the area is also described. (Note: The purple box shows result obtained from this study) (Modified after Tate <i>et. al.</i> , 2008).15	
Figure 2.3: Map shows the distribution of Bukit Tinggi Fault Zone and Kuala Lumpur Fault Zone and adjacent areas. Modified after Ng (1994).....	19
Figure 3.1: Geological map of the study area and the sample locations in Kuala Kubu Bharu, Selangor.....	23
Figure 3.2: Geological map of the study area and the sample locations in Bukit Tinggi, Pahang.....	24
Figure 3.3: Geological map of the study area and the sample locations in Kuala Kelawang, Negeri Sembilan.....	25
Figure 3.4: A cross-section through a shear zone showing the main types of fault rocks and deformation with depth of the crust (After Passchier and Trouw, 2005). The zone typically broadens and changes in geometry and dominant types of fault rocks with increasing depth.....	26
Figure 3.5: Fault rocks nomenclature. Modified after Brodie <i>et al.</i> , (2007).....	32
Figure 3.6: $^{40}\text{Ar}/^{39}\text{Ar}$ age temperature spectra diagram for a) PM11, age value of 92.4 ± 0.8 Ma. b) PM23, age value of 84.3 ± 0.8 Ma.....	43
Figure 3.7: Inverse isochron age diagram for the mylonite from BTFZ. Inverse isochron age a) PM11 = 87.0 ± 1.0 Ma, MSWD = 2 b) PM23 = 78.3 ± 3.3 Ma, MSWD = 1.6.....	44
Figure 3.8: Schematic illustration of the recovery process. a) Dislocations dispersed over the crystal result in undulose extinction. b) Recovery process causes concentration of dislocations in deformation bands and eventually c) in a subgrain boundary (tilt wall). After Passchier and Trouw (2005).....	49

Figure 3.9: An approximate deformed temperature and deformation mechanisms range for different minerals in mylonites of BTFZ. Bars indicate the transition zones. Arrows indicate the effect of strain rate. BLG, SGR, GBM – main types of recrystallization. The ornamented domain is the domain of crystal plastic deformation. Modified after Passchier and Trouw (2005).....	60
Figure 3.10: A conceptual model of a fault zone showing mylonites location at depth and temperature from Sibson (1977).....	60
Figure 4.1: Idealised S-C fabric. The C-surface is internal shear or slipped surface parallel to shear zone boundary and has the same sense of shear as the main shear zone. The S-surface is related to the accumulation of finite strain and it is defined the mylonitic foliation. After Trouw <i>et al.</i> (2010).....	62
Figure 4.2: Schematic diagram showing the relationship between regional foliation and S-C fabrics in the mylonites of BTFZ. Blue dotted box demonstrate how the oriented sample was taken at the field. The small block (right below) represents the oriented rock sample.....	63
Figure 4.3: Idealised oblique foliation defined by preferred orientation of elongated quartz grains in a quartz rich band embedded in a mylonite, with the mylonitic foliation (C-surface) as reference frame. After Trouw <i>et al.</i> , (2010).....	68
Figure 4.4: a) Idealised sigma porphyroclast structure. Note that the wings are composed of recrystallized feldspar derived from the porphyroclast. b) Idealised delta porphyroclast structure. After Trouw <i>et al.</i> , (2010).....	71
Figure 4.5: The mica fish types commonly found in the mylonite. After Trouw <i>et al.</i> (2010).	73
Figure 4.6: a) Domino type fragmented porphyroclast. Notice that the movement along the porphyroclast is antithetic to the sense of shear and the angle between these faults and the C-surface is usually larger than 45°. b) Shear band type fragmented porphyroclast. Notice the movement along the faults in the porphyroclast is synthetic with the sense of shear in the surrounding mylonite and the angle between the microfaults and the C-surface is smaller than 45°. After Trouw <i>et al.</i> , (2010).....	76
Figure 4.7: Equal area stereonet plot of pole to mylonitic foliations (C-surfaces) of the BTFZ.....	78
Figure 4.8: The granite mylonite shows large stretched drawn-out cylindrical grains defining the stretching lineations (L). The grains are quartz and feldspar pointing to the NE. Bukit Tinggi, Pahang.....	80

Figure 4.9: Equal area stereonet plot of lineations measurements with arrows indicating the movement of the hanging wall. (Note: point with no direction is due to uncertain movement direction).....	81
Figure 4.10: Schematic diagram of a steep reverse anatomosing shear zone. The dominant slip will be reversed but some normal-slip will also be present due to the change in dip direction. Both reverse and normal slip sections will have the similar vergence direction.....	83
Figure 5.1: XRF whole-rock major element data in wt% unit for protolith.....	90
Figure 5.2: XRF whole-rock major element data in wt% unit for mylonites.....	91
Figure 5.3: XRF whole-rock trace element data in ppm unit for protolith.....	92
Figure 5.4: XRF whole-rock trace element data in ppm unit for mylonites.....	93
Figure 5.5: Protolith-normalised major element geochemical transects the BTFZ from NE to SW.....	96
Figure 5.6: Protolith-normalised trace element geochemical transects the Bukit Tinggi Fault Zone from NE to SW.....	97

LIST OF PLATES

- Plate 3.1:** The Bukit Tinggi Pluton is consisted of megacrystic medium to coarse-grained biotite granite, with hypidiomorphic granular texture of tabular or oval K-feldspar megacrysts.29
- Plate 3.2:** Sample of Bukit Tinggi Granite under the microscope. The K-feldspar megacrysts exhibit weakly rounded corners. Quartz occurs as anhedral interstitial grains interlocking and polycrystalline aggregates. Biotite is the dominant mafic mineral in this rock. Inclusions of zircon in biotite are common. Muscovite occurs as interstitial plates and also as minute flakes or aggregates in feldspar and biotite.....29
- Plate 3.3:** Chloritization tends to initiate along the cleavages and margins of the biotites. In some cases, more than quarter of the grains is chloritized.....30
- Plate 3.4:** Mica-chlorite schist is a roof-pendant in the western flank of Main Range Granite found in Kuala Kubu Bharu, Selangor..... 30
- Plate 3.5:** An oriented sample of mylonite shows S-C surfaces. The surface shown is cut parallel to the lineation and perpendicular to the foliations (S-C surfaces). It shows dextral-normal slip with the vergence points to the NE.....36
- Plate 3.6:** A sample of protomylonite from BTFZ. The preferred orientation of tabular to ellipsoidal feldspar porphyroclasts is parallel to S-surfaces. The elongated quartz aggregates and mica strings are mainly aligned parallel to S-surfaces but some are aligned along the C-surfaces.....37
- Plate 3.7:** Photomicrograph of protomylonite from BTFZ. C-planes are made of trails of mica band and aggregate shape of preferred orientation (aspo) of quartz, while S-planes are formed of feldspar porphyroclasts and ribbon quartz.....37
- Plate 3.8:** A sample of mesomylonite from BTFZ. The grain size is finer than the protomylonite and it has higher matrix content (50-90%). The C-surfaces are more distinct than the faint S-surfaces.....38
- Plate 3.9:** The recrystallized quartz grains (neocrysts) in mesomylonite form aggregate shape preferred orientation (aspo) to build the C-surfaces while the S-surfaces are made of grain shape preferred orientation (gsपो) of feldspar porphyroclasts and quartz neocrysts. The inclined aspo combined with the gsपो in the mica rich band (C-plane) point to a dextral sense of shear.....38
- Plate 3.10:** An ultramylonite sample from the BTFZ. It is very fine grains with matrix more than 90%. Only the C-surfaces can be seen in the hand specimen.....39
- Plate 3.11:** An ultramylonite under microscope. The C-surfaces are clearly indicated by compositional banding and the S-surfaces are less developed and indicated by grain shape preferred orientation (gsपो) in the quartz-rich bands.....39

- Plate 3.12:** a) Quartz grains are strongly deformed in protomylonite by crystal-plastic mechanism forming ribbon-shaped quartz, some with aspect ratio more than 4:1. Visible recrystallization is started at the the ribbon-shaped quartz edges by bulging recrystallization (BLG). b) In mesomylonite, almost all of the ribbon-shaped quartz experiencing dynamic recrystallization to form neocrysts.....47
- Plate 3.13:** a) In protomylonite, the feldspars form angular clasts through fracturing and microcracking. Minor sericitization occurs in the feldspar clasts. b) With increasing shear, plagioclase frequently fold, kink and experiencing undulose extinction due to internal deformation. Bending or folding in plagioclase caused the twinning lamellae to curve. Flame perthite is common.....50
- Plate 3.14:** a) Photomicrograph showing K-feldspar clast with fracture along the cleavages. Recrystallization by bulging recrystallization (BLG) in the feldspar occurs at the grains boundary between the same minerals. b) Alternate quartz and feldspar neocrysts-rich layers parallel to the C-surface. Notice the different in size of quartz and feldspar neocrysts. The new recrystallised quartz are polygon in shape at about the same size.....51
- Plate 3.15:** In mylonite mica behaves ductilely. Undulose extinction, folds and kinks are common, generally associated with deflection of basal planes and lead to fish shaped boudinage grains. With increasing shear and strain, mica recrystallized to form very fine plate-shaped grains.....52
- Plate 4.1:** An oriented protomylonite with S-C foliations, cut parallel to the lineation and perpendicular to the foliations. The S-C fabric and porphyroclasts show dextral reverse movement top-to-NE vergence. C-surface = 150° , 68° SW; Lineation = 072° → 243°64
- Plate 4.2:** a) Photograph of a stained polished rock slab of protomylonite indicates dextral sense of shear. b) The S-C fabric is inclined in reverse direction to the NE.....67
- Plate 4.3:** Oblique foliation in (a) protomylonite and b) ultramylonite from the sample indicate dextral sense of shear.....69
- Plate 4.4:** Sigma porphyroclasts of K-feldspar. (a) Minor recrystallization along the rim shows initiating the core-mantle structure in protomylonite (b) Note the porphyroclast show advanced recrystallization (upper right) forms stair step in the matrix. The sigma shape fabric stepping to the right around the large porphyroclast and S-C structure indicate dextral sense of shear in the protomylonite.....72
- Plate 4.5:** a) Biotite fish surrounded by quartz showing internal deformation and recrystallization along the rims. Note that the mineral cleavage is parallel to the side of the fish in protomylonite. b) A lens-shaped mica fish indicates dextral sense of shear by stair stepping and a weak oblique fabric in quartz in ultramylonite.....74

Plate 4.6: Photomicrographs show the fractures in K-feldspar porphyroclasts with apparent sinistral displacement along the microfaults that separate the three fragments. These domino type antithetic fragmented porphyroclasts indicate dextral sense of shear in the protomylonite.....77

University of Malaya

LIST OF TABLES

Table 2.1: Summary of major faults in Peninsular Malaysia. All these faults are young brittle fault post-date mylonitisation episode. Modified after Shuib (2009a).....	20
Table 3.1: $^{40}\text{Ar}/^{39}\text{Ar}$ analytical data for the mylonite from BTFZ.....	42
Table 3.2: Table shows the evolution of the deformation microstructures in mylonite of BTFZ. Relative development indicator (o: absent, x : minor, xx : moderate, xxx : high).....	53
Table 3.3: Summary of the temperature correspond to the deformed microstructures in mylonites of BTFZ.....	58
Table 5.1: Summary of concentration for major elements in protolith and mylonites...87	87
Table 5.2: Summary of concentration for trace elements in protolith and mylonites....88	88

LIST OF ABBREVIATIONS

$^{40}\text{Ar}/^{39}\text{Ar}$	Argon/Argon	NW	North-West
BF	Bukit Fraser	Pl	Plagioclase
BG	Biotite Granite	PM	Protomylonite
BLG	Bulging recrystallisation	P-T-t	Pressure-Temperature-
Bt	Biotite		time
BT	Bukit Tinggi	Qtz	Quartz
BTFZ	Bukit Tinggi Fault Zone	S	South
cm	centimeter	SE	South-East
E	East	Sg.	Sungai (river)
ENE-WSW	East-North-East— West-South-West	SGR	Subgrain rotation recrystallisation
E-W	East-West	SRTM	Shuttle Radar
GBM	Grain boundary	Topographic	
migration			Mission
	recrystallisation	SW	South-West
K-Ar	Potassium Argon	UM	Ultramylonite
Kfs	K-feldspar	U-Pb	Uranium Lead
Kg.	Kampung (village)	W	West
KK	Kuala Kelawang	WNW-ESE	West-North-West-East-
KKB	Kuala Kubu Bharu	South-East	
KL	Kuala Lumpur		
Km	Kilometre		
Ma	Million year age		
MCS	Mica-Chlorite Schist		
MM	Mesomylonite		
N	North		
NE	North-East		

LIST OF APPENDICES

APPENDIX A: Detail of major faults in Peninsular Malaysia.....	119
APPENDIX B: Description of samples used in the study.....	127
APPENDIX C: Measurements of the samples.....	128
APPENDIX D: Detail geochemical data for the samples.....	133

University of Malaya

CHAPTER 1: INTRODUCTION

1.1 General introduction

A fault zone is a zone of sheared, crushed or foliated fault-rocks deformed by faulting or shearing. The type of fault rocks produced is related to the characteristics of the protolith and deformation conditions. Generally, brittle fault-rocks such as cataclasite are formed at shallow crustal level where the temperature and pressure are relatively low, while at deeper level mylonites are formed where plastic deformation predominates (Sibson, 1977).

According to Brodie *et al.* (2007) mylonites is a cohesive fault rock occurring in a tabular zone characterised by a well developed foliation resulting from tectonic reduction of grain size, and commonly porphyroclastic. Throughout the formation, some minerals are affected by deformation and some are recrystallised to new form of minerals at different physico-chemical conditions. Microstructures formed during the shearing process are very important to understand the mechanisms and conditions during the fault formation.

There are two main faults cut through the middle of the Western Peninsular Malaysia, particularly in the east of Kuala Lumpur known as Kuala Lumpur Fault Zone and Bukit Tinggi Fault Zone (Shu, 1969, 1989; Tjia, 1972). The Bukit Tinggi Fault Zone (BTFZ) is one of many major faults in Peninsular Malaysia. It cuts the Main Range granite and strongly expressed by prominent lineaments and a broad zone of mylonites which has been traced from Kuala Kubu Bharu through Bukit Tinggi down to Kuala Kelawang (Shu, 1969).

The Bukit Tinggi Fault Zone is an ideal zone to study the relationship between deformation, mineralogy and chemical changes hence, a direct comparison can be made with the protolith adjacent to it. Difference in the process involved can be explicitly known in this setting.

1.2 Objectives

The objectives of this research are:

- i) To characterise the deformation and recovery microstructures of the mylonites.
- ii) To investigate the history of deformation by determining the temperature of deformation and the kinematics of the fault zone.
- iii) To determine the geochemical changes during mylonitisation by comparing the chemical contents of the mylonites from the undeformed protolith.

1.3 Study area

The Bukit Tinggi Fault Zone (BTFZ) is situated just north of Kuala Lumpur Fault Zone (Stauffer, 1968) with length over than 100 km and strike nearly 140° (Shu, 1969; Tjia, 1972). The fault can be traced across the states of Selangor, Pahang, Negeri Sembilan and Perak (Figure 1.1).

Exposures of mylonites is located near the Sg. Selangor dam immediately northeast of the Kuala Kubu Bharu, Selangor town, cut slopes between km 45 and km 53 of Karak Highway, and several small outcrops in Bukit Tinggi, Pahang and along the way from Genting Peres to Kuala Kelawang, Negeri Sembilan (Kuala Lumpur Fault Zone). The extent of the study area covers approximately 120 km long, bounded by longitudes $101^{\circ}40'E$ to $101^{\circ}54'E$ and latitudes $3^{\circ}20'N$ to $3^{\circ}35'N$.

1.4 Previous works

Faults in the Kuala Lumpur and adjacent areas have been of great interest to geologists for many years. Among the earlier geological research held in this area was done by Alexander (1955). Burton (1965) was the first to document the large scale strike-slip fault while he was undertaking a geological regional survey in Baling, Kedah. Stauffer (1968, 1969) proposed a major strike-slip fault zone, the Kuala Lumpur

Fault Zone extending all the way across the western part of Peninsular Malaysia at an orientation of about 105° and passing very near Kuala Lumpur coinciding in part with the quartz reefs. Alexander (1965) noted lithological offsets in map by Gobbett (1965a) of order of several kilometres associated with the lineaments, prominent stream alignments, quartz reefs and a variety of other features all correspond to this fault zone. He inferred a sinistral strike slip movement of this fault.

The Bukit Tinggi Fault Zone (BTFZ) was proposed by (Shu, 1969) for a major NW-SE trending lineament and related mylonitic rocks cutting the Main Range Granites between Bukit Tinggi, Pahang and Jelebu, Negeri Sembilan. The most persistent faults in the Kuala Lumpur area are exhibited by the main set of strike-slip faults trending at 310° - 320° , with associated splays trending at 280° - 290° (Shu, 1969). He reported the presence of a set of north-south striking faults to be the oldest in the area and cut by both the Bukit Tinggi Fault Zone and a few relatively minor complimentary northeast-southwest trending faults. He interpreted all faults to be sinistral strike-slip faults with the exception of the north-south striking set, which he believes to be right lateral strike-slip in nature.

Tjia (1972, 1975a, 1978) concluded that left lateral offsets are evident along fault zones that trend approximately NW to WNW in the Kuala Lumpur area. He came to the conclusion that the N-S trending faults exposed in the center of Peninsular Malaysia were dextral strike-slip faults. According to him, the Bukit Tinggi Fault Zone is apparently the oldest fault in the Kuala Lumpur area and is transacted by the N-S trending fault, which he terms the Kelau-Karak Fault Zone.

Ng (1992, 1994) and Shuib (2009a) also reported the existence of two main fault zones with NW-SE strike in eastern part of Kuala Lumpur which is Bukit Tinggi Fault Zone and Kuala Lumpur Fault Zone. Ng (1994) also noted that Kuala Lumpur granitic

rocks experienced several episodes of displacements which produce various kinds of deformed granites.

Geochemical transformation during the faulting process in granitic mylonites has been studied by many authors (Kerrick *et al.*, 1980; Hippertt, 1998; Roberts and Nissen, 2006; Kwon *et al.*, 2009). However, no such studies have been done for the deformed rocks along the BTFZ. The deformation history of BTFZ is also poorly understood. Radiometric dating of mylonites from Kuala Kelawang, Negeri Sembilan by Harun (2002) gave an age of 83.6 Ma.

1.5 Research methodology

A combined microstructural, geochemistry and geochronological approach, utilizing both field and laboratory studies, was used to determine the microstructural and geochemical characteristics of mylonites along the Bukit Tinggi Fault Zone.

1.5.1 Literature review

Literature review is crucial. Approximately 300 journal articles have been collected as references. Thesis, books, maps and memoirs also used to complete the study. Relevant information related to the research objective were traced and adopted when the problems are identified. This process is essential to enable us to understand and prepare the study to be undertaken.

1.5.2 Fieldwork

The fieldworks have been carried out from January 2012 to early of 2013. The field methods included sampling and mapping transect the area of Bukit Tinggi Fault Zone. Those are included several spots from the road of Kuala Lumpur to Fraser Hill, Karak highway, Kampung Bukit Tinggi and road from Genting Peres to Kuala

Kelawang. Mesoscopic characteristics of the mylonites are noted and orientation of foliations and lineations are recorded. When suitable mesoscopic kinematic indicators are present, the sense of shear was recorded. The kinematic analysis was done on surfaces that are parallel to the lineation and perpendicular to the foliation. About 100 samples were collected, including oriented samples for microscopic kinematic analysis. Location of each rock samples were marked by GPS. Each rock samples were given specific code for identification.

1.5.3 Laboratory works

The laboratory work consists of petrographic study and geochemical analysis. Thirty fresh rock samples were selected for geochemical analysis. Two samples were selected for $^{40}\text{Ar}/^{39}\text{Ar}$ radiometric dating.

a) Petrographic analysis

About 30 thin sections were prepared to the standard 30 μm thickness. Fifteen oriented thin sections were made perpendicular to the foliation and parallel to the lineation for microscopic kinematic analysis. Thin sections were examined using a petrology microscope to determine the mineral constituent, the texture, microstructure and alteration. Besides that, the same rock samples were used for geochemical analysis.

b) Geochemical analysis

The analysis was done to determine the major and trace element contents in the protolith and mylonites. The collected samples were crushed into smaller pieces using a jaw crusher and pulverized to fine powder using a tema mill. The pulverizing and grinding process was carried out at the Department of Geology, University of Malaya.

Geochemical analysis (XRF and ICP-MS) for the study was performed by Acme Analytical Labs Ltd., Vancouver, Canada using the following procedures:

X-ray Fluorescence (XRF)

First loss of ignition (LOI) of the sample is determined. After then, the sample is fused with flux to form a fusion bead. The finished bead will then be analyzed by the XRF machine.

To determine LOI of the samples, about 1g of dry rock sample in powder form is put into a crucible and sintered at 1000°C in an oven for 1 hour. The crucible is then cooled (about 10 minutes). The value of LOI (in weight %) can be determined from using the formula below :

$$\text{LOI} = [(a-b) / (a-c)] \times 100\%$$

a : weight of the crucible with sample before sintering (in gram)

b : weight of the crucible with sample after sintering (in gram)

c : weight of the empty crucible (in gram)

12 g of sintered powder is mixed with flux (lithium metaborate, LiBO₂) and fused in a platinum crucible using an automated fusion machine, before the molten sample is casted into a glass bead. The glass bead is then analyzed by a XRF machine using acceptable values of standard samples for major elements.

Reference materials used for XRF analysis are STD SY-4(D) and STD OREAS72B.

Inductively coupled plasma-mass spectrometry (ICP-MS)

The technique used by Acme Labs is a type of acid digestion; lithium tetraborate Li₂B₄O₇ fusion followed by diluted acid digestion. This decomposition technique is suitable for rare earths and refractory elements. The bead preparation and fusion process is similar the one described for XRF analyses,

except that 5 g of sample and a different flux is used instead. The resulting molten bead is rapidly digested in a weak nitric acid solution. It is only with this attack that major oxides including SiO₂, REE and other high field strength elements are put into solution. Precious metals, base metals and their associated pathfinder elements are generated from an aqua regia digestion. Sample splits of 0.5g are leached in hot (95°C) aqua regia. Reference materials used for ICP-MS analysis are STD SO-18, STD DS9 and STD OREAS45EA.

c) Geochronology

For ⁴⁰Ar/³⁹Ar dating purposes 2 whole rock samples of mylonites were sent to Activation Laboratories Ltd., Ontario, Canada. Thin section examination was carried out to make sure that the biotite of these 2 samples is completely recrystallized. The biotite separates were obtained by crushing several kg of sample, sieving, washing and separation using magnetic methods and heavy liquids. The separates were wrapped in Al foil and loaded in an evacuated and sealed quartz vial with K and Ca salts and flux monitors (LP-6 biotite, with and assumed age of 128.1 Ma) (Ingamells and Engels, 1976; Odin *et al.*, 1982). They were irradiated in the McMaster University, Ontario, Canada, nuclear reactor for 48 hours. After the flux monitors were run, J values were calculated, using the measured flux gradient. Neutron gradients did not exceed 0.27% on sample size. The Ar isotope composition was measured in a Micromass 5400 static mass spectrometer. 1200°C blank of ⁴⁰Ar did not exceed 2–5*10⁻¹⁰ cc STP. Heating time for each step was 10 minutes. After each analysis, the extraction temperature is elevated to 1800°C for few minutes and the furnace is prepared for next analysis.

For the Ar analysis an aliquot of the sample was weighted into an Al container, loaded into the sample collector of the extraction system, and degassed at ≈100°C for two days to remove the surface gases (Miranda *et al.*, 2009). Argon was extracted from the sample in a double vacuum furnace at 1700 °C. The Ar concentration was then

determined using isotope dilution with a ^{38}Ar spike, which is introduced to the sample system prior to each extraction. The extracted gases are cleaned up in a two steps purification system. Pure Ar was then introduced into a custom built magnetic sector mass spectrometer (Reynolds type) with a Varian CH5 magnet. The ion source has an axial design (Baur-Signer source), that provides more than 90% transmission and extremely small isotopic mass discrimination. Ar isotope ratios measurements were corrected for mass discrimination and atmospheric argon was removed assuming that ^{36}Ar is of atmospheric origin. The concentration of radiogenic ^{40}Ar was calculated using a ^{38}Ar spike. After each analysis the extraction temperature is elevated to 1800°C for few minutes and the furnace is prepared for the next analysis.

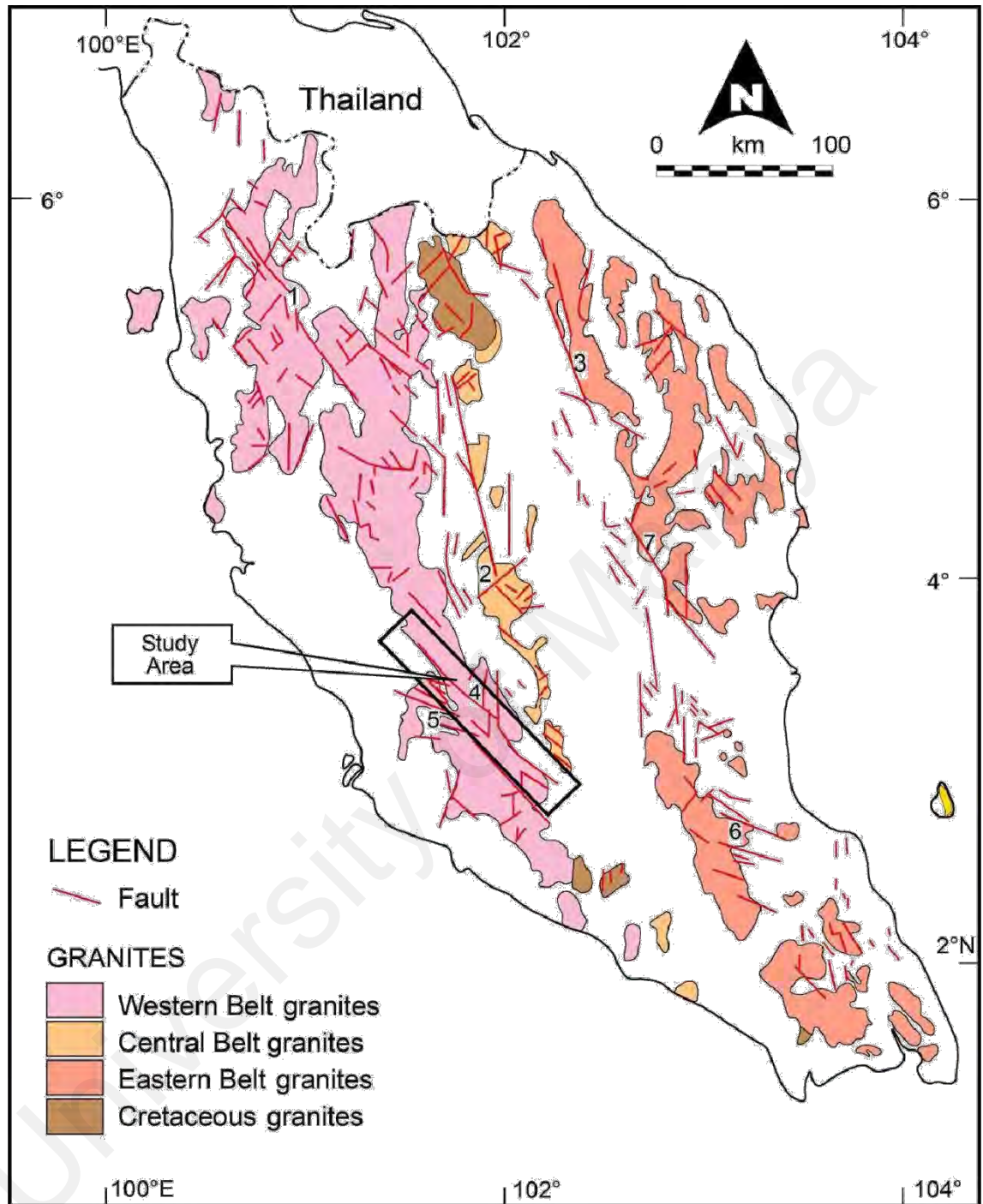


Figure 1.1: Map of main faults in Peninsular Malaysia. Bukit Tinggi Fault Zone (study area) transects the Main Range Granite. 1) Bok-Bak fault 2) Kerak-Karak fault 3) Lebir fault 4) Bukit Tinggi fault 5) Kuala Lumpur fault 6) Endau fault 7) Lepar fault. Modified after Ng (1992).

CHAPTER 2: REGIONAL GEOLOGY AND TECTONIC SETTING

2.1 Introduction

The structure, stratigraphy, magmatism, geological evolution and geophysical signatures distinctly distinguish the Western, Central and Eastern belts of Malay Peninsula. Sibumasu region detached from NW Australian Gondwana margin to form the Western Belt of Malay Peninsula (Metcalf, 2013). The Western Belt is mostly covered by coarse grained megacrystic biotite granite. The country rocks intruded by the granites are mainly Lower Paleozoic formations and have Gondwana affinity (Metcalf, 2000, 2013) and sequence of folded Upper Paleozoic clastic metasediments. These Paleozoic rocks were intruded by granites mainly during the Late Triassic.

A number of faults trending NW-SE, N-S and NE-SW cut the Western Belt granite and the Paleozoic rocks including the Bukit Tinggi Fault Zone. This fault zone is a NW-SE striking fault that penetrated the western flank of Western Belt granite from Kuala Kubu Bharu to Bukit Tinggi until north of Kuala Kelawang district (Shu, 1969).

2.2 Regional geology and tectonic setting

The Western Belt granite (Figure 2.1) forms an enormous mountain range stretching from the Thai border to as far south as Melaka (Cobbing *et al.*, 1992). The belt exists to the west of Bentong-Raub Suture Zone (Metcalf, 2000, 2013) which separated the Western Belt from the Eastern Belt. Two main batholiths of the Western Belt granite are the Main Range and Bintang batholiths (Cobbing and Mallick, 1987). The Western Belt granite magma is generated during the eastward collision between Sibumasu and Indochina block in Triassic. The belt has restricted rocks composition from granite to granodiorite. The granite can be divided into three facies based on the

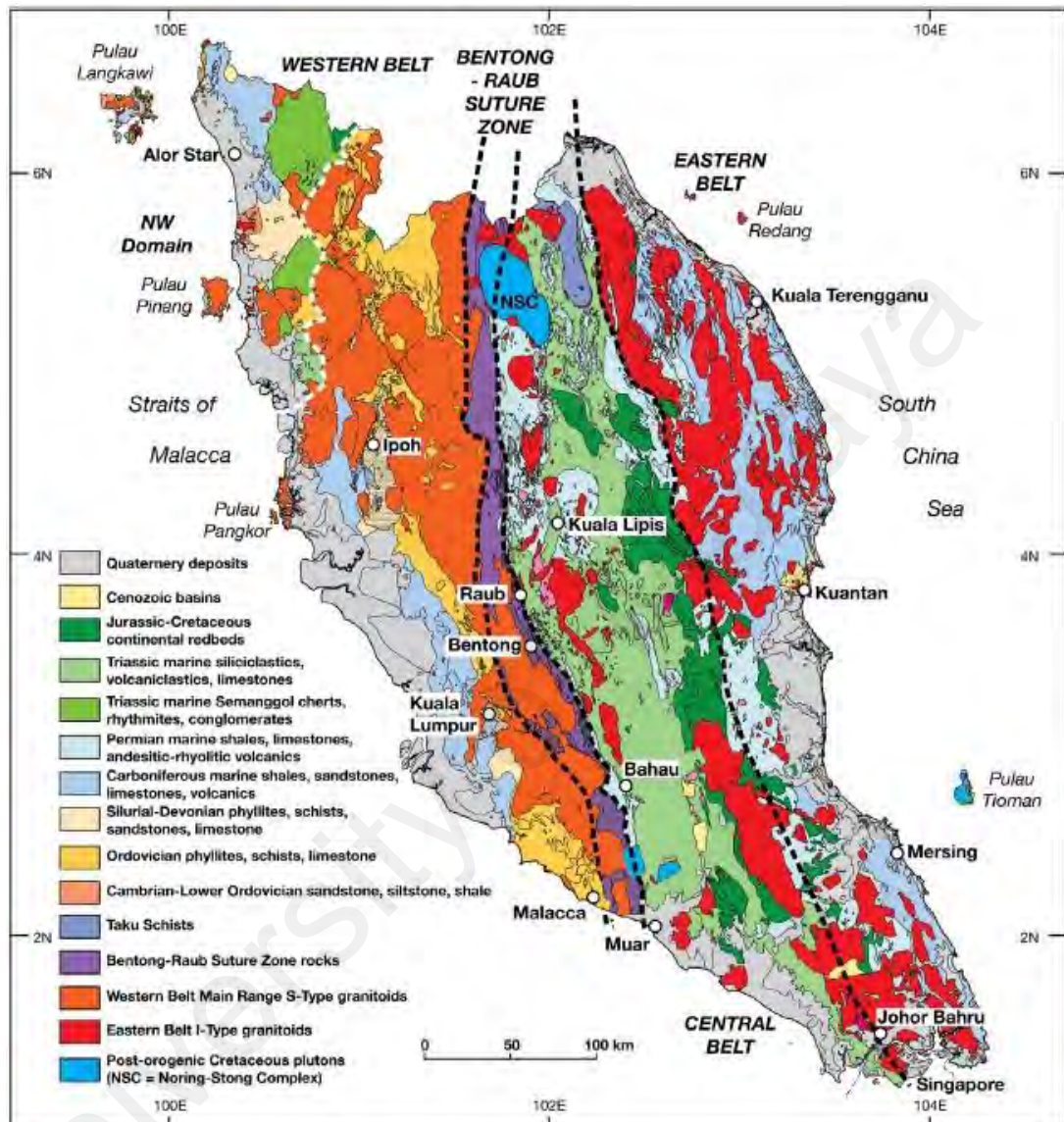


Figure 2.1: Simplified geological map of the Malay Peninsula. After Tate *et al.* (2009) and Metcalfe (2013).

mineral content and textures that is biotite granite, amphibole bearing granite and late stage microgranite and mesogranite (Cobbing *et al.*, 1992; Ghani *et al.*, 2013).

The granite in the study area is known as the Bukit Tinggi pluton and composed of coarse grained biotite granite. The Bukit Tinggi pluton is cut by a set of faults known as the Bukit Tinggi Fault Zone.

The Bukit Tinggi pluton which lies to the east of the Bukit Tinggi Fault Zone is a large, elliptical complex and in contact with schists and other metasediments of Devonian to Silurian age. It is made up of several units of granite such as Gap unit, Ulu Kali unit, Sg. Senaling unit and Sg. Rodah Microgranite unit (Bignell and Snelling, 1977). The NW-SE trending fault zone cuts across the Gap unit in the Bukit Tinggi pluton from Kuala Kubu Bharu in the north down to Kuala Kelawang area.

Towards the western margin of the Bukit Tinggi pluton, the granitic rocks show evidence of retrograde metamorphism resulted from the rocks being deformed under the greenschist metamorphic facies (Ng, 1994). It is coarse grained, composed of quartz, K-feldspar, plagioclase, biotite and accessory minerals include apatite and zircon. The granite shows fabrics varying from undeformed primary igneous to deformation fabrics exhibiting mylonitic textures. Several meter-scale wide shear zones are well exposed in small outcrops. A complete gradation from slightly deformed to strongly sheared granite can be observed in the area studied.

2.3 Major faults in Peninsular Malaysia

Major faults in Peninsular Malaysia are parallel to the main structure trend and generally strike NW-SE and N-S. Some of them have undergone complex repeated history of deformation such as the Bukit Tinggi Fault Zone (Ng, 1994), Bok Bak Fault (Burton, 1965) and the Alur Lebey Fault (Harun, 1994).

The earlier developed fault zones are the Bentong-Raub Suture Zone, Lebir Fault Zone, Kisap thrust, Alur Lebey Fault and Balau Fault (Shuib and Abd. Rahman, 1999; Shuib, 2000a). It is followed by few sets of NW-SE to N-S fault zones which developed after the emplacement of the Main Range Granite such as the Bukit Tinggi and Bok Bak fault zones (see Figure 1.1). Details of the major faults in Peninsular Malaysia were summarized in Table 2.1.

2.4 Bukit Tinggi Fault Zone

The Bukit Tinggi Fault Zone (BTFZ) is made of prominent sets of sub-parallel NW-SE striking lineaments (Figure 2.2). The fault zone is near vertical and in places it has been traced dipping both to the SW and NE. It is best shown by the exposures sheared granites parallel to the fault zone which has a thickness up to about 5 km wide to the east of Kuala Lumpur area.

2.4.1 Geology of BTFZ

Approaching the boundary of the Bukit Tinggi pluton, the fault zone is characterized by strongly deformed granites, with mylonitic textures. The strain distribution in this sheared zone is variable on a local scale, forming rocks ranging from protomylonite to ultramylonite.

Granite exposed along the road from Kuala Kubu Bharu town to the Fraser Hill (Figure 2.2) is megacrystic and medium to coarse grained. The granite comprises about 40% of alkali feldspar (1.0-7.5cm), 15-20% quartz and plagioclase respectively, whereas the megacrystic granite exposed along the KL-Karak highway has 35-40% alkali feldspar, 30-35% quartz and about 10% plagioclase. The undeformed granite exhibits primary textures which typically comprise of oval K-feldspar megacrysts

surrounded by grey quartz clusters and groundmass containing biotite, muscovite, chlorite, sphene, epidote and sometime magnetite or hematite.

Few outcrops of microgranite are exposed along the road to Berjaya Hills Resort. Cobbing and Mallick (1987) classified the microgranite as the Sg. Rodah unit of the Bukit Tinggi pluton. It is generally in the form of dikes and may also be present as stocks or small plutons. The size of the dikes varies from place to place up to 1m thick. The microgranite characterized by non-porphyritic granular and fine grained size K-feldspar, plagioclase, quartz, biotite and muscovite.

The fault zone is also found to cut the Belata Formation and Trolak Formation at Kuala Kubu Bharu and Jelevu Schist in Kuala Kelawang area. The Belata Formation is made of argillaceous facies of phyllite in the lower part and marginal arenaceous facies of metasandstone and metaquartzite in the upper part, and minor bedded chert within the argillaceous facies. The Belata Formation is thought to be Carboniferous to Permian in age and can be correlated to the Kenny Hill Formation of Kuala Lumpur (Lee, 2004). The Trolak Formation is comprised of argillaceous facies of quartz-mica schist, graphitic schist and phyllite, minor arenaceous facies of metaquartzite and quartz schist, and minor limestone facies (Lee, 2004). It is Ordovician to Silurian in age. It correlated to Kuala Lumpur Limestone and Hawthornden schist (Gobbett, 1964) of the Kuala Lumpur area (Lee, 2004).

The Lower Palaeozoic Jelevu Schist consists of quartz-mica schist, quartz schist, quartz sericite-chlorite schist, quartz graphite and graphitic phyllites with minor lenses of calcareous rocks and amphibole schist (Lee, 2004).

In the central part of Kuala Kubu Bharu area, the metasedimentary rocks occur as a roof pendant in the granite batholith. The rock is hard and has hornfelsic texture near the granite contact. These metasedimentary rocks have undergone regional metamorphism, contact metamorphism by the granite intrusion and also deformed by faulting.

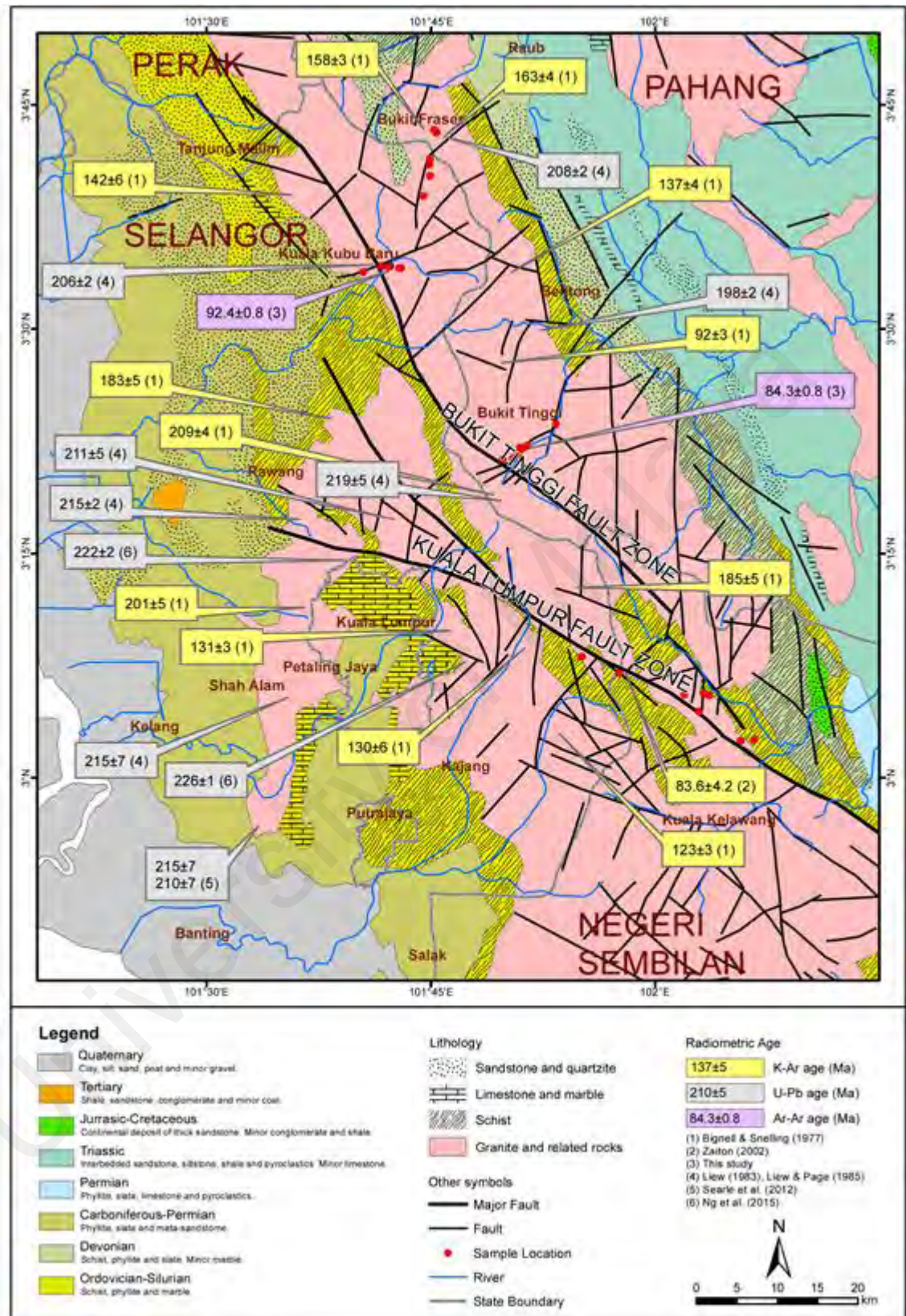


Figure 2.2: The tectonic map of the western flank of Main Range. The red dots show the sample locations. The age of tectonic events in the area is also described. (Note: The purple box shows result obtained from this study) (Modified after Tate *et. al.*, 2008).

metasedimentary rocks, which mostly located on the flat areas along the Sungai Selangor, whereas the alluvium covers the eastern part of Kg. Bukit Tinggi area in the form of alluvial terraces. The alluvium comprise of varying proportions of unconsolidated sand, silt, clay and gravel.

2.4.2 Structures of BTFZ

The trend of foliations in mylonites is NW-SE subparallel to the Bukit Tinggi Fault Zone. The other set of NW-SE fault present near to the study area is the Kuala Lumpur Fault Zone. Several lineaments representing younger faults are also known to cut the Bukit Tinggi Fault Zone at Kg. Janda Baik, Bukit Tinggi area.

Although the strike of the foliations in the mylonites are quite consistent (100° to 170°), the dips are variable from 40° - 89° SW to 23° - 78° NE. The lineations are plunging at moderate angles towards 190° - 254° for the SW dipping foliations and towards 030° - 065° for the NE dipping foliations. The vergence, however is consistently towards the NE. Foliations in the metasediments are steep and strike about 125° - 305° .

A prominent quartz vein found just south of the Kuala Kubu Bharu town is vertical and trending 102° - 108° dip NE. Post-date mylonitisation, the brittle episode of BTFZ is determined as a sinistral strike-slip fault by Zaiton (2002) and Shuib (2009).

2.5 Kuala Lumpur Fault Zone

The Kuala Lumpur Fault Zone (KLFZ) and BTFZ are adjacent to each other (Figure 2.3) with some close characteristics. They are oriented in the same direction and the granite mylonite formed during the Late Cretaceous age (Harun, 2002). The fault zone is one of the two major NW-SE trending fault zones (Stauffer, 1968; Shu, 1969; Shuib, 2009a) in west central Peninsular Malaysia. It cuts the Kuala Lumpur granite at the east of Kuala Lumpur area (see figure 2.3). The granite is a part of the Main Range

Granite which intruded into folded and regionally metamorphosed clastic and calcareous Paleozoic rocks. It is separated from the Genting Sempah Microgranite by a metasedimentary screen at its eastern margin. However, the outcrop is poorly exposed and only found in few spots along the road from Semenyih dam to Kuala Kelawang.

The Kuala Lumpur Granite is a large irregular granitic body on the western side of the Main Range Granite. It comprises western and eastern lobe. To the east it is separated from the Genting Sempah microgranite by a major fault and by a sedimentary screen which runs along the line of the fault. The pluton is emplaced into Permo-Carboniferous Kenny Hill Formation, Kuala Lumpur Limestone of Silurian age and Hawthornden Formation of Ordovician age. It is predominantly megacrystic consisting of K-feldspar megacrysts set in an allotriomorphic to hypidiomorphic groundmass. The major minerals are K-feldspar, quartz and plagioclase, while biotite, muscovite and tourmaline usually occur in minor amounts, except in the late phase differentiates where these minerals may be dominant.

On imagery images, the fault zone is made up of five main strands (Noraini and Taylor, 2000). These are the Ulu Kelang fault, Bukit Tajoh fault, Kongkoi fault, Ampang fault and Ulu Langat fault (see figure 2.3). The fault zone has a minimum width of 10 km and a total displacement of more than 20 km. It passes through the Batu Arang Tertiary basin and can be traced up to Pulau Jemur, Indonesia (Tjia, 1989a). This basin is situated on overlapping segments of right-stepping en-echelon splays of the Kuala Lumpur Fault Zone. The mylonite occurs in Jelebu-Kuala Kelawang area is along the Kongkoi fault.

Batu Arang Basin is believed to rise after the transtensional stress at the overlapping segments (Mahendran *et al.*, 1991; Raj *et al.*, 1998; Shuib and Abd. Rahman, 1999). Thus, it is suggested that the Kuala Lumpur Fault Zone was activated until the Late Miocene.

The Kuala Lumpur Fault Zone is defined by sets of steep brittle faults and shear zones (Shuib, 2009a). These are the sinistral NW-SE and N-S, dextral NE-SW, and

ENE-WSW and a less prominent normal to sinistral E-W set. Based on the orientation of the vertical quartz reefs, the Kuala Lumpur Fault Zone was formed due to WNW-ESE maximum compressive stress, determined from fault kinematics to have acted from 100° - 114° to 280° - 294° , similar to the results obtained by Ng (1994) and Tjia (1997).

University of Malaya

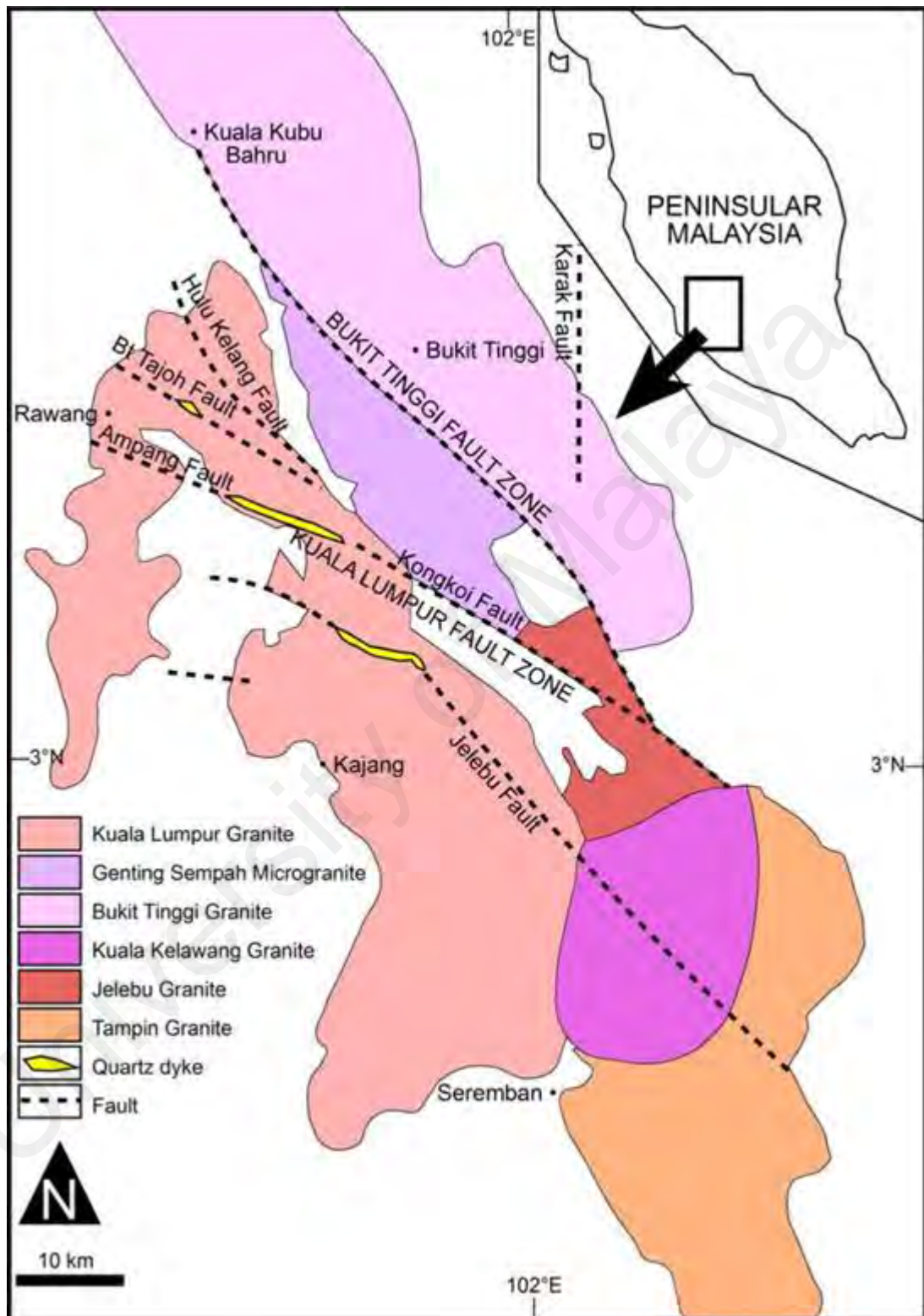


Figure 2.3: Map shows the distribution of Bukit Tinggi Fault Zone and Kuala Lumpur Fault Zone and adjacent areas. Modified after Ng (1994).

Table 2.1: Summary of major faults in Peninsular Malaysia. All these faults are young brittle fault post-date mylonitisation episode. Modified after Shuib (2009a).

Name of fault	Type of fault	Location
Balau-Murau Fault Zone	Dextral strike slip fault.	<ul style="list-style-type: none"> - From Batu Layar northwards to the Balau Fault Zone (Shuib and Jamaluddin, 1999). - Through Tanjong Leman, Tanjong Murau and Mersing.
Bok Bak Fault Zone	Sinistral strike-slip (NNW-SSE), Dextral strike-slip (NNE-SSW).	<ul style="list-style-type: none"> - Transects the Main Range Granite at the Western part of the Peninsular Malaysia from southwest Kelantan, passing through central Perak, Bukit Perak (Kedah) and ends near Pokok Sena (Kedah). - Extended southward to central Perak and southwest Kelantan based on LANDSAT lineament study (Raj, 1982c).
Bukit Keluang Fault	Dextral strike-slip fault.	<ul style="list-style-type: none"> - Terengganu.
Bukit Tinggi Fault Zone (BTFZ)	Sinistral strike-slip fault.	<ul style="list-style-type: none"> - North of Kuala Kubu Bharu until south to Kuala Kelawang (Shu, 1969).
Galas Fault Zone	Oblique sinistral reverse fault.	<ul style="list-style-type: none"> - Extend across the Thailand border, near Bukit Saiong (Kedah) to the Tembeling area.
Kapas Fault	Dextral transpression fault.	<ul style="list-style-type: none"> - Pulau Kapas (Terengganu).

Kisap Thrust	Thrust fault.	- From southern part of Langkawi (tip of Pulau Dayang Bunting), through the main island up to Pulau Dangli at the northernmost tip.
Kuala Lumpur Fault Zone (KLFZ)	Sinistral fault	- Kuala Lumpur.
Lebir Fault Zone	Sinistral normal fault.	- Along Sungai Lebir near Manek Urai (Kelantan).
Lepar Fault Zone	Sinistral strike-slip fault.	- Parallel to Sungai Lepar (Pahang).
Mersing-Endau Fault Zone	Sinistral strike slip	- From Endau (north) to Kota Tinggi (south), through Layang-layang and Segamat (west).
Ruok Fault Zone	Sinistral strike-slip, reactivated as normal faulting.	- From the Pattani river (Thailand) into Malaysia along Sungai Kenerong, then along the Temenggor lake before ending just north of the Bok Bak Fault Zone.
Seremban Fault Zone	Sinistral strike-slip fault.	- Trace from NW of Gunung Ledang, northwestward into the Main Range Granite at Bahau and passing through Seremban.

University of Malaya

CHAPTER 3: PETROGRAPHY AND DEFORMATION MICROSTRUCTURES

3.1 Introduction

The study areas are located at Kuala Kubu Bharu (Selangor), Bukit Tinggi (Pahang) and Kuala Kelawang (Negeri Sembilan) area. These areas are largely underlain by granitic rocks with minor occurrence of metasedimentary rocks at the eastern part of Kuala Kubu Bharu. The locations have been selected as the rocks in the areas were significantly shown changes in the structural and chemical features. The samples used were unweathered and in good condition as well. Detail sample locations used in the study are shown in Figure 3.1-3.3. The subdivision of granite pluton by Cobbing and Mallick (1987) is adopted in this study. They classified the granitic rocks in the study area as part of the Bukit Tinggi Pluton.

The numerous faults have deformed the Bukit Tinggi Granite to produce a diverse assemblage of fault rocks (Figure 3.4). The fault related granites found in the study area include mylonites, cataclasites, fault breccia and fault gouge. However, the thesis is focusing on mylonites.

Mylonites occur in localized zone of intense deformation in the study area. The shear zones occur in different scales, vary in width from a few millimeters to several kilometers. The millimeter wide shear zones are observed under the microscopic and the Bukit Tinggi Fault Zone along the Karak highway is estimated to be about 5 kilometers wide.

The mesoscopic and microscopic characteristics of the undeformed granite, metasediment and mylonites will be discussed here from the aspect of petrography, deformational microstructures behaviour of the constituent minerals, the deformation mechanisms and conditions as well as the age of the fault during mylonitisation.

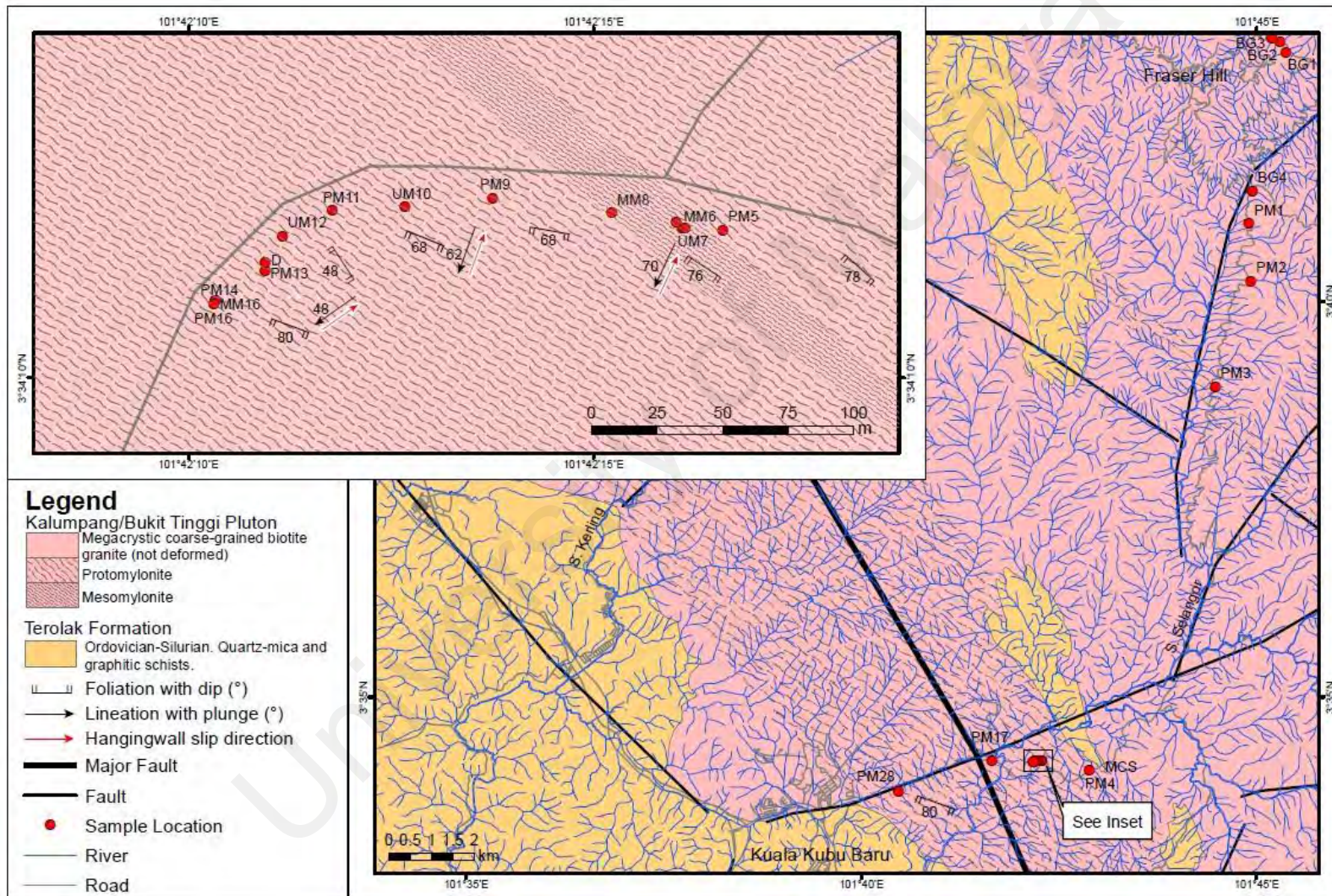


Figure 3.1: Geological map of the study area and the sample locations in Kuala Kubu Bharu, Selangor.

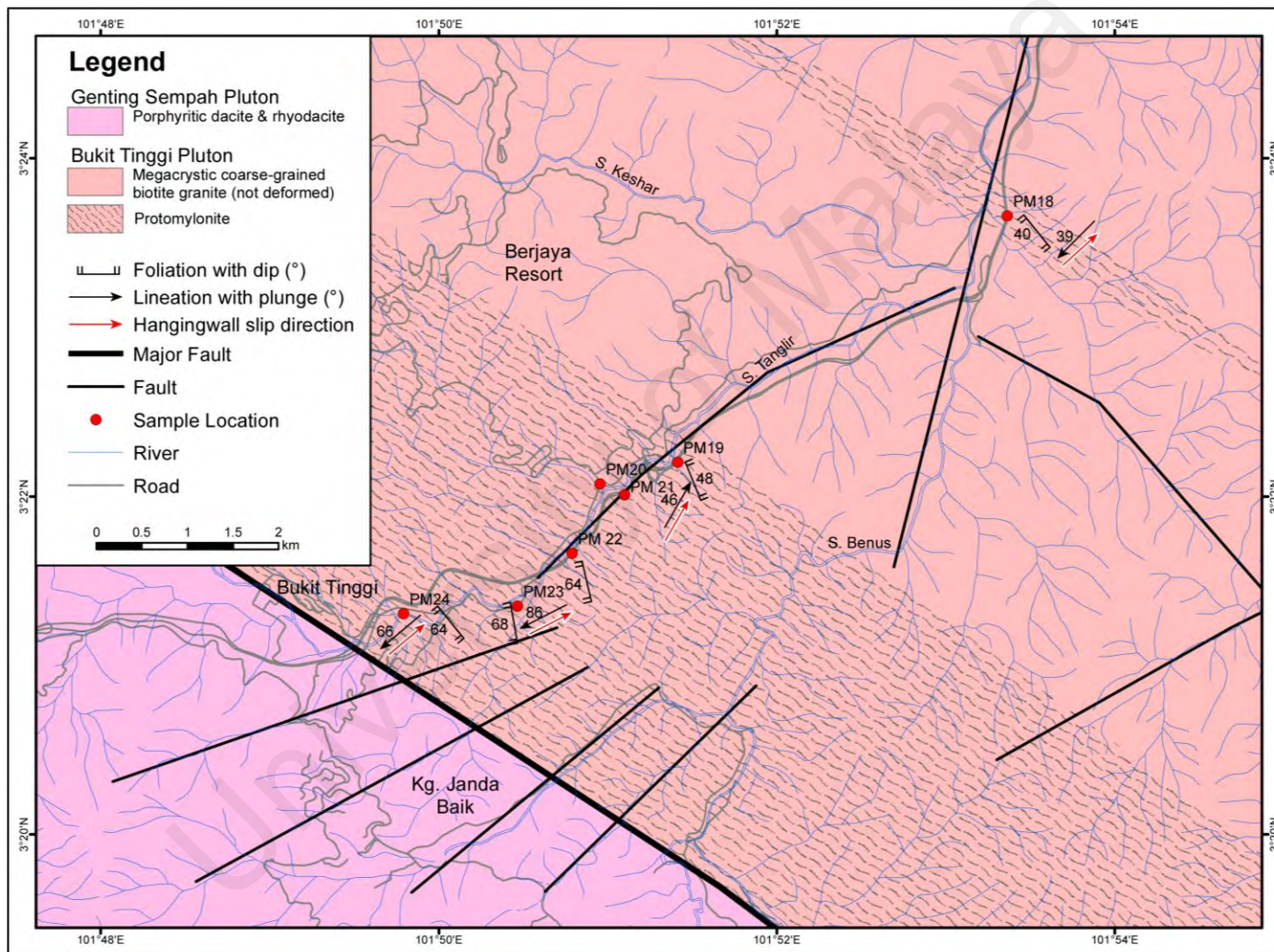


Figure 3.2: Geological map of the study area and the sample locations in Bukit Tinggi, Pahang.

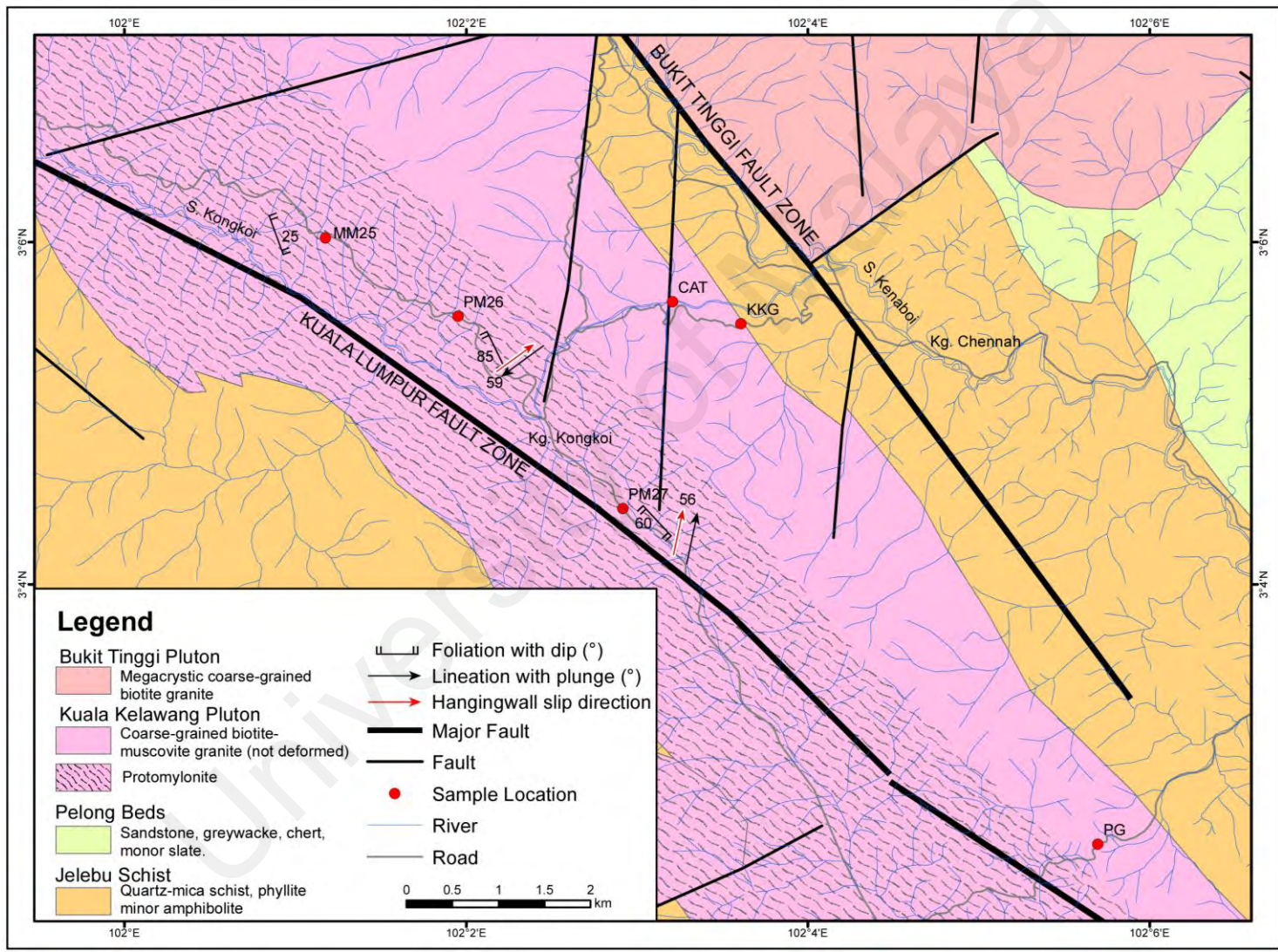


Figure 3.3: Geological map of the study area and the sample locations in Kuala Kelawang, Negeri Sembilan.

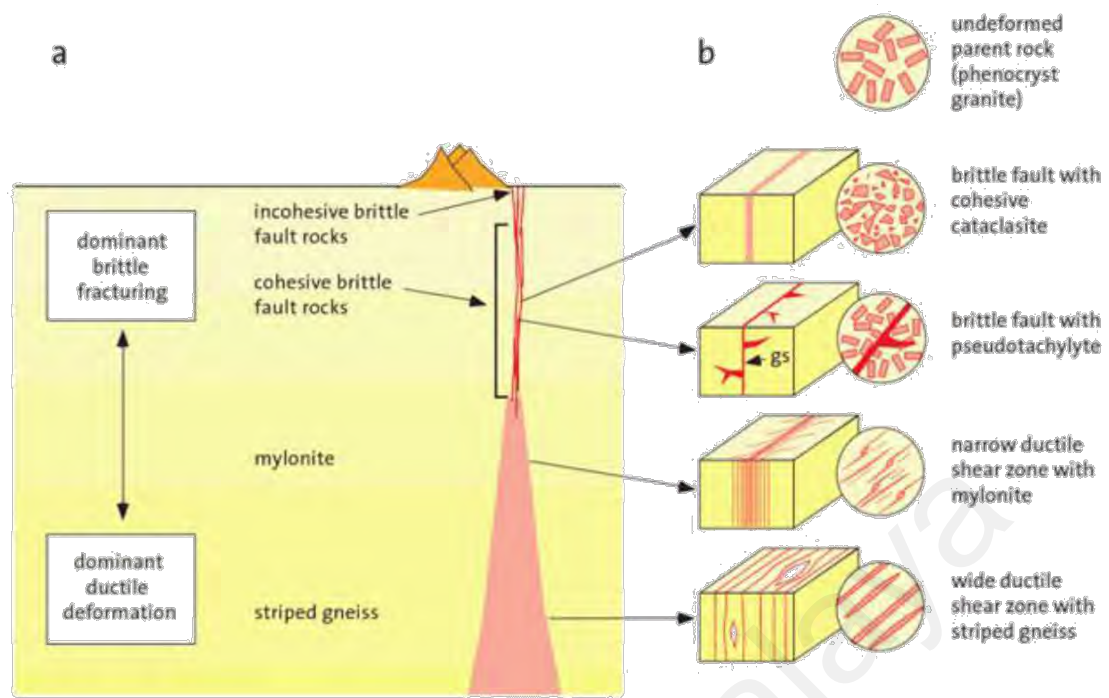


Figure 3.4: A cross-section through a shear zone showing the main types of fault rocks and deformation with depth of the crust (After Passchier and Trouw, 2005). The zone typically broadens and changes in geometry and dominant types of fault rocks with increasing depth.

3.2 Petrography of rocks at the Bukit Tinggi Fault Zone vicinity

The minerals occurred in every type of rocks in the Bukit Tinggi Fault Zone (BTFZ) vicinity will be explained in detail mesoscopically and microscopically below.

3.2.1 Bukit Tinggi Granite

The Bukit Tinggi granite is a medium to coarse-grained biotite granite, with hypidiomorphic granular texture and tabular or oval K-feldspar megacrysts (Plate 3.1). According to Cobbing and Mallick (1987) and Cobbing *et al.* (1992) the granite unit is a primary-textured granite, that is original texture of the rock is still preserved. The granite is characterized by megacrystic texture and presence of biotite clots. The grains are inequigranular, with interlocking grain boundaries, and quartz occurs as clusters of crystals. The K-feldspar megacrysts are set in a grey groundmass of quartz, feldspar and dark biotite. The granite is typically greyish with black specks of biotite and prominent

white plagioclase. Size of the K-feldspar grains varies from 0.5 mm in the groundmass up to 5.0 cm megacrysts.

Microscopically, the granite consists of approximately 35-40% K feldspar, quartz (15-35%), plagioclase (8-20%), biotite (2-10%) and muscovite (<5%). Allanite, sphene, apatite, zircon and magnetite are present as accessory minerals. Secondary minerals such as chlorite and sericite are common in which chlorite formed from biotite and sericite from feldspar as their alteration products.

The edges of the euhedral to subhedral K-feldspar phenocrysts are often slightly rounded and irregular (Plate 3.2). K-feldspar usually displays perthitic texture, which is commonly observed in the megacrysts. Tartan twinning is also common. Inclusions of plagioclase and quartz are observed in the megacrysts.

Plagioclase is euhedral to subhedral and display polysynthetic twinning. Some plagioclase shows zoning and sericitization is common. Quartz usually occurs as anhedral interstitial interlocking grains and interconnected polycrystalline aggregates between K-feldspar and plagioclase.

Biotite is the dominant mafic mineral in the rock. It occurs as single subhedral to euhedral flakes and also occurs as clusters (Plate 3.2). Inclusion of zircon is common which are often surrounded by pleochroic haloes. Other inclusions observed are quartz, apatite, and opaque minerals. Alteration of biotite to muscovite and chlorite is commonly observed. Near to the shear zone boundary, the biotite crystals show partially chloritized. Chloritization tends to formed often along the cleavages and margin of the biotites (Plate 3.3).

Muscovite occurs as interstitial plates and also as minute flakes or aggregates in plagioclase, K-feldspar and biotite (Plate 3.2). The coarse-grained crystals are primary muscovite, while the fine muscovite flakes and aggregates are secondary alteration

product of plagioclase and biotite. Although in some cases it is difficult to positively ascertain whether the muscovite is primary or secondary.

The most common accessory minerals observed in thin sections are apatite and zircon. They are found as minute subhedral to euhedral inclusions, particular in biotite. Zircon is less common compared to apatite, which is found as subrounded crystals probably due to magmatic corrosion. Secondary chlorite also found and is associated with alteration of biotite (Plate 3.3). Magnetite occurs as the main opaque phase.

3.2.2 Mica-Chlorite Schist

In hand specimen, the mica-chlorite schist is fine-grained, dark grey with mottled appearance. It contains few if any recognizable minerals. The handspecimen is strongly foliated with compositional colour banding. The foliation generally trends in the northwest-southeast direction. Banding occurs as alternation of light grey quartz-rich bands and black bands rich in mafic minerals (Plate 3.4).

Under the microscope, the minerals observed in the dark bands are quartz, plagioclase, K-feldspar, chlorite, andalusite, epidote, biotite and opaque minerals. The light grey bands are composed of quartz, K-feldspar, plagioclase and has hypidiomorphic texture indicating that they are probably granitic materials that injected into the host rock.



Plate 3.1: The Bukit Tinggi Pluton is consisted of megacrystic medium to coarse-grained biotite granite, with hypidiomorphic granular texture of tabular or oval K-feldspar megacrysts.

Sample: BG3

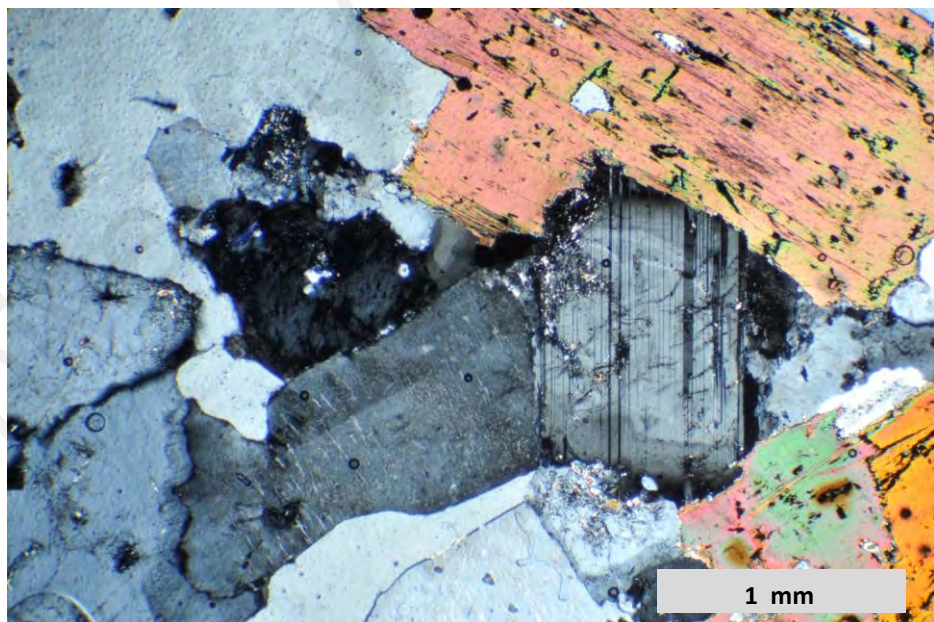


Plate 3.2: Sample of Bukit Tinggi Granite under the microscope. The K-feldspar megacrysts exhibit weakly rounded corners. Quartz occurs as anhedral interstitial grains interlocking and polycrystalline aggregates. Biotite is the dominant mafic mineral in this rock. Inclusions of zircon in biotite are common. Muscovite occurs as interstitial plates and also as minute flakes or aggregates in feldspar and biotite.

Sample: BG1

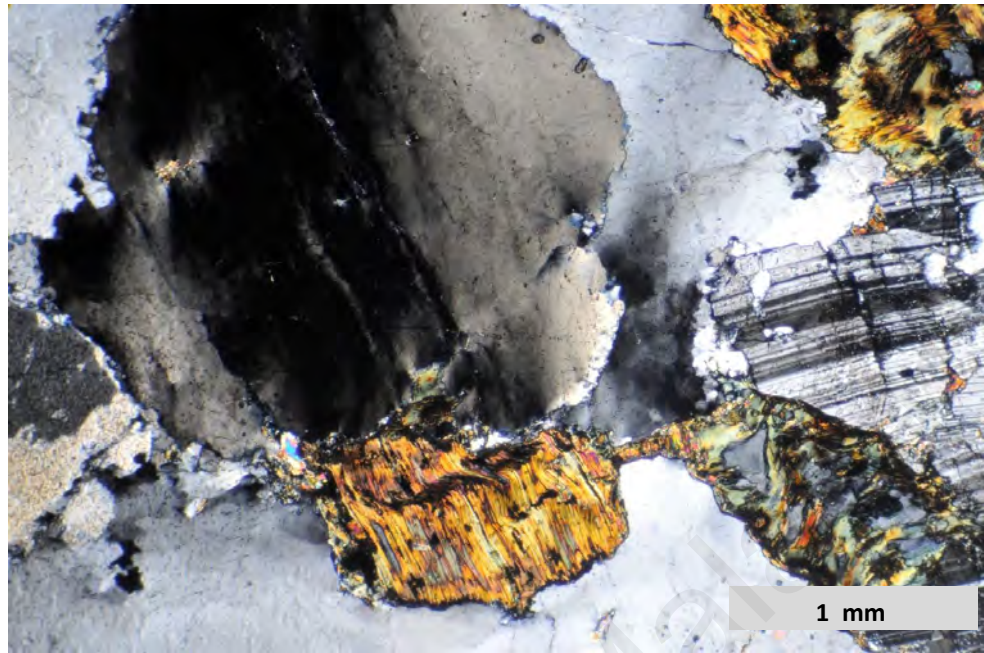


Plate 3.3: Chloritization tends to initiate along the cleavages and margins of the biotites. In some cases, more than quarter of the grains is chloritized.

Sample: PM1



Plate 3.4: Mica-chlorite schist is a roof-pendant in the western flank of Main Range Granite found in Kuala Kubu Bharu, Selangor.

Sample: MCS

3.3 Petrography of Mylonites

Mylonites are regularly associated with shear zones (Figure 3.4), with a clear structure indicative of stronger ductile deformation than adjacent rocks. This structure is further specified by the presence of a strong SL (both foliation and lineation) fabric, the presence of a relatively fine-grained matrix with porphyroclasts (only absent in ultramylonites) and the frequent occurrence, especially in low-grade mylonites, of asymmetric structures like C/S fabrics, mineral fish, stair stepping in porphyroclast, oblique foliation etc.

Deformed granites occur along the Bukit Tinggi Fault Zone comprises largely of protomylonite, minor mesomylonite and rare bands of ultramylonite. The division of the mylonites is based on the fault rocks nomenclature by Brodie (2007) (Figure 3.5) on the percentage of grain size reduction. According to it, the protomylonite has less than 50% of the rock volume has undergone size reduction while a mesomylonite has 50-90% of the rock volume has undergone size reduction and an ultramylonite has more than 90% of the rock volume has undergone size reduction.

Granite mylonites found at the Bukit Tinggi Fault Zone are classified as S-C mylonite as they developed sets of asymmetric S-surfaces (from French "schistosité"), transected by planar distinct C-type shear band or C-surface (from French "cisaillement", meaning shear (Berthé *et al.*, 1979a) (Plate 3.5). The C-surface is internal shear or slipped surface parallel to shear zone boundary and has the same sense of shear as the main shear zone. The S-surface is related to the accumulation of finite strain and it is defined the mylonitic foliation. Stretching lineation observed on the foliation can be distinguished by orientation of muscovite flakes and ribbon quartz. Petrographic study was carried out to examine the development and changes in microstructure and mineralogy during mylonitisation.

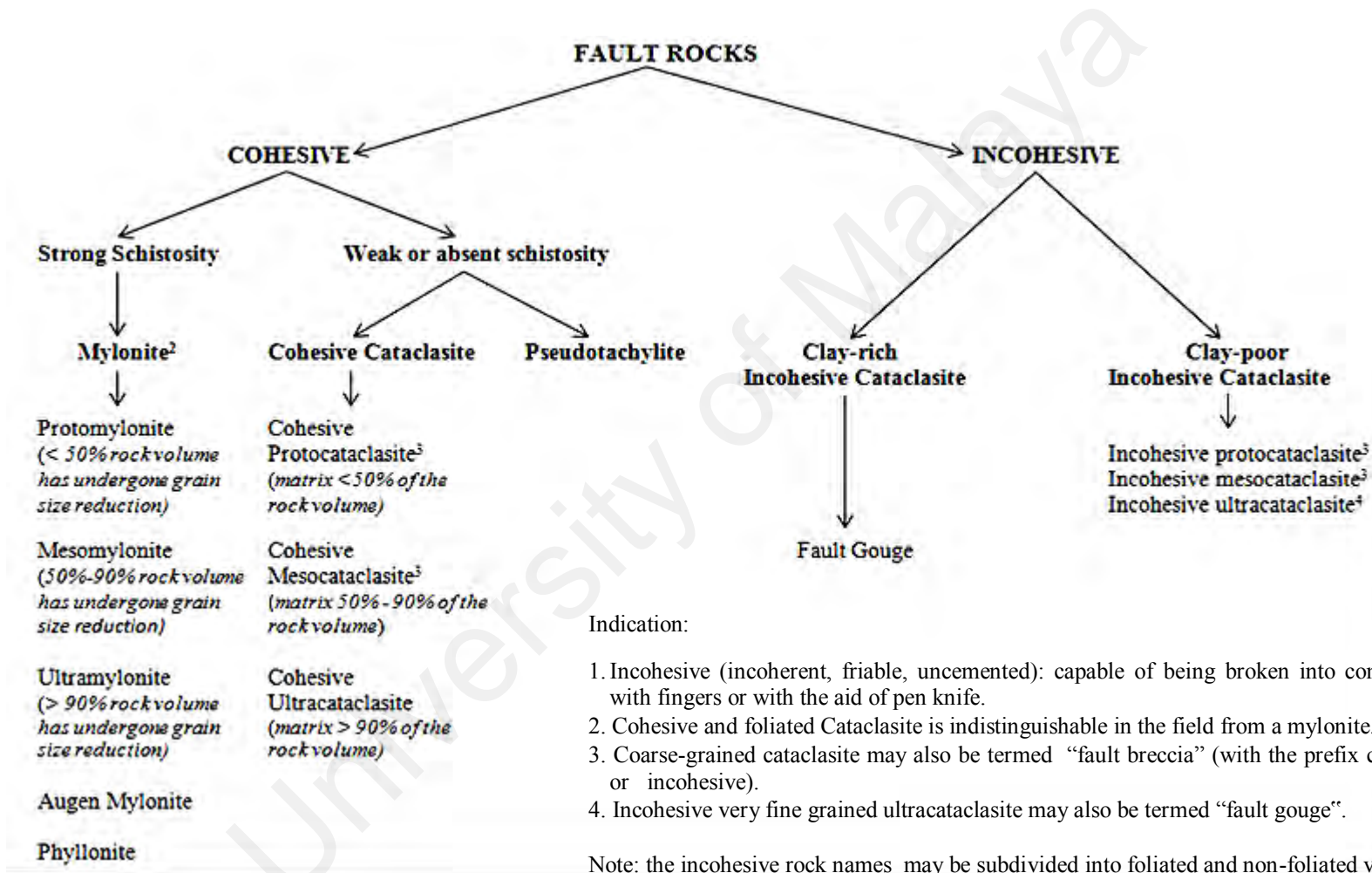


Figure 3.5: Fault rocks nomenclature. Modified after Brodie *et al.*, (2007).

3.3.1 Protomylonite

Protomylonite in the BTFZ is a medium to coarse-grained porphyroclastic mylonite. It is the least strained mylonitic rock in the area and the most abundant mylonite type. The granite protomylonite shows two sets of foliation (C/S surfaces). The S-surfaces are well developed, while the C-surfaces and stretching lineations are often less well defined. The S-surfaces make an angle between 30° to 60° to the C-surfaces.

In hand specimen, the foliation is identified by preferred orientation of tabular to ellipsoidal feldspar porphyroclasts especially K-feldspar, elongated quartz grains and some mica strings. The K-feldspar porphyroclasts are set in quartz and mica-rich matrix. Size of the porphyroclasts is variable, ranging from 1 cm up to 4 cm (Plate 3.6).

Under the microscope, the protomylonite is composed of feldspar porphyroclasts, elongated quartz grains with strong undulose extinction, elongated aggregates of recrystallized quartz (quartz neocrysts) and mica strings (Plate 3.7). The matrix is made of fine quartz neocrysts, feldspar clasts and mica. Epidote and allanite is observed in some thin sections. Apatite, zircon and opaque minerals are common accessory minerals. The feldspar porphyroclasts are often fractured, show undulose extinction and minor recrystallization to very fine neocrysts concentrated at the grain edges and the strain shadows. Flame perthite occurs along the margins of K-feldspar clasts towards the center of the grains. Fractures in K-feldspar porphyroclasts often occur along cleavages and displacement along the fractures forms offset fractured grains with “book shelf” texture. Fractures in plagioclase are less intense compared to K-feldspar. Bending of plagioclase clasts indicated by curved twins is also observed. Quartz shows contrasting microstructures compared to the feldspars. Quartz is deformed to elongated clasts with strong undulose extinction and development of subgrains at the margins. They are enclosed by quartz neocrysts, and some quartz are completely

recrystallized to elongated granular aggregates. Recrystallization of quartz also occurs along boundary of deformation bands. Some quartz clasts have serrated to lobate contacts with some fine quartz neocrysts along the contact.

Biotite forms small porphyroclasts (mica fish) and most are recrystallized to form fine biotite s with preferred orientation and concentrated along thin bands or biotite string. Chloritization of biotite is common. Fine epidote aggregates forming thin discontinuous bands along the foliation is observed in a few thin sections.

3.3.2 Mesomylonite

The mesomylonite zone at Kuala Kubu Bharu is tens of meter wide and along the Karak highway it is only a few meter wide. The granite mesomylonite has distinct preferred orientation of small elongated porphyroclasts, particularly the K-feldspar porphyroclasts, enclosed by dark grey fine foliated matrix (Plate 3.8). The C-surfaces are often more conspicuous than the S-surfaces. The foliations are shown by thin colour banding formed by segregation of strongly deformed quartz aggregates (light-colour bands) and mica (dark-colour bands). The angle between the S and C surfaces are smaller (10° - 30°) than that of the protomylonite.

Microscopically, besides preferred orientation of the porphyroclasts, the S-surfaces are also demarcated by preferred orientation of elongated recrystallized quartz grains and aggregates and fine elongated feldspar clasts (Plate 3.9). The C-surfaces generally form dark-coloured continuous shear bands that are rich in biotite, have finer grain size and more intensely recrystallized, that cut the S-surfaces. The C-surfaces occasionally form discrete shear bands and cause the S-surfaces to curved towards, and become parallel to the shear bands. The dark colour of these bands is caused by the abundant aligned biotite plates and lenses and finer grain size. Fine-scale banding (both compositional and grain size banding) along the C-surfaces, which is uncommon in the

protomylonites, is clearly discernible in mesomylonite. Mineralogically, the mesomylonite is similar to the protomylonite. The main difference is the increase in grain size reduction, mineral segregation, recrystallisation and to a lesser extent chloritization of biotite in the mesomylonite.

3.3.3 Ultramylonite

Ultramylonite occurs as rare thin bands in the BTFZ. It is dark grey to black in colour with scarce porphyroclasts appear as fine white and grey specks a few mm in diameter (Plate 3.10). The foliation is defined by alternating dark and light coloured bands and in the mesoscopic scale only 1 set of foliation is observed. In the hand specimen, individual grain of the granite ultramylonite is indiscernible.

Under the microscope, foliation is defined by distinct compositional banding, preferred orientation of elongated porphyroclasts and recrystallized quartz (Plate 3.11). The compositional banding (C-surfaces) is demarcated by alternating thin (about 0.05 to 0.1 mm) dark mica-rich bands and thicker (about 0.1 to 0.5 mm) quartzo-feldspatic bands. The quartz in the quartzo-feldspatic bands are completely recrystallized and are slightly elongated, with aligned long axis (oblique foliation – S-surfaces) that makes a small angle to the compositional bands. The angle between S and C surface is oftensmall (10° - 30°), and in some ultramylonite, the S and C surface almost coincide. K-feldspar occurs in the quartzo-feldspatic bands as fine fragmented clasts, lesser very fine elongated recrystallized grains and a few rounded porphyroclasts can be seen. The mineralogy of the ultramylonite is also similar to the previous mylonites, but there is lesser plagioclase clasts due to transformation of plagioclase to very fine white mica (sericite).

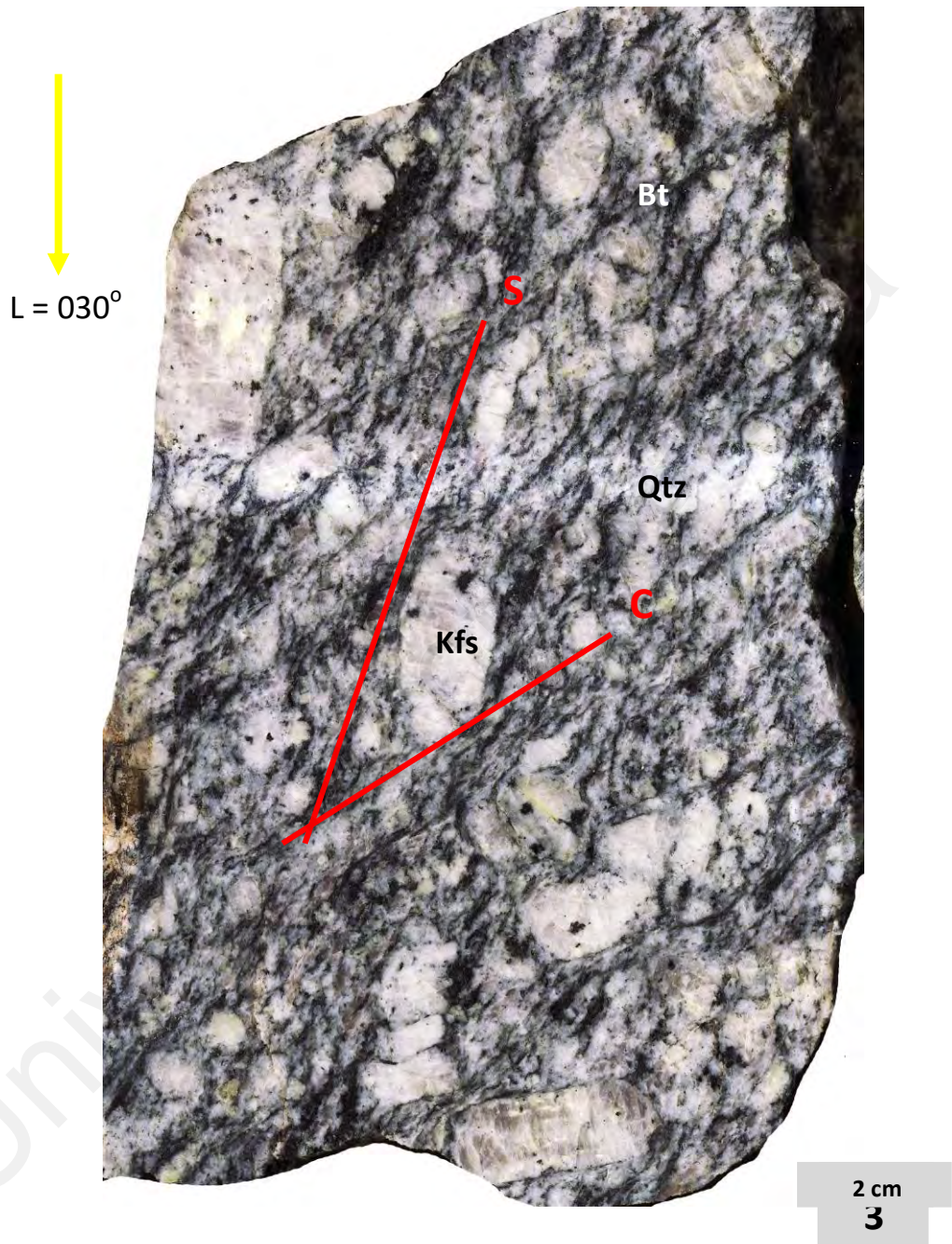


Plate 3.5: An oriented sample of mylonite shows S-C surfaces. The surface shown is cut parallel to the lineation and perpendicular to the foliations (S-C surfaces). It shows dextral-normal slip with the vergence points to the NE.

Sample: PM21



Plate 3.6: A sample of protomylonite from BTFZ. The preferred orientation of tabular to ellipsoidal feldspar porphyroclasts is parallel to S-surfaces. The elongated quartz aggregates and mica strings are mainly aligned parallel to S-surfaces but some are aligned along the C-surfaces.

Sample: PM18

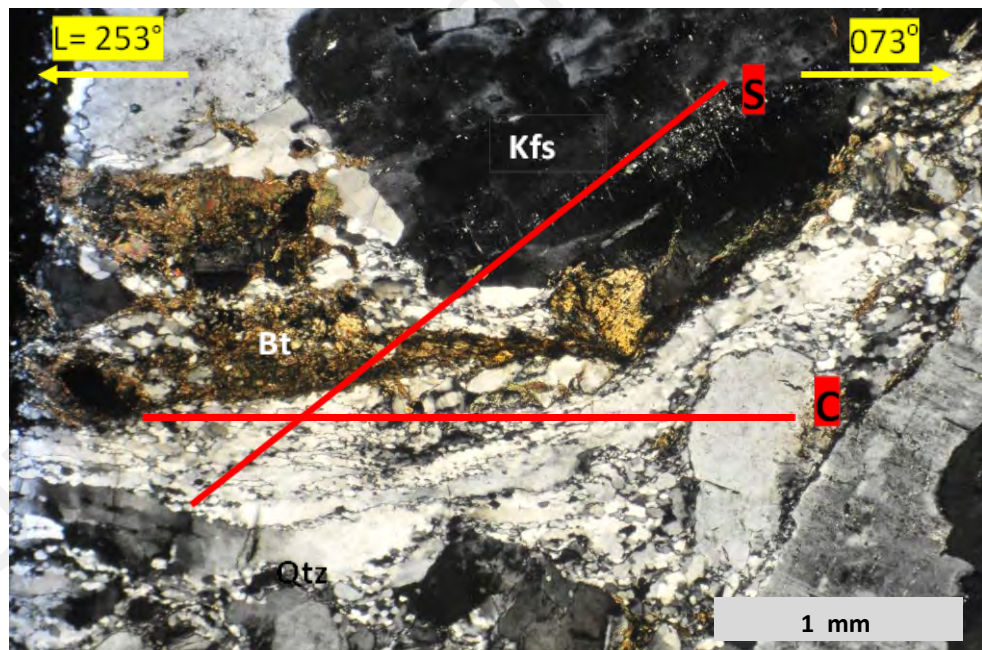


Plate 3.7: Photomicrograph of protomylonite from BTFZ. C-planes are made of trails of mica band and aggregate shape of preferred orientation (aspo) of quartz, while S-planes are formed of feldspar porphyroclasts and ribbon quartz.

Sample: PM 22



Plate 3.8: A sample of mesomylonite from BTFZ. The grain size is finer than the protomylonite and it has higher matrix content (50-90%). The C-surfaces are more distinct than the faint S-surfaces.

Sample: MM 8

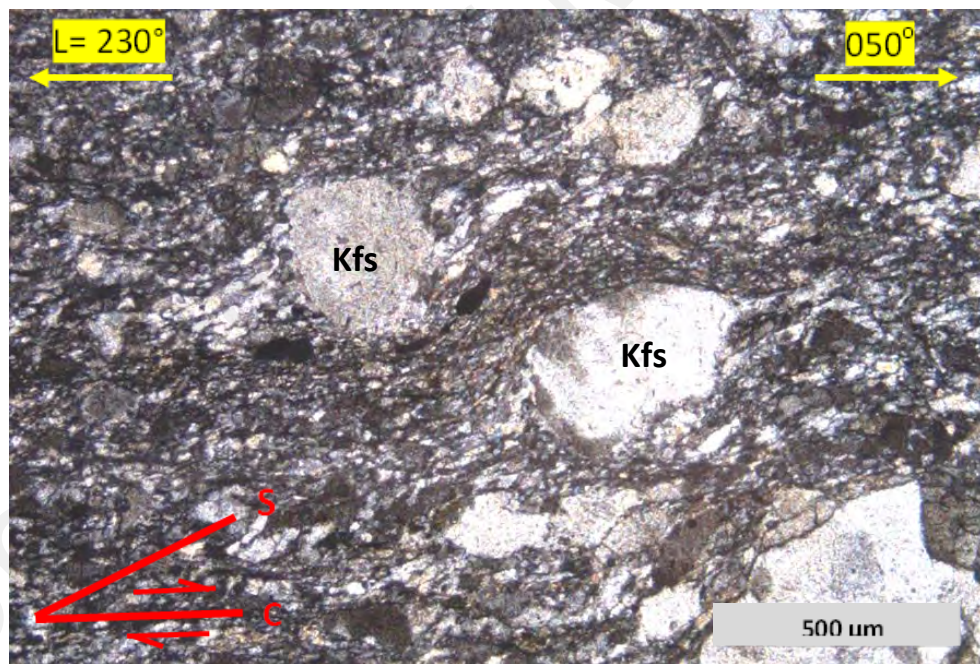


Plate 3.9: The recrystallized quartz grains (neocrysts) in mesomylonite form aggregate shape preferred orientation (aspo) to build the C-surfaces while the S-surfaces are made of grain shape preferred orientation (gspo) of feldspar porphyroclasts and quartz neocrysts. The inclined aspo combined with the gspo in the mica rich band (C-plane) point to a dextral sense of shear.

Sample: MM8

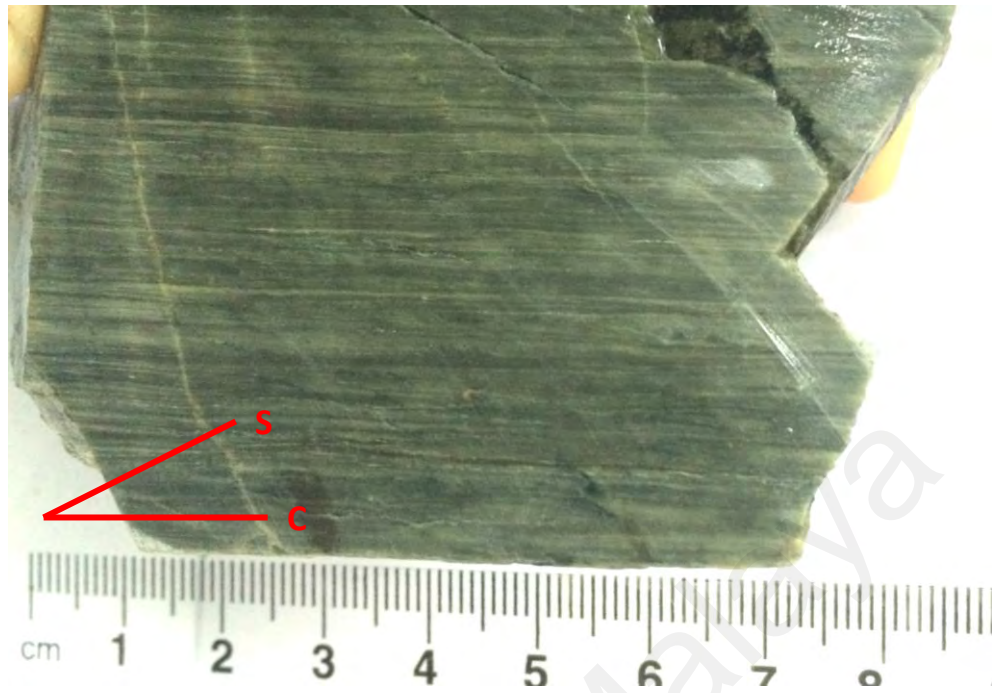


Plate 3.10: An ultramylonite sample from the BTFZ. It is very fine grains with matrix more than 90%. Only the C-surfaces can be seen in the hand specimen.

Sample: UM7

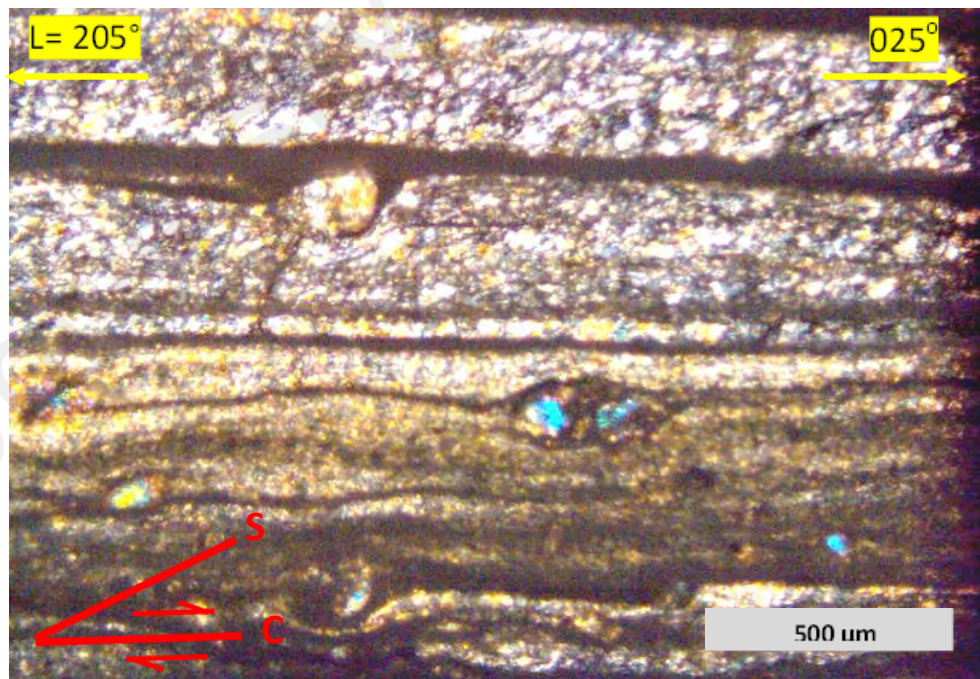


Plate 3.11: An ultramylonite under thin section sample. The C-surfaces are clearly indicated by compositional banding and the S-surfaces is less well developed and indicated by grain shape preferred orientation (gspe) in the quartz-rich bands.

Sample : UM 7

3.4 Magmatism age

The age of the granite on Peninsular Malaysia was dated using isotopic methods (Bignell and Snelling, 1977; Liew, 1983; Krahenbuhl, 1991; Cobbing *et al.*, 1992; Searle *et al.*, 2012; Ng *et al.*, 2015). Several studies have made to date the age of fault (Harun, 2002), but there has yet been a broad study on the dating of faulting events. For this study, radiometric dating using $^{40}\text{Ar}/^{39}\text{Ar}$ method of recrystallized biotite extracted from the mylonite was carried out. The result was compared with the previous record on the age of the tectonic events (Figure 2.2).

Early studies on the radiometric dating of granitic rocks in Peninsular Malaysia typically done on traditional isotopic method such as Rb-Sr and K-Ar dating (Snelling *et al.*, 1968; Bignell and Snelling, 1977; Krahenbuhl, 1991). Alongside these dating methods, several recent studies have utilized U-Pb zircon age dating to the granitic bodies in Peninsular Malaysia (Liew and Page, 1985; Searle *et al.*, 2012; Ng *et al.*, 2015), where Late Triassic igneous age was reported for the Main Range Granite.

The U-Pb age of the Bukit Tinggi Granite is ranging from 208 Ma to 198 Ma (Liew and Page, 1985). The Kuala Lumpur Granite has been dated by several workers (Liew and Page, 1985; Searle *et al.*, 2012; Ng *et al.*, 2015) with U-Pb age between 226 Ma and 210 Ma (Figure 2.2).

Ages from the Rb-Sr and U-Pb dating of the Main Range Granite of Peninsular Malaysia generally show older ages than those achieved through K-Ar dating of the same rock unit. Ages obtained from K-Ar dating range from Late Jurassic-Eocene; these younger ages were attributed to argon loss in the granite as a result young fault related disturbance, with area cut by WNW-ESE faults showing clear argon loss in granite (Bignell and Snelling, 1977). These younger K-Ar ages therefore does not necessarily represent the igneous age of the granitic rocks.

3.5 $^{40}\text{Ar}/^{39}\text{Ar}$ thermochronology

There are limited radiometric studies of fault rocks in Peninsular Malaysia with the work by Harun (2002) providing radiometric ages as the main reference in reconstructing the tectonic evolution of the main faults of the Peninsular Malaysia. Combined with a lack of studies on fault rocks, the age of ductile shearing of major faults of Peninsular Malaysia is still poorly constrained. From the radiometric dating of granite mylonite in this study, it is possible to place a limitation on the timing of the faulting event that generates the mylonites.

For this study, two mylonite samples were sent for $^{40}\text{Ar}/^{39}\text{Ar}$ thermochronology dating. The recrystallized biotites that were resulted from fault deformation, separated from the samples for analysis purpose.

Location of the samples collected for $^{40}\text{Ar}/^{39}\text{Ar}$ analyses are shown in figure 2.2. After examination in thin section to determine the character of secondary biotite, the most suitable samples were selected for $^{40}\text{Ar}/^{39}\text{Ar}$ dating. The two samples were taken from the main outcrop at Kuala Kubu Bharu and Karak highway (KM 45.6) respectively. Both of the samples represent a typically deformed and mylonitised biotite granite of Bukit Tinggi Granite. They contain of feldspar porphyroclasts, quartz, biotite, muscovite, chlorite and sericite. Apatite, zircon, sphene and epidote are found as accessory phases. The samples are located in the fault zone and display a well-developed stretching lineation and mylonitic foliation. As stated in Chapter 1, the analyses were performed at the ActLab, Canada and standard mineral separation techniques were used.

Table 3.1 contains $^{40}\text{Ar}/^{39}\text{Ar}$ analytical data for secondary biotite in the study area. The result is presented in the age spectrum diagrams (Figure 3.6). Secondary

biotite was selected from both samples as they recrystallized syntectonically to preserve the age of the latest deformation in mylonites.

Both samples yielded ages from both plateau and isochron methods. The secondary biotite for Kuala Kubu Bharu sample displays a plateau age of 92.4 ± 0.8 Ma for 48.8 % of the gas released, and the inverse isochron age is 87.0 ± 1.0 Ma (Figure 3.7a). The plateau age of secondary biotite from Karak Highway is 84.3 ± 0.8 Ma for 78.5 % of the gas released and inverse isochron age is 78.3 ± 3.3 Ma (Figure 3.7b).

A study on the brittle-ductile deformation age of the nearest fault zone, Kuala Lumpur Fault Zone (sample location: KM 54 Kajang-Kuala Kelawang road) has been done by Harun (2002) using the K/Ar method. It has resulted in the mylonite deformed at the age of 83.6 Ma (Late Cretaceous).

Table 3.1: $^{40}\text{Ar}/^{39}\text{Ar}$ analytical data for the mylonite from BTFZ.

Sample	IIA (Ma) $\pm 1\sigma$	TFA $\pm 1\sigma$	WMPA (Ma)$\pm 1\sigma$	Ca/K	Comments
PM11	87.0 \pm 1.0	88.5 \pm 0.6	92.4\pm0.8	0.06-5.28	Three steps plateau
PM23	78.3 \pm 3.3	83.1 \pm 0.7	84.3\pm0.8	0.06-5.93	Four steps plateau

Explanation:

$\pm 1\sigma$ = Estimated uncertainty (1 sigma);

TFA = Total fusion age;

Ca/K = Apparent Ca / K ratios;

IIA = Inverse Isochrone age

WMPA = Weighted mean plateau age;

WMIPA = Weighted mean Intermediate Plateau age

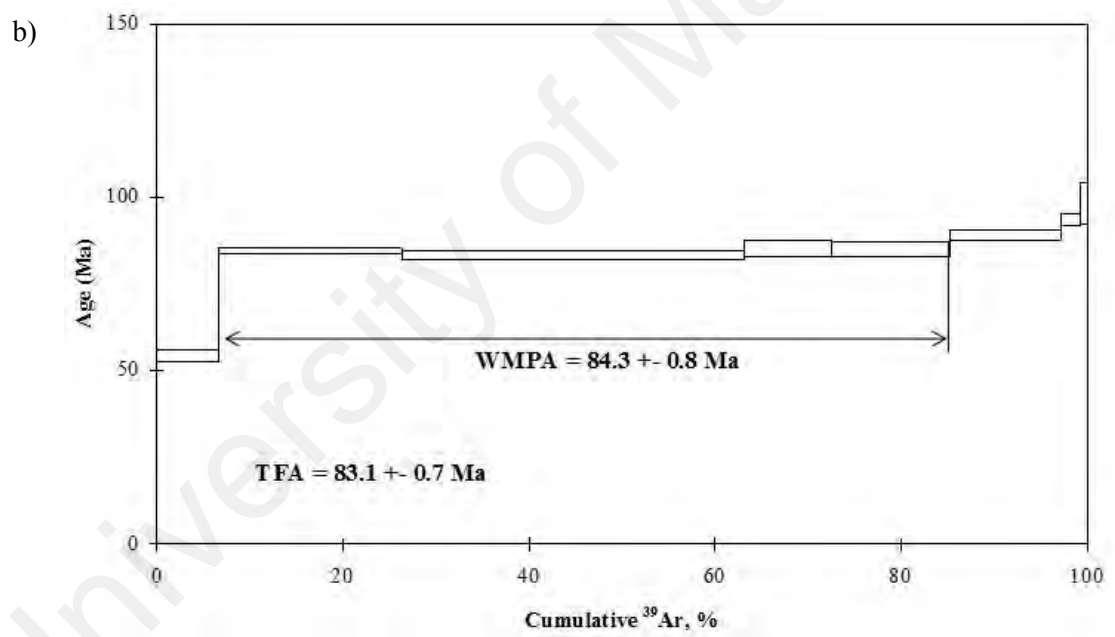
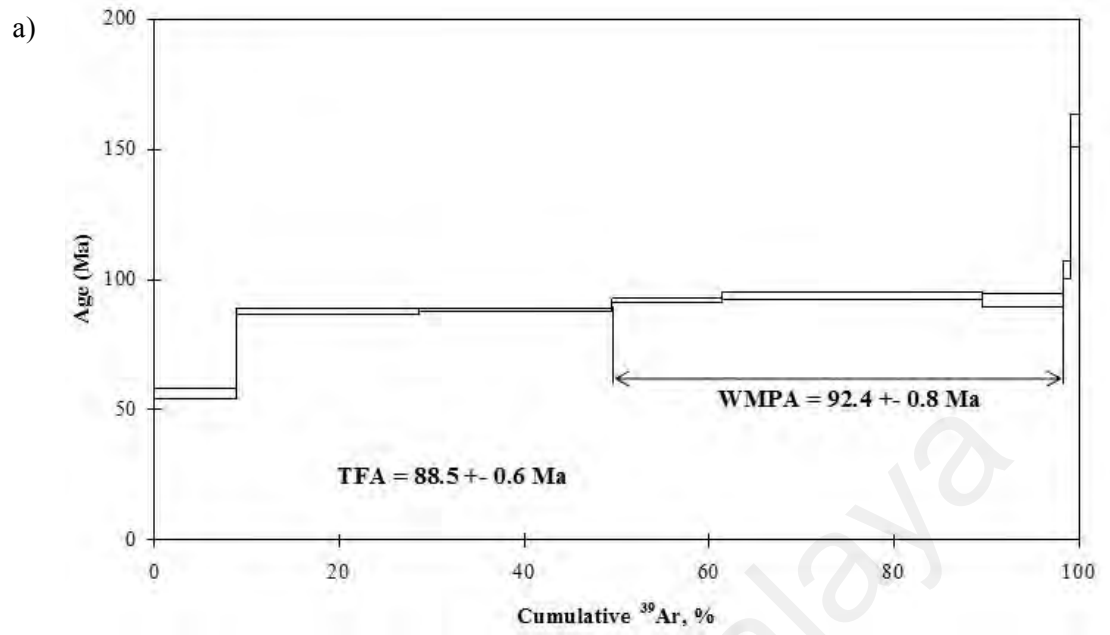


Figure 3.6: $^{40}\text{Ar}/^{39}\text{Ar}$ age temperature spectra diagram for a) PM11, age value of $92.4 \pm 0.8\text{Ma}$.
b) PM23, age value of $84.3 \pm 0.8\text{Ma}$.

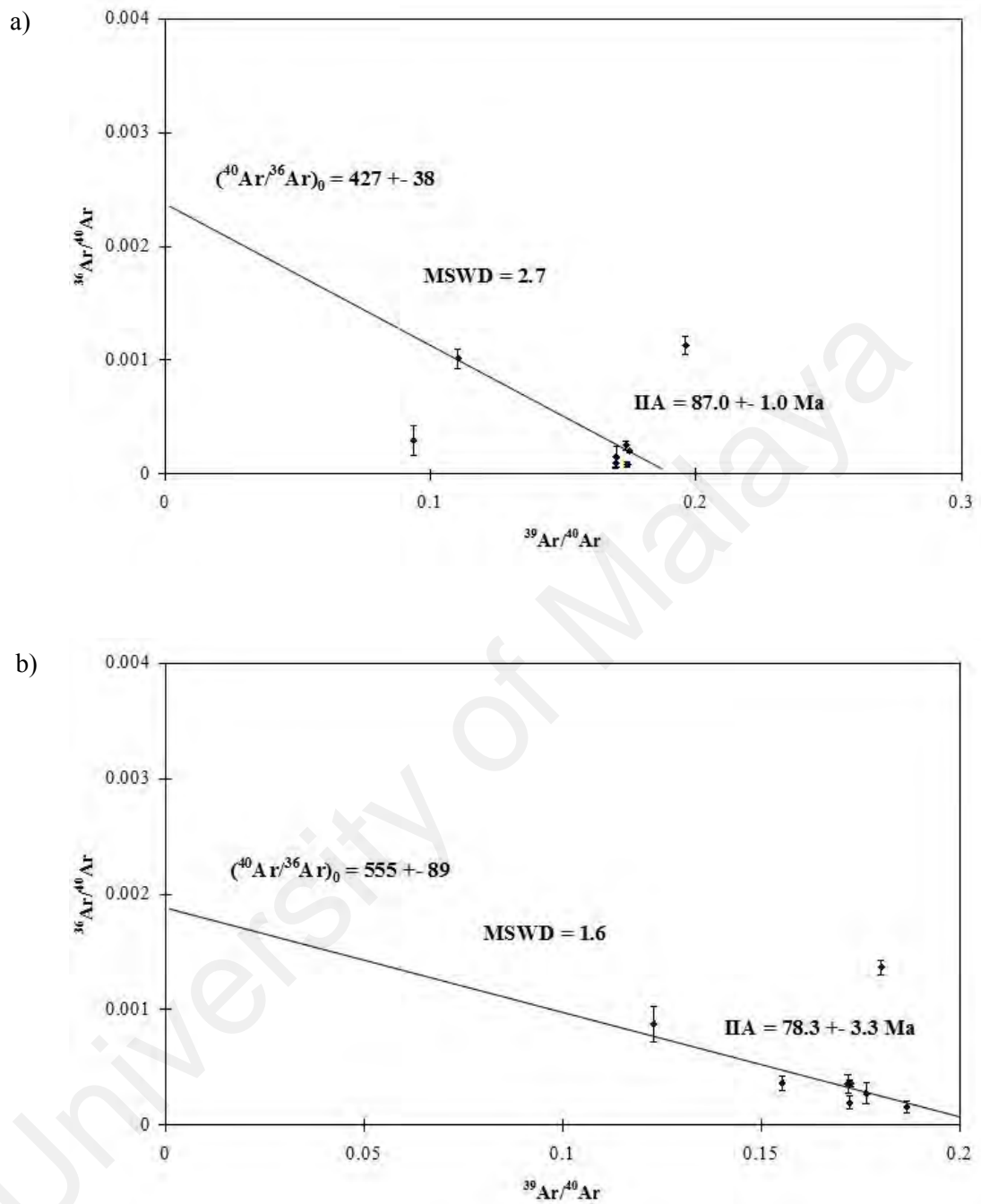


Figure 3.7: Inverse isochron age diagram for the mylonite from BTFZ. Inverse isochron age a) PM 11 = $87.0 \pm 1.0 \text{ Ma}$, MSWD = 2 b) PM 23 = $78.3 \pm 3.3 \text{ Ma}$, MSWD = 1.6.

3.6 Discussion

Mechanism of deformation, deformation temperature, grain size reduction, strain softening and influence of fluid occurred in the mylonites will be discussed below.

3.6.1 Mechanism of deformation

The foliation within the mylonites shows by flow, where every individual band accommodated by specific deformation mechanism. Based on the microstructural observations, the deformation mechanisms were interpreted for the principal minerals below:

a) Quartz

When subjected to strain, atoms in the quartz grains started to slide caused the grains lengthen parallel to the direction of strain. This process is controlled by lattice defects movement, in a process driven by intracrystalline deformation and crystal plasticity (Passchier and Trouw, 2005) mechanisms. This resulted in the formation of undulatory extinction, deformation band and ribbon-shaped quartz well developed in the protomylonite and to the least extent in the mesomylonite (Plate 3.12a). In the ultramylonite, the quartz is completely recrystallized.

The intense deformation initiated recovery process (Figure 3.7) which begins with the formation of subgrains (polygonization) and ending with complete recrystallization by the forming of neocrysts that are free from strain and separated from other grains. The process is triggered by dislocation slip mechanism to reflect the ductile deformation of quartz (Passchier and Trouw, 2005) in mylonites. The subgrains often occur near the margin of the quartz grains. There is often a progression from strained quartz forming the core of the quartz grains, followed by subgrains surrounding the relict quartz, and quartz neocrysts at the outer-most margin. This indicates that the neocryst are formed as a result of rotation in the subgrains. The neocrysts formed by

subgrain rotation recrystallization (SGR) have straight boundaries and dominated by high angle boundaries (approximately 120°) (Plate 3.12b). The polygonal subgrains and neocrysts are almost the same size and often slightly elongated and they show shape preferred orientation. . Polygonal subgrains and neocrysts having same shape, size and aspect ratio are also reported by Kruhl (1986); Nishikawa and Takeshita (2000); Schmid *et al.* (1980) and Vernon *et al.* (1983).

There is also minor occurrence of quartz grains with serrated boundaries and occasional small rounded to polygonal neocrysts along the boundaries in the protomylonite. This indicates that there is minor recrystallization through bulging recrystallization (BLG).

b) Feldspar

Cataclasis is the main mechanism of reduction in size of feldspar. It causes the comminution of feldspar grains by fracturing and microcracking (Plate 3.13a). There are many microcracks in the feldspars, which produces angular grain fragments, microfaults, and antithetic bookshelf fractures, often along cleavages. The dominance of these deformed microstructures to recrystallization reflects the largely brittle behaviour of K-feldspar. Fracturing of feldspar in mylonite is also reported by Hadizadeh and Tullis (1992) and Tullis and Yund (1992) and other low temperature ductile shear zone (Stünitz *et al.*, 2003; Hippertt and Hongn, 1998).

Despite the dominance of fracturing, feldspars in the mylonites of BTFZ also show ductile deformation shows by the existence of undulose extinction (Plate 3.13b) and minor recrystallization. Bending or folding of the feldspars is observed, particularly in the plagioclase (Plate 3.13b). It causes the cleavage and twin lamellae to become curved. Intragranular microcracks may appear at the hinge line. Bending or folding

often appears in grains that are not aligned to the foliation, and it occurs near to the grains edges that curve towards the foliation.

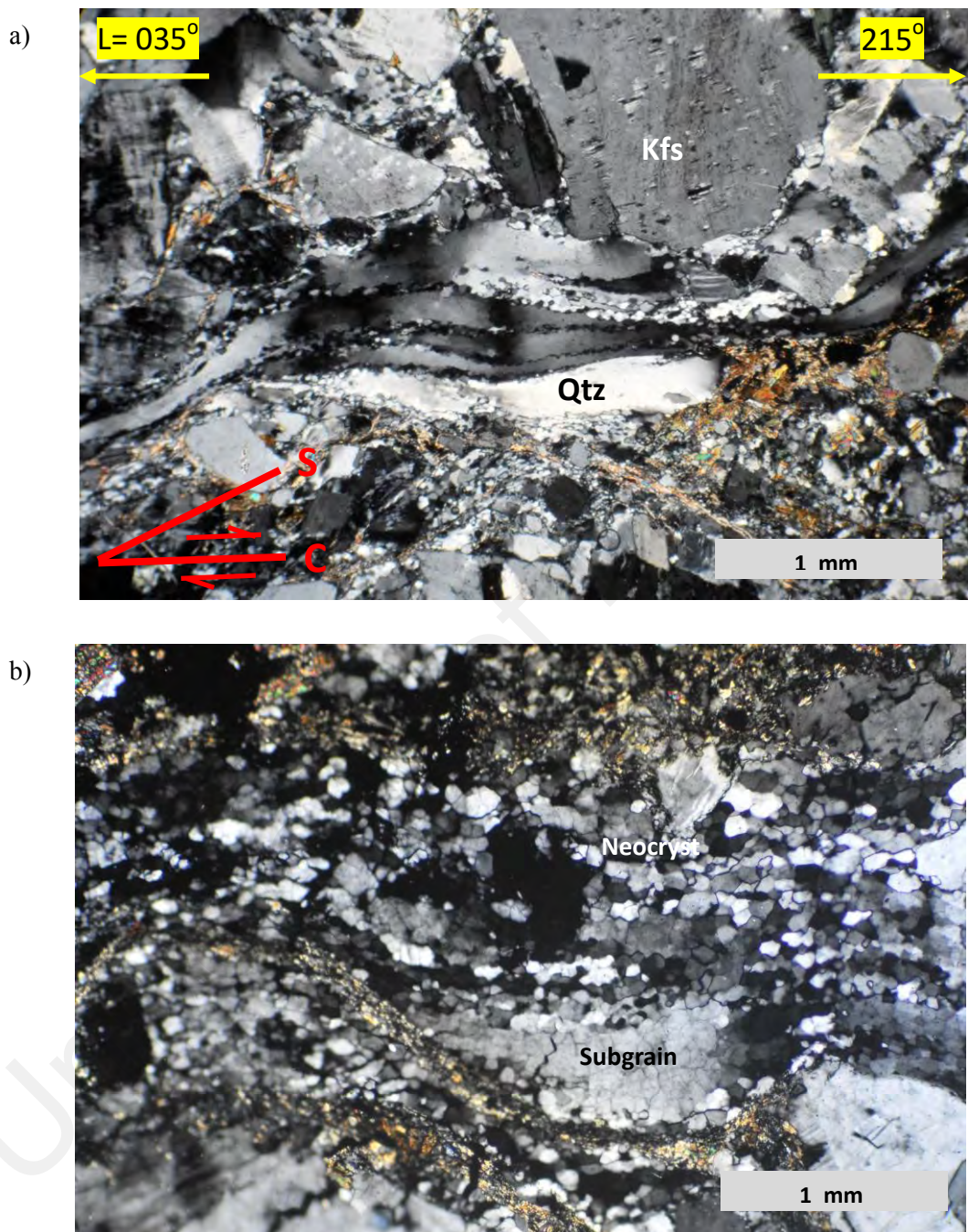


Plate 3.12: a) Quartz grains are strongly deformed in protomylonite by crystal-plastic mechanism forming ribbon-shaped quartz, some with aspect ratio more than 4:1. Visible recrystallization is started at the the ribbon-shaped quartz edges by bulging recrystallization (BLG). b) In mesomylonite, almost all of the ribbon-shaped quartz experiencing dynamic recrystallization to form neocrysts.

Sample a: PM21

Sample b: PM23

The limited occurrence of recrystallization in feldspars is characterized by lobate boundary and associated fine elongated feldspar neocrysts. This indicates that bulging recrystallization (BLG) likely acted as the mechanism that leads to the formation of the neocrysts (Plate 3.14a). The neocrysts are more prevalent in the mylonite at higher deformations intensity (i.e. mesomylonite and ultramylonite). However, neocrysts are mainly constrained to the K-feldspar. Recrystallization of plagioclase is rarely observed.

K-feldspar also form flame perthite, usually occur near the boundary of K-feldspar with the perthite flame oriented towards the center of the clast. They are often developed at high stress areas such as clast contacts and along microfaults. The albite flame is formed by the replacement of K-feldspar by albite during deformation by retrograde breakdown of plagioclase and hydration of K-feldspar (Pryer and Robin, 1996). The flames have been reported by Pryer and Robin (1996) to be preferentially oriented subparallel to the maximum compression direction but preferred orientation of flame perthite is not observed in the mylonites of BTFZ. The absence of preferred orientation may be due to rotation of feldspar clasts during shearing.

c) Mica

In biotite, muscovite and chlorite, the evidence of strain is ubiquitous. The existent of undulatory extinction, bending, and kinking is common, and recrystallization is observed in biotite (Plate 3.15). These deformation features are caused by dislocation glide mechanism (Mares and Kronenberg, 1993) and reflect the ductile behaviour of mica. The new recrystallised grains are driven by grain boundary migration recrystallization (GBM) mechanism (Bell, 1998). Biotite and muscovite are mechanically rotated and some of the large grains of biotite occur as mica fish.

Summary of the deformed microstructures evolution in mylonites of BTFZ is presented in the Table 3.2.

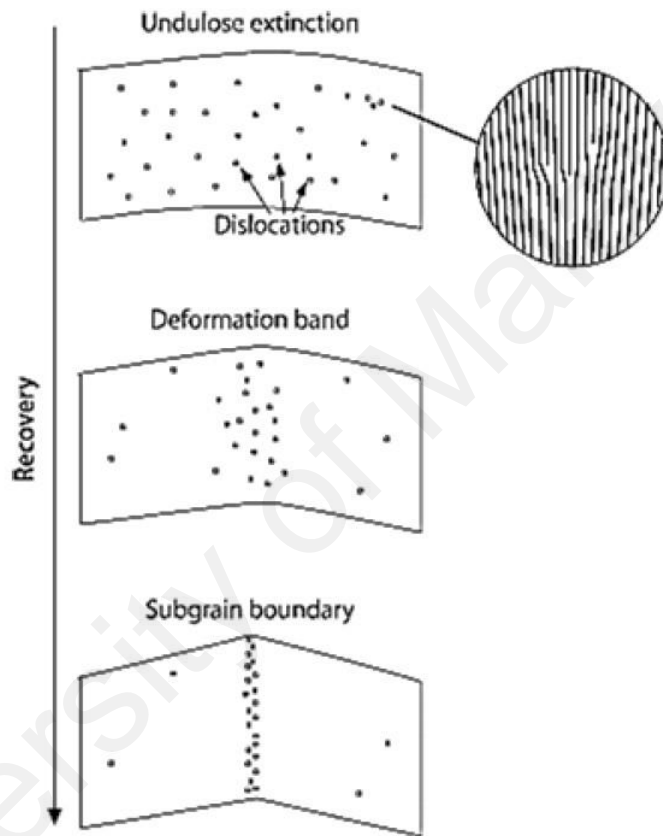
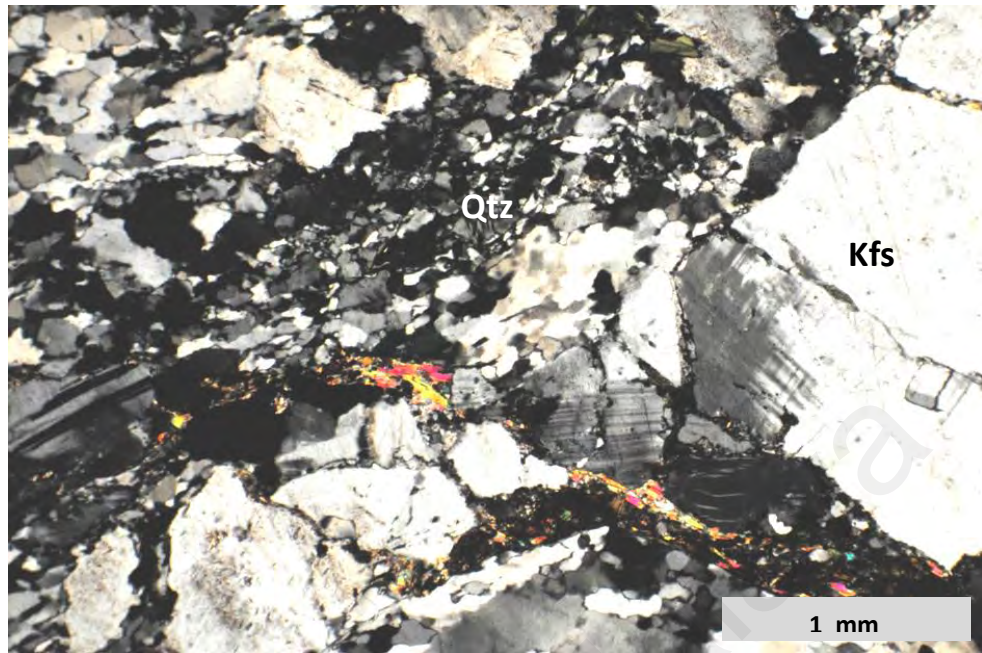


Figure 3.8: Schematic illustration of the recovery process. a) Dislocations dispersed over the crystal result in undulose extinction. b) Recovery process causes concentration of dislocations in deformation bands and eventually c) in a subgrain boundary (tilt wall). After Passchier and Trouw (2005).

a)



b)

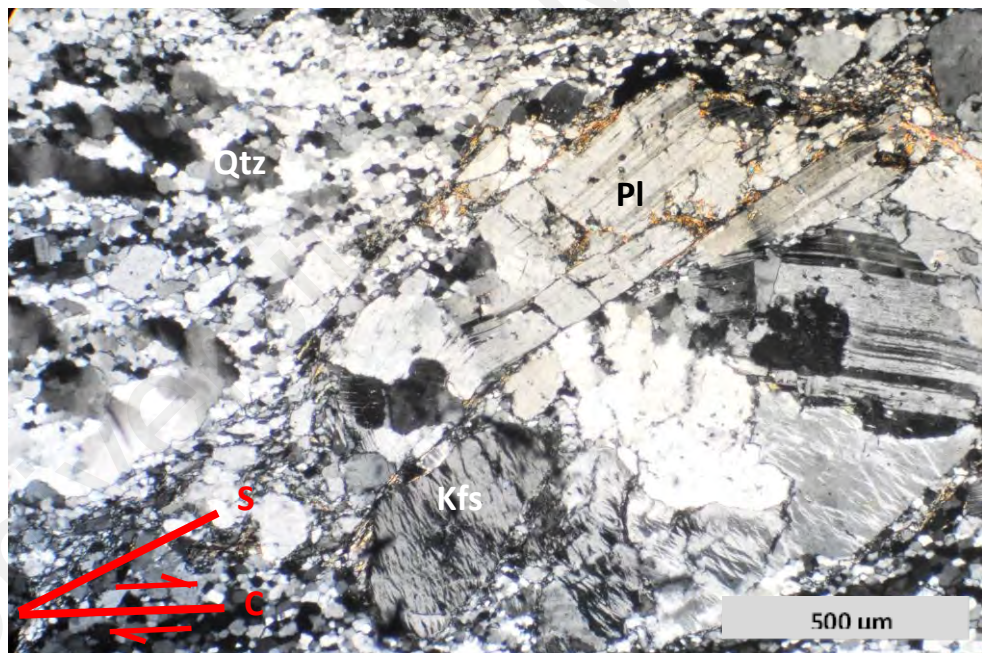


Plate 3.13: a) In protomylonite, the feldspars form angular clasts through fracturing and microcracking. Minor sericitization occurs in the feldspar clasts. b) With increasing shear, plagioclase frequently fold, kink and experiencing undulose extinction due to internal deformation. Bending or folding in plagioclase caused the twinning lamellae to curve. Flame perthite is common.

Sample a: PM5

Sample b: PM21

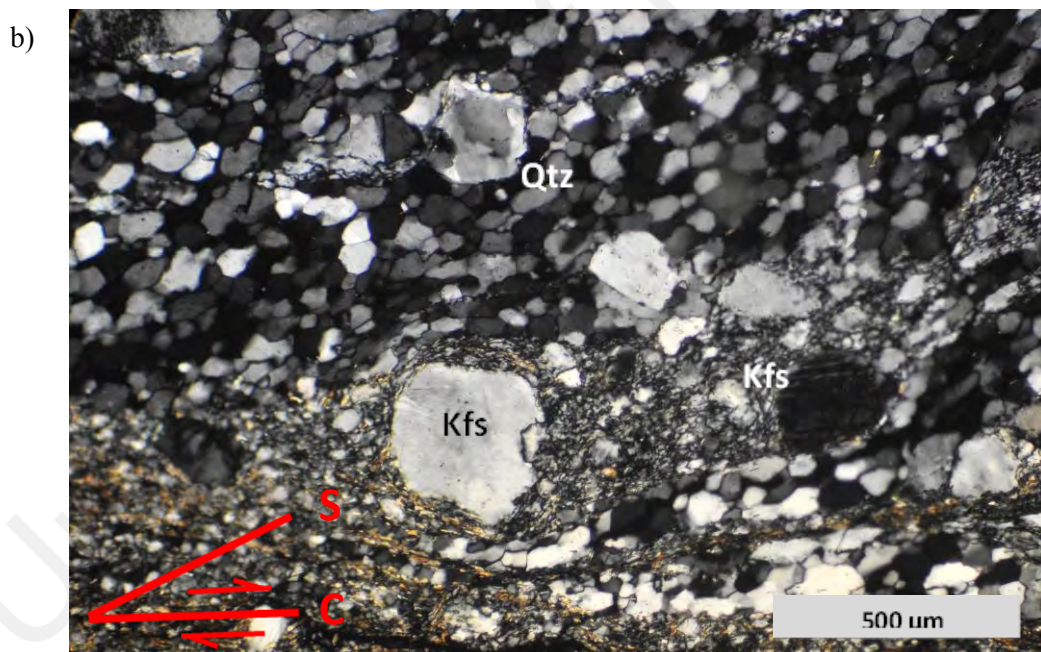
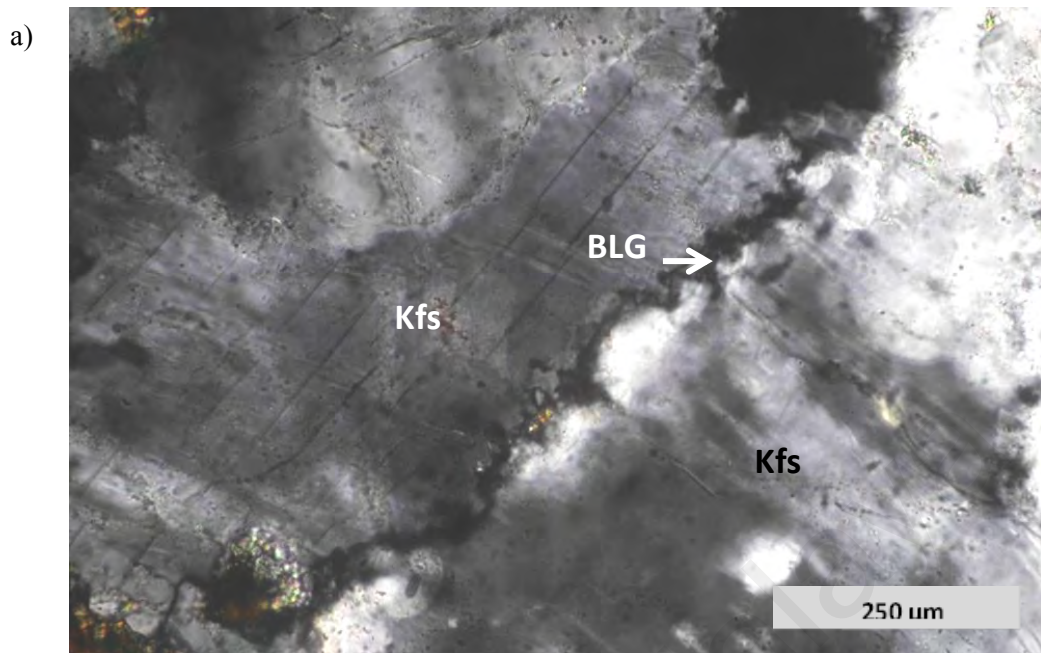


Plate 3.14: a) Photomicrograph showing K-feldspar clast with fracture along the cleavages. Recrystallization by bulging recrystallization (BLG) in the feldspar occurs at the grains boundary between the same minerals. b) Alternate quartz and feldspar neocrysts-rich layers parallel to the C-surface. Notice the different in size of quartz and feldspar neocrysts. The new recrystallised quartz are polygon in shape at about the same size.

Sample a: PM21

Sample b: PM23

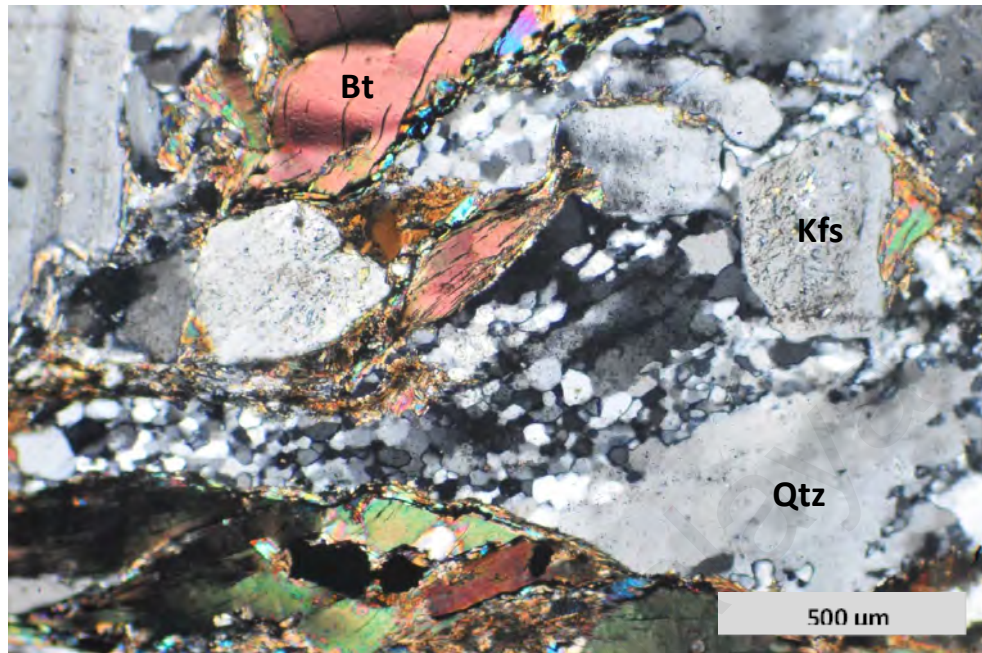


Plate 3.15: In mylonite mica behaves ductilely. Undulose extinction, folds and kinks are common, generally associated with deflection of basal planes and lead to fish shaped boudinage grains. With increasing shear and strain, mica recrystallized to form very fine plate-shaped grains.

Sample: PM22

Table 3.2: Table shows the evolution of the deformation microstructures in mylonite of BTFZ. Relative development indicator (o: absent, x: minor, xx: moderate, xxx: high).

Minerals	Deformation Microstructures	Proto mylonite	Meso mylonite	Ultra mylonite
Quartz	Ribbon quartz	xxx	xx	o
	Deformation band	xxx	xxx	o
	Polygonization	xx	xxx	o
	Recrystallized grains by BLG	x	x	o
	Recrystallized grains by SGR	x	xxx	xxx
	Neocryst grain shape preferred orientation	xx	xxx	xxx
	Aggregate shape preferred orientation	xx	xxx	xx
K-feldspar	Undulose extinction	xx	x	x
	Deformation band	x	xx	xx
	Fracture	xxx	xx	x
	Microfault	o	x	x
	Flame perthite	xx	xx	x
	Recrystallized grains	x	xx	xxx
	Antithetic bookshelf fracture	o	xx	o
Plagioclase	Undulose extinction	xx	xx	xx
	Fracture	xxx	xx	x
	Microfault	x	xx	x
	Recrystallized grains	o	o	x
	Bending	x	xx	o
	Kink	o	x	x
Mica	Undulose extinction	xx	xx	xx
	Recrystallized grains	x	xx	xxx
	Shear band	x	xx	xxx
	Bending	x	xx	o
	Mica fish	x	xx	o

3.6.2 Deformation Temperature

In mylonites of the BTFZ, the presence of undulose extinction is ubiquitous in relict quartz clasts. According to Nishikawa and Takeshita (1999) and Stipp *et al.* (2002a), this microstructure takes place at very low grade condition (below 300°C). The occurrence of deformation lamellae in quartz is reported to occur at higher temperature, between 300° - 400°C (Passchier and Trouw, 2005). At this temperature, dislocation glide and creep become important, mainly on basal glide surfaces in the (c) <a> direction. At the temperature range of 280° - 400°C quartz neocrysts are formed by bulging recrystallization (BLG) (Stipp *et al.*, 2002a; Tullis, 1978; Wu and Groshong, 1991a; Faleiros *et al.*, 2010).

Ribbon-shaped quartz started to develop at more than 400°C to 500°C (Stipp *et al.*, 2002a; Passchier, 1985; Hongn and Hippertt, 2001). At this range, dislocation creep is dominant, and prism {m} <a> slip becomes more important. This was accentuated by the presence of subgrain rotation recrystallization (SGR) mechanism as the dominant recrystallization mechanism for polygonisation in the mylonite (Stipp *et al.*, 2002a; Faleiros *et al.*, 2010; Lloyd and Freeman, 1994) and oblique foliation (Stipp *et al.* 2002a; Passchier and Trouw, 2005).

Deformation behaviour of K-feldspar and plagioclase in the mylonites of BTFZ is rather similar and therefore the feldspars are treated together. Laboratory experiments and observation of naturally deformed feldspars have shown that feldspar deformation is strongly dependent on metamorphic conditions (Passchier and Trouw, 2005). Here, the feldspar deformed mainly by brittle fracturing (Plate 3.13a). Fracturing typically occurs at low temperature (below 300°C; Pryer, 1993). White (1975) and Boullier (1980) believes that antithetic book-shaped porphyroclasts (Plate 4.6) are common in the low temperature range between 300° and 400°C. Above 400°C, feldspar still deforms by microfracturing aided strongly by minor dislocation glide. Undulose

extinction and deformation twinning may be present (Pryer, 1993; Ji, 1998a,b; Tullis and Yund, 1980).

At the temperature above 450°C, flame-shaped albite lamellae in K-Feldspar is distributed in mylonite (Pryer and Robin, 1996; Pryer, 1993) (Plate 3.13b). The minor occurrence of feldspar recrystallization in the mylonite of BTFZ indicates that the temperature of above 450°C has just been reached (Gates and Glover, 1989; Tullis and Yund, 1991).

Undulose extinction, kink band and folding of micas are common in the mylonites (Plate 3.15). These features can exist at temperature below 400°C (Mares and Kronenberg, 1993). Biotite behaves in a ductile manner at temperatures above 250°C (Stesky, 1978). Summary of deformation microstructures versus temperature is shown in Table 3.3. From the microstructures, it is indicated the mylonites of the BTFZ are deformed at the brittle-ductile transition at temperatures between about 300°C and 500°C (Figure 3.9). Location of the mylonites at depth and temperature is shown by the conceptual model of a fault from Sibson (1977) (Figure 3.10).

3.6.3 Grain size reduction

The grain size reduction can be achieved by cataclasis and dynamic recrystallization (Jefferies, 2006). In addition to relieving stress, cataclastic failure created fine-grained regions that might be expected to be rheologically weaker than the protolith. Not only was the grain size significantly reduced the original rock fabric was destroyed, resulting in a more homogeneous distribution of phases in the rock. The more random distribution of phases could prevent the growth to equilibrium grain size (Twiss, 1977) of the individual mineral constituents, effectively stabilizing this fine grain size. However, in the mylonites of BTFZ, cataclasis is constrained to feldspars, thus the homogenization of phases is limited. In contrast, segregation occurs in some

protomylonite, where feldspar clasts are concentrated in thin layers parallel to the S-surfaces, and they alternate with bands rich in fine recrystallized quartz and quartz ribbons, and mica-rich bands. Etheridge and Wilkie (1979) point out that very small, non-equilibrium grain sizes may be maintained during dynamic recrystallization in a multiphase rock, where the growth to equilibrium grain size of the mineral of interest is inhibited by another phase.

Dynamic recrystallisation is a recrystallization process during active deformation including bulging recrystallization (BLG) and subgrain rotation (SGR). Recrystallization contributes to the reduction of dislocation density in deformed crystals (Poirier, 1985; Gottstein and Mecking, 1985; Drury and Urai, 1990). As a result, new small grains (neocrysts) replace the old grains with a change in grain size, shape and orientation. This process results in weakening due to increase in grain-boundary sliding and grain-boundary diffusion creep (Jaroslow *et al.*, 1996; Warren and Hirth, 2006). Therefore grain size reduction by dynamic recrystallization process possibly plays a fundamental role in weakening a long large shear zones and large-scale displacement. Finer grain size, due to an increase in grain boundary surface area is more susceptible to reaction softening than coarser grained rocks (Brodie and Rutter, 1985).

3.6.4 Strain softening

The high finite strain reached in mylonite imply that strain rates in the mylonite zone have exceeded that in the wall rock for some time and the material in the zone have been softer than the wall rock (Passchier and Trouw, 2005).

The changes occur in the rheology of the materials in the ductile zone. This effect is known as strain-softening. A number of mechanisms lead to strain softening and that results in shear instabilities in shear zones (White *et al.*, 1980). Decrease in grain size, growth of new minerals, development of lattice preferred orientation and











shear bands (c-surface) are the prime mechanisms that contribute to softening (White *et al.* 1980; Tullis *et al.* 1990). Softening indicated for decreasing differential stress at constant strain rate. It may lead to the ductile deformation in shear zones (Passchier and Trouw, 2005). The grain size reduction and foliation development of the mylonites of the BTFZ contribute to strain softening, which is also suggested by the development of localized zones of mesomylonite and ultramylonite.

3.6.5 Influence of fluid

The minerals weakened due to diffusion of water into the lattice (Luan and Paterson, 1992; Kronenberg, 1994; Post and Tullis, 1998). Water infiltrates into the quartz lattice slowly and affected quartz rheology for quartz under greenschist facies conditions. The presence of water/fluids during deformation is an important factor that influences the breakdown and alteration of anhydrous minerals (feldspar) to low grade assemblages of hydrous minerals (phyllosilicates) (Jefferies, 2006). The extent to which mineral and bulk rock compositions are modified in shear zones appears to be influenced by fluid access and the temperatures of deformation. As a result, fine-grained fluid rich fault zones are expected to be weak. Rocks in the shear zone are surrounded by granite and there is no obvious source for the fluids needed to produce the shear zone mineral assemblages; but deforming rock itself, by dehydration reactions, could be the fluid source (Gundersen and Gates, 1995). The influence of fluid in the mylonites of BTFZ is indicated by the sericitization of feldspar and chloritization of biotite. Quartz veins which may indicate the presence of hydrothermal fluid is rare in the mylonites, except those that are affected by subsequent brittle deformation (cataclasites).

Table 3.3: Summary of the temperature correspond to the deformed microstructures in mylonites of BTFZ.

Minerals	Temperature (°C)								References
	250	300	350	400	450	500	550	600	
Quartz									
Undulose Extinction								Stipp <i>et. al.</i> (2002a,b), Nishikawa and Takeshita (1999)
Deformation Lamellae								Passchier and Trouw (2005)
Ribbon-shaped quartz								Stipp <i>et. al.</i> (2002a,b), Passchier (1985), Hongn and Hippert (2001)
Core and Mantle								Stipp <i>et. al.</i> (2002a,b), Passchier and Trouw (2005)
Subgrains by BLG								Tullis (1978), Stipp <i>et. al.</i> (2002a,b), Wu and Groshong (1991a), Faleiros <i>et. al.</i> (2010)
Subgrains by SGR								Stipp <i>et. al.</i> (2002a,b), Faleiros <i>et. al.</i> (2010), Lloyd and Freeman (1994)
Oblique Foliation								Stipp <i>et. al.</i> (2002a,b), Passchier and Trouw (2005)

Feldspars		
Microfaults (antithetic)		White (1975), Boullier (1980).
Undulatory Extinction		Pryer (1993), Ji (1998a,b), Tullis and Yund (1980).
Deformation twins		Pryer (1993), Ji (1998a,b).
Flame Perthite		Pryer (1993), Pryer and Robin (1995).
Subgrains by BLG		Gates and Glover (1989), Tullis and Yund (1991).
Mica		
Undulose Extinction		Lister and Snoke (1984), Bell <i>et. al.</i> (1986b).
Folding		Lister and Snoke (1984), Bell <i>et. al.</i> (1986b), Passchier and Trouw (2005).
Kinking		Lister and Snoke (1984), Bell <i>et. al.</i> (1986b), Nishikawa and Takeshita (1999), Wu and Groshong (1991a), Passchier and Trouw (2005).
Mica Fish		Passchier and Trouw (2005).
Subgrains by GBM		Bell (1998).

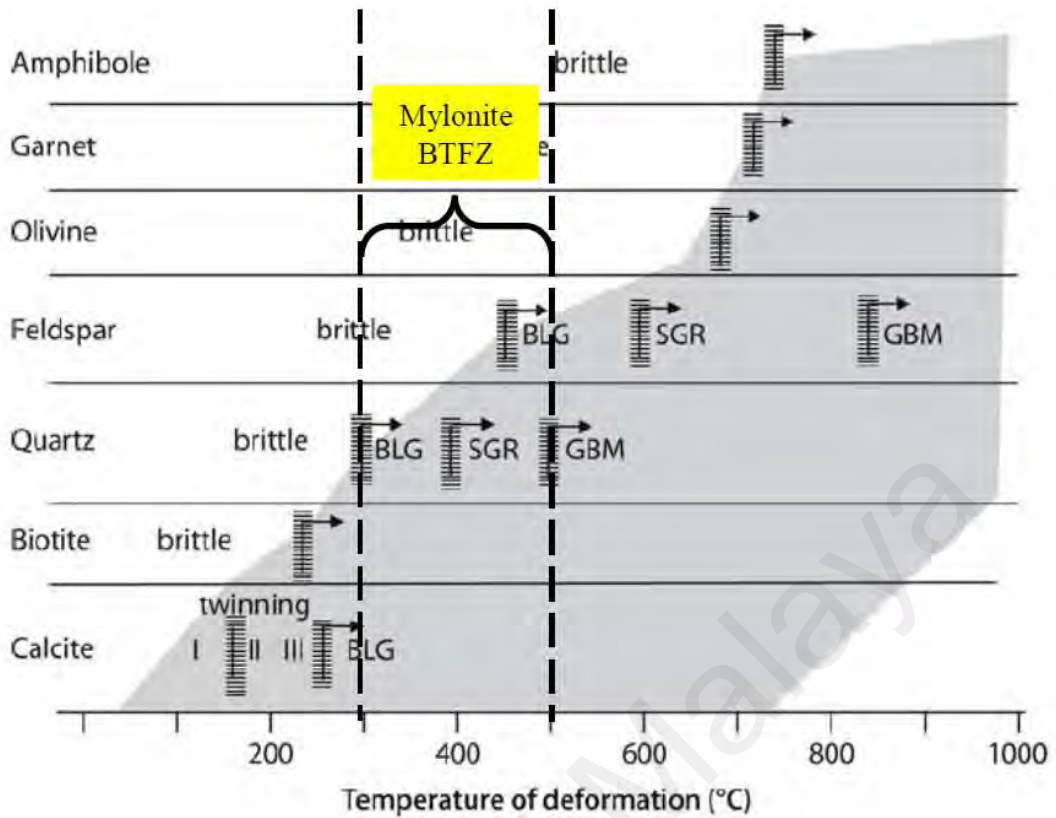


Figure 3.9: An approximate deformed temperature and deformation mechanisms range for different minerals in mylonites of BTFZ. Bars indicate the transition zones. Arrows indicate the effect of strain rate. BLG, SGR, GBM – main types of recrystallization. The ornamental domain is the domain of crystal plastic deformation. Modified after Passchier and Trouw (2005).

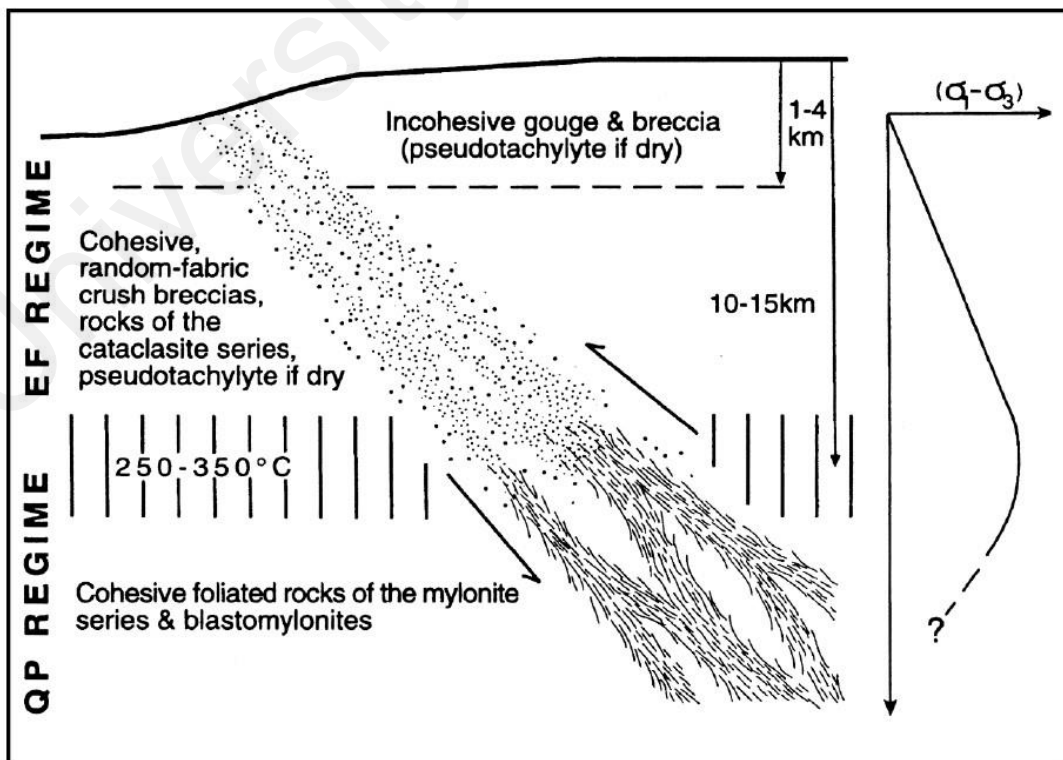


Figure 3.10: A conceptual model of a fault zone showing mylonites location at depth and temperature from Sibson (1977).

CHAPTER 4: KINEMATIC ANALYSIS OF THE MYLONITES

4.1 Introduction

Kinematic analysis is the study of indicators of the flow regime operating during deformation. The structures that allow reliable inferences about the displacement (flow) of material in the rock during progressive deformation are known as kinematic indicators. The direction of movement of a ductile shear zone is usually assumed to lie subparallel to stretching mineral lineations (Passchier and Simpson, 1986) according to the strain model of simple shear. The lineation measured in the field closely tracks the shear direction in sheared rocks (Hanmer and Passchier, 1991).

Shear sense observations are best viewed in the XZ surface of the finite strain ellipsoid. Foliation is a planar fabric element that occurs penetratively on a mesoscopic scale in a rock (Passchier and Trouw, 2005). Foliation is taken to lie approximately parallel to the XY surface of the finite strain ellipsoid, and the lineation is taken to mark the X direction. Shear sense indicators are a subset of kinematic indicators that indicate the sense of shear in progressively noncoaxially (simple shear) (Hobbs *et al.*, 1976; Ramsay, 1980a; Hanmer and Passchier, 1991; Passchier and Trouw, 2005) deformed materials.

In the field, shear sense is recorded on this sense of shear surface, which is parallel to the lineation and perpendicular to the foliations. Similarly, thin sections were prepared from oriented samples in the same orientation. The strike slip fault could be differentiated from the dip slip fault as the stretching lineation is horizontal with pitch value 90° while dip slip fault has inclined stretching lineation and pitch degree less than 90° .

The Bukit Tinggi Fault Zone contains a wide range of well-developed shear sense indicators, such as S–C fabrics (Lister and Snoke, 1984; Hanmer and Passchier,

1991; Figure 4.1) and asymmetric porphyroclasts (Passchier and Simpson, 1986), and provides a natural laboratory for kinematic studies of regional-scale ductile shear zones in the western flank of Main Range Granite.

This contribution will describe the kinematic analysis done using mesoscopic features and microstructure of lattice-preferred orientation. These studies were performed to confirm the flow direction of the fault zone during the brittle-ductile fault episode that generated the granite mylonite.

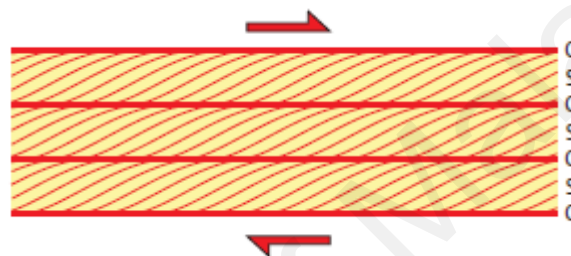


Figure 4.1: Idealised S-C fabric. The C-surface is internal shear or slipped surface parallel to shear zone boundary and has the same sense of shear as the main shear zone. The S-surface is related to the accumulation of finite strain and it is defined the mylonitic foliation. After Trouw *et al.* (2010).

4.2 Mesoscopic features

Foliation and lineation are major mesoscopic structures documented in the Bukit Tinggi Fault Zone. Mylonitic deformation has resulted in the formation of a penetrative fabric consisting of several mesoscopic and microscopic fabric elements. The most conspicuous of these features is mylonitic compositional layering (parallel to C-surface), which consist of biotite-rich layers and lenses of mylonitic granite, especially in the mesomylonite and ultramylonite. The planar preferred orientation of micas (biotite, muscovite and chlorite), together with flattened elongated quartz grains and aggregates, and feldspar porphyroclasts, impart an additional fabric (S-surface) that may

be planar or sigmoidal, which is prominent in the protomylonite. S-surfaces may be inclined at angles up to 60° to the C-surface (Figure 4.2, Plate 4.1).

Stretching lineation is observed on the foliation surface and is parallel to the S-surface and C-surface intersection. The lineation preserved direction of maximum elongation that prevailed, at least, during the final stages of mylonitisation. The lineation lies in a direction defined by preferred orientation of elongated prophyroclasts, quartz aggregates and platy minerals.

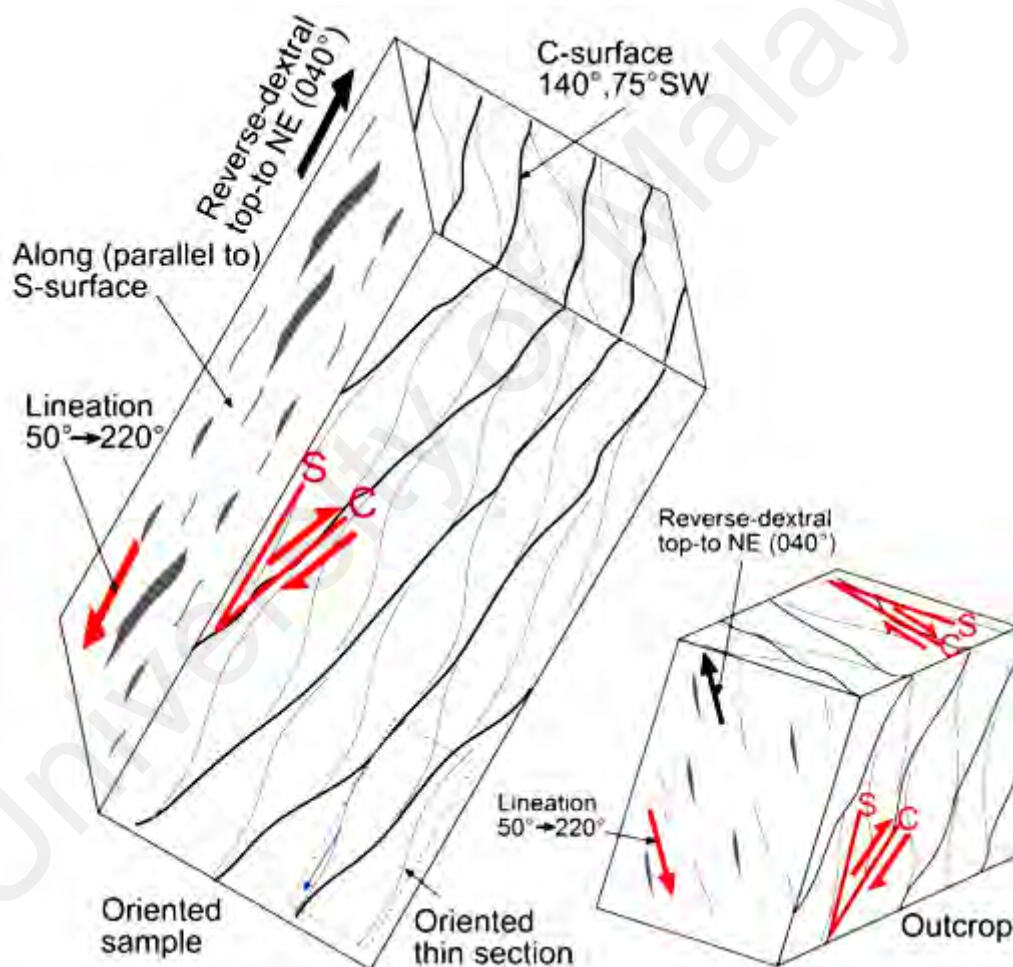


Figure 4.2: Schematic diagram showing the relationship between regional foliation and S-C fabrics in the mylonites of BTFZ. Blue dotted box demonstrate how the oriented sample was taken at the field. The small block (right below) represents the oriented rock sample.

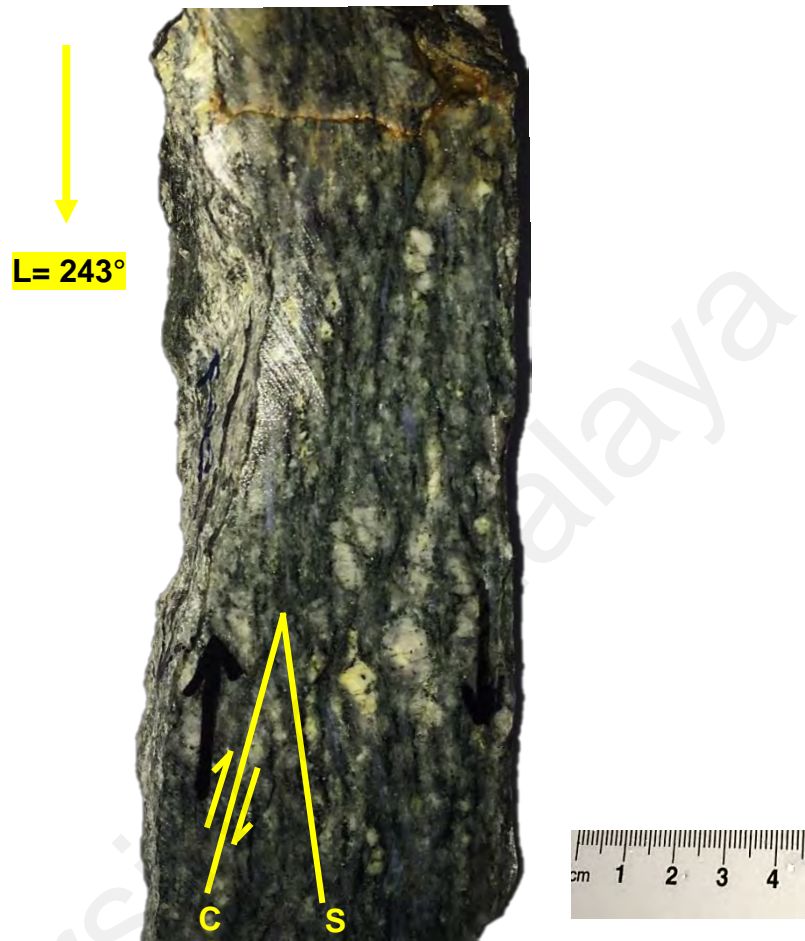


Plate 4.1: An oriented protomylonite with S-C foliations, cut parallel to the lineation and perpendicular to the foliations. The S-C fabric and porphyroclasts show dextral reverse movement top-to-NE vergence. C-surface = $150^{\circ}, 68^{\circ}$ SW; Lineation = $072^{\circ} \rightarrow 243^{\circ}$.

Sample: PM 22

S-C fabric is the most useful sense of shear indicator in ductile shear zones in both mesoscopic and microscopic scales (Berthé *et al.*, 1979a; Simpson and Schmid, 1983; Lister and Snoke, 1984; Hanmer and Passchier, 1991). It is a composite planar fabric formed during non-coaxial deformation (Berthé *et al.*, 1979a; Lister and Snoke, 1984). They consist of two sets of foliations that are S-surface and C-surface (figure 4.1). The S-surface is oblique to C-surface in zones of low apparent strain. Since the C-surface is parallel to the boundary of the mylonite zone, it is presumed to parallel the surface of shear. The S-surface records the orientation of preserved surfaces of flattening, and the relationship between S-surface and C-surface could be used to determine the direction of shear (Ramsay and Graham, 1970; Berthé *et al.*, 1979a). In the example shown in Plate 4.1, using oriented sample cut parallel to the lineation and perpendicular to the foliations, the S-C surfaces give a reverse-dextral sense of shear requiring the hanging wall to have moved northeast (063°) relative to the footwall. The σ -porphyroclasts (will be described in 4.3.3) also indicate the same sense of shear.

4.3 Microstructure features

Microstructural features encountered from different parts of the Bukit Tinggi Fault Zone are including S-C fabrics, oblique foliation, winged porphyroclasts, mica fish and bookshelf antithetic microfracturing. They were used to decipher the information on the movement directions of mylonites in the ductile shear zone (Passchier and Simpson, 1996).

4.3.1 S-C fabric

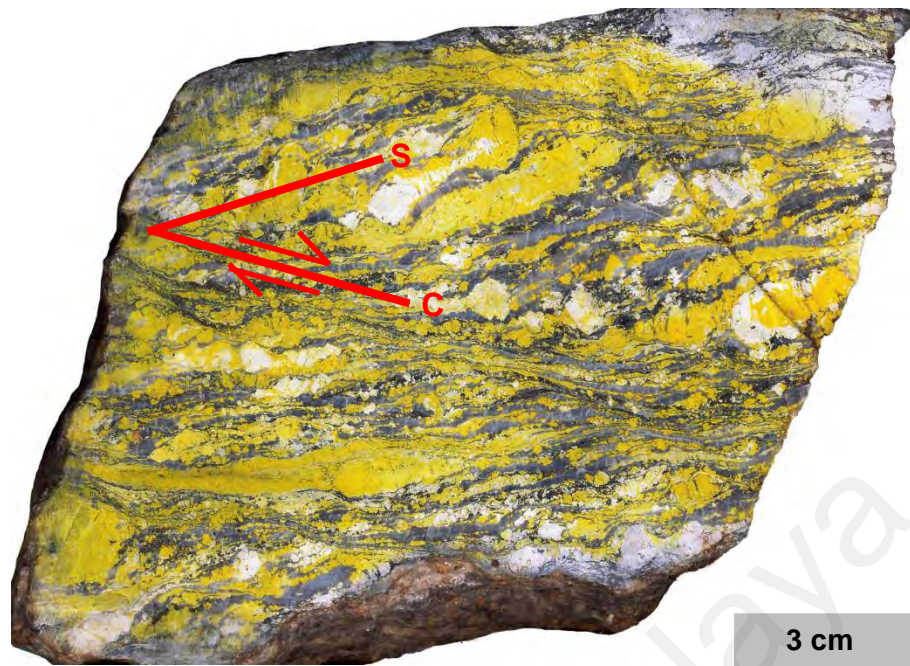
Under the microscope, S-C fabric is clear in the mesomylonite and ultramylonite. In the protomylonite, the S-C fabric is often less clear because of the relatively coarser grain size. According to Passchier and Simpson (1996), there are two

types of S-C fabrics, type 1 and type 2. Type 1 is common in granitoid rocks and consists of S-surface (define by feldspar porphyroclasts) and transected by C-surface (defined by concentrated flow of mica and quartz ribbons) that are continuous, and analogous to shear zone boundaries. Type 2 S-C fabric (or S-C' fabric) is common in micaceous quartzite and is dominated by C-surfaces.

Type 1 S-C fabrics are found in the Bukit Tinggi Fault Zone. As the rock progressively deforms in non-coaxial deformation, the S-surface generally forms first and with increasing shear strain C-surface starts to form then, S and C surfaces continue to develop together. The S-surface is defined by elongated quartz ribbons and is approximately parallel to the XY surface of finite strain ellipsoid whereas the C-surface is a zone of high shear strain approximately parallel to the shear zone boundary and is marked by mica rich zones. With increasing deformation, S-surface progressively rotated toward parallelism with C surface and the surface may become more closely spaced and better developed. At very high strain, S-surface becomes subparallel to and indistinguishable from C-surface.

The angle between S-surfaces and C-surfaces was measured and generally varies from 10° to 60° . The variation of angles between S and C surfaces reflect the heterogeneity of strain in the shear zone with lower angles corresponding to higher shear strain. The S-C fabrics in the fault zone show top to east (Plate 4.2).

a)



b)

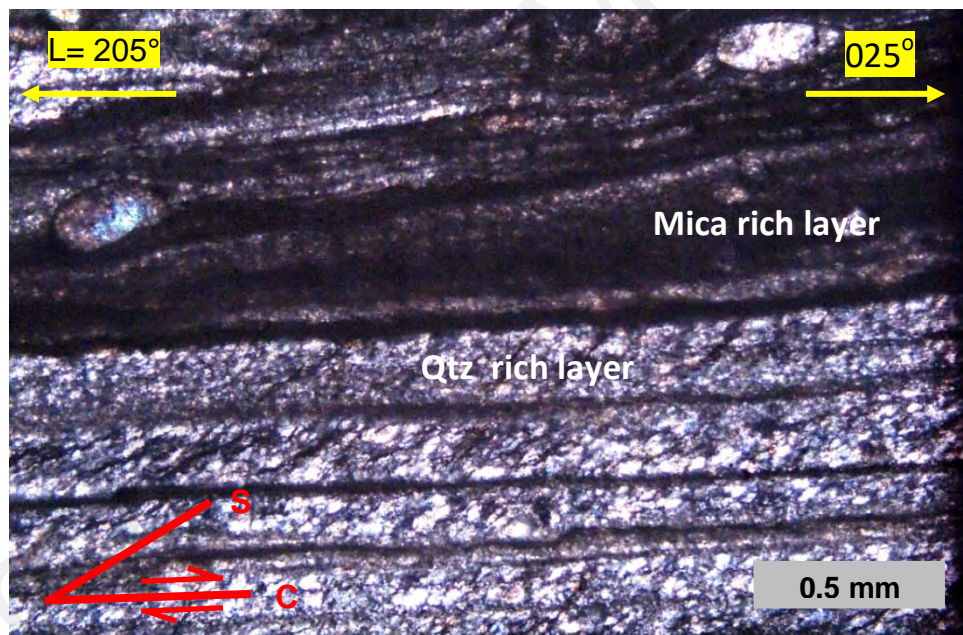


Plate 4.2: a) Photograph of a stained polished rock slab of protomylonite indicates dextral sense of shear. b) The S-C fabric is inclined in reverse direction to the NE.

Sample a: Karak highway

Sample b: UM7

4.3.2 Oblique foliation

An oblique foliation is a grain shape preferred orientation. In the mylonites of BTFZ it is parallel to the S-surface and defined by aligned elongated subgrains and dynamically recrystallized new grains (neocrysts) oblique the C-surface. In the protomylonite and mesomylonite, oblique foliation mainly occurs in partially to completely recrystallized elongated quartz aggregates. The elongation of the aggregates as a whole is parallel to the C-surface, while the individual subgrain and neocryst are slightly elongated and the elongation is parallel to the S-surface (Plate 4.3a). In the ultramylonite, oblique foliation occur in the light colour quartz-feldspar layers, the layers are parallel to the C-surface, while the elongated quartz neocrysts have preferred orientation parallel to the S-surface (Plate 4.3b).

Aggregates of dynamically recrystallized small grains in monomineralic aggregates, showing a preferred alignment oblique to the mylonitic foliation have been observed by many previous workers (Law *et al.*, 1986; Means 1981; Lister and Snoke, 1984) and used as a sense of shear indicator (Figure 4.3). They are assumed to develop by rotation of grains in non-coaxial flow resulting in increasingly elongate grains (Passchier and Trouw, 2005).

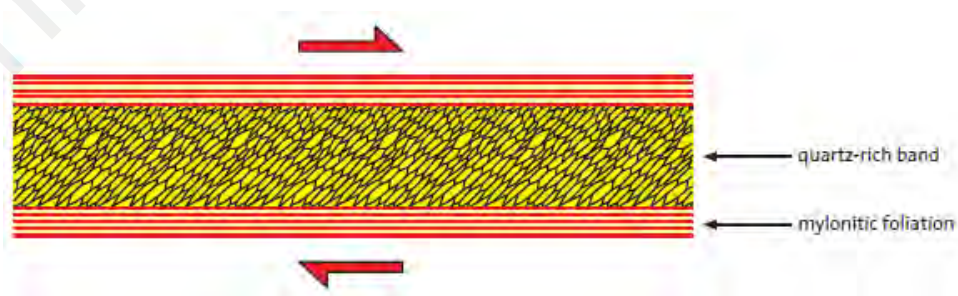


Figure 4.3: Idealised oblique foliation defined by preferred orientation of elongated quartz grains in a quartz rich band embedded in a mylonite, with the mylonitic foliation (C-surface) as reference frame. After Trouw *et al.*, (2010).

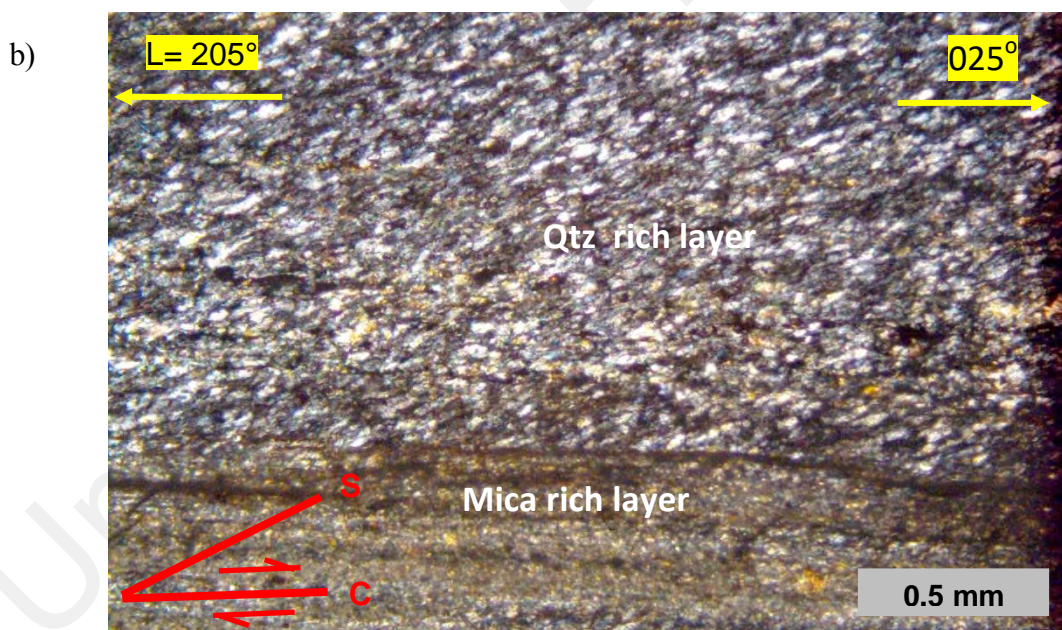
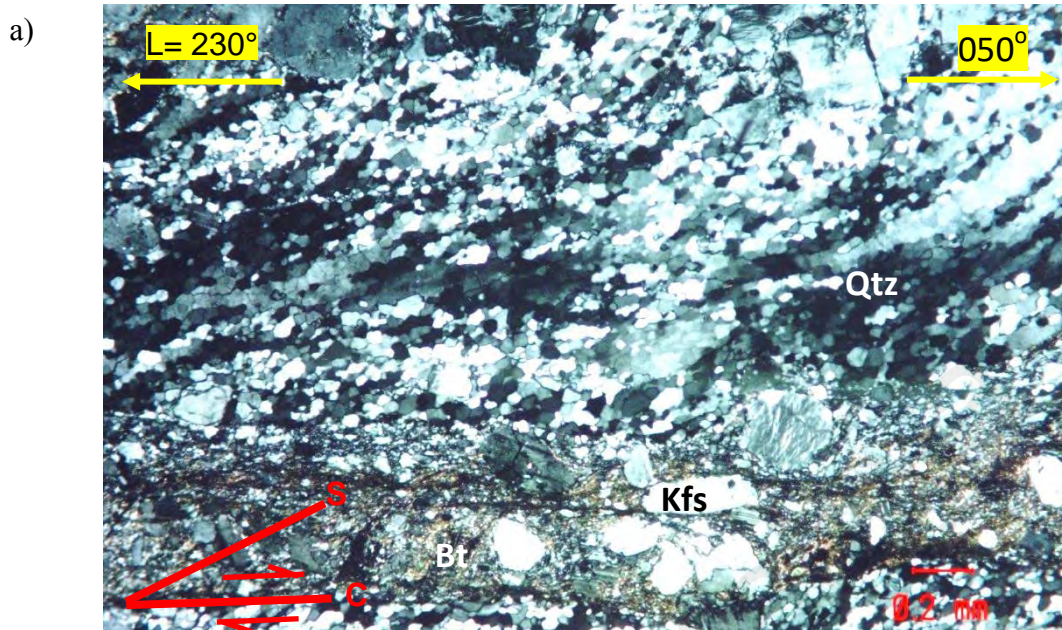


Plate 4.3: Oblique foliation in (a) protomylonite and b) ultramylonite from the sample indicate dextral sense of shear.

Sample a: PM23

Sample b: UM7

4.3.3 Mantled porphyroclast

Mantled porphyroclasts with recrystallized tails are extremely important for deducing the sense of shear in high strain zones (Simpson and Schmid, 1983; Lister and Snoke, 1984; Passchier and Simpson; 1986). Mantled porphyroclast consists of a central clast and a fine-grained mantle of the same mineral. The fine grained soft mantle can be deformed into wings (or trails) that extend both sides of the porphyroclast parallel to the preferred orientation in the mylonites (Passchier and Trouw, 1986). Wings are thought to stretch and changed shape while the porphyroclast core remains rigid or continues to recrystallize along the contact with the rim, shrinking in size. Wing shape can be used as a shear sense indicator and contains information on rheology of the matrix and the matrix-clast coherence.

The porphyroclasts can be divided into 5 types, and three types of winged porphyroclasts with stair stepping (sigma, delta and complex) can be used for kinematic analysis (Passchier and Simpson; 1986). Sigma type porphyroclast (σ) usually occurs at lower strain whereas delta (δ) type mainly occurs in high strain mylonites (Figure 4.4). The sense of shear is given by the sense of stair stepping of the tails (wings) on either side of the porphyroclasts. In the Bukit Tinggi Fault Zone, sigma type K-feldspar and quartz porphyroclasts (σ) are commonly observed in the protomylonite and mesomylonite (Plate 4.4). The K-feldspar porphyroclasts are often fractured.

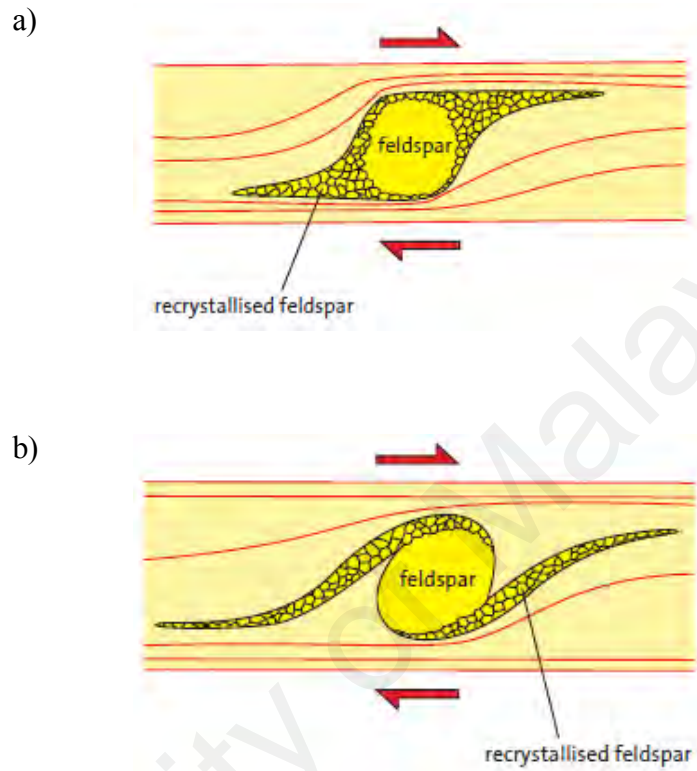


Figure 4.4: a) Idealised sigma porphyroblast structure. Note that the wings are composed of recrystallized feldspar derived from the porphyroblast. b) Idealised delta porphyroblast structure. After Trouw *et al.* (2010).

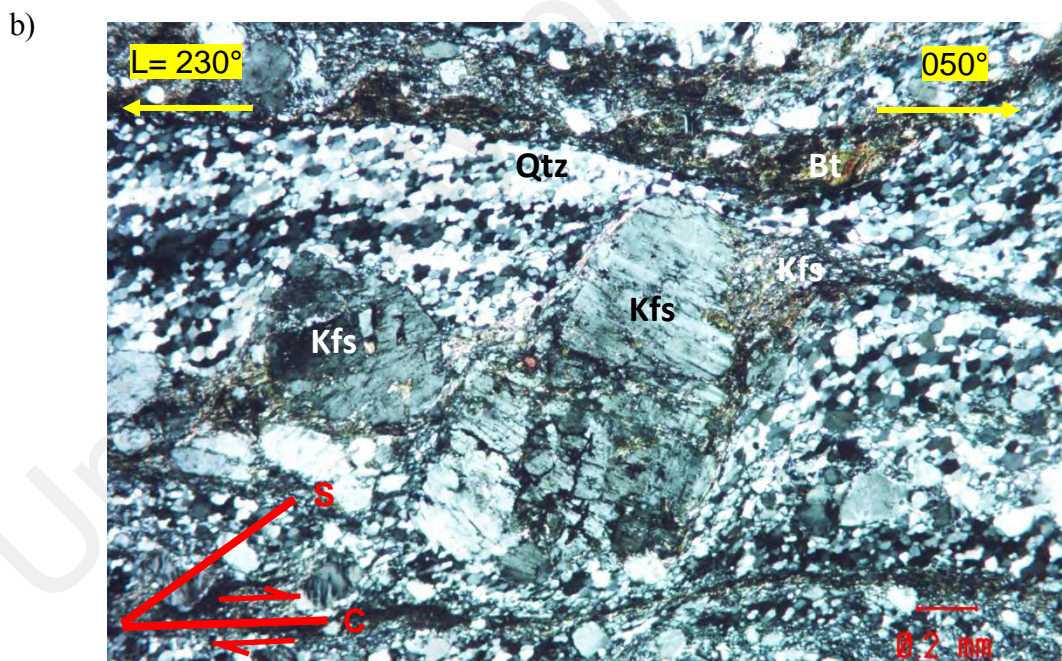
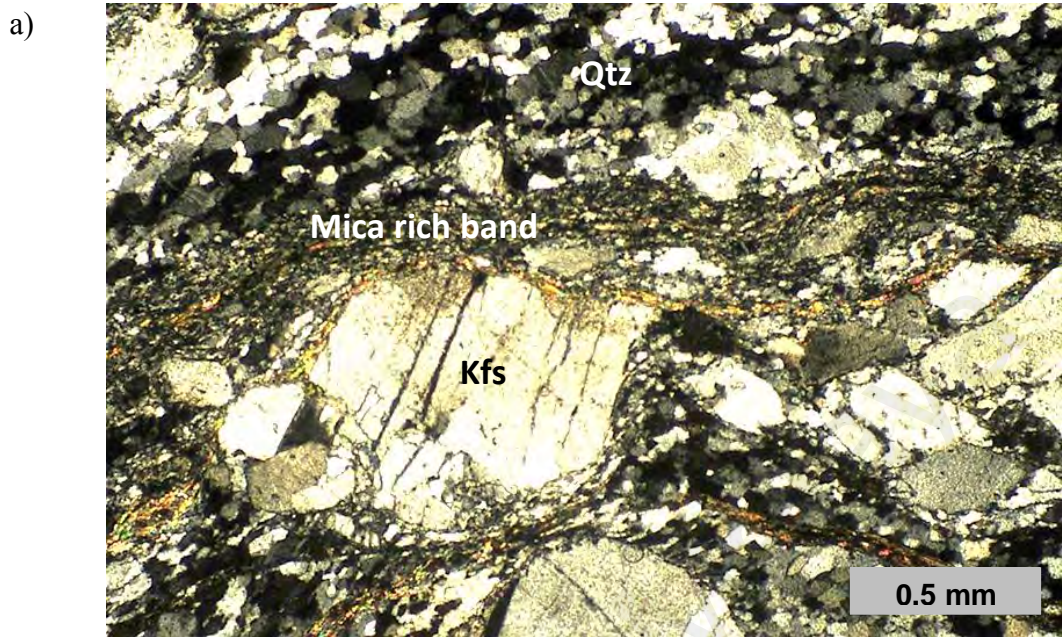


Plate 4.4: Sigma porphyroclasts of K-feldspar. (a) Minor recrystallization along the rim shows initiating the core-mantle structure in protomylonite (b) Note the porphyroclast show advanced recrystallization (upper right) forms stair step in the matrix. The sigma shape fabric stepping to the right around the large porphyroclast and S-C structure indicate dextral sense of shear in the protomylonite

Sample a: PM9

Sample b: PM23

4.3.4 Mica fish

Mica fish is elongate lozenge or lens-shaped single mica clast, which is common in mica-bearing mylonites (Figure 4.5). It lies with the longest dimension at a small angle to the mylonitic foliation. The fabric of mica fish, with trails of fine-grained mica extending from the tips of the fish into the matrix combined with the oblique foliation of the quartz in the matrix, show resemblance to mylonites with an S–C fabric as suggested by Lister and Snoke (1984).

Mica fishes are reliable sense of shear indicator (Lister and Snoke, 1984). In most cases, trails of shredded mica or recrystallized mica extend into the matrix from the tips of isolated mica fish defining C-surfaces (Lister and Snoke, 1984).

In the protomylonite and mesomylonite of BTFZ, biotite is commonly found to form as mica fish. The stair-stepping across the fish can be used as a sense of shear indicator (Plate 4.5).

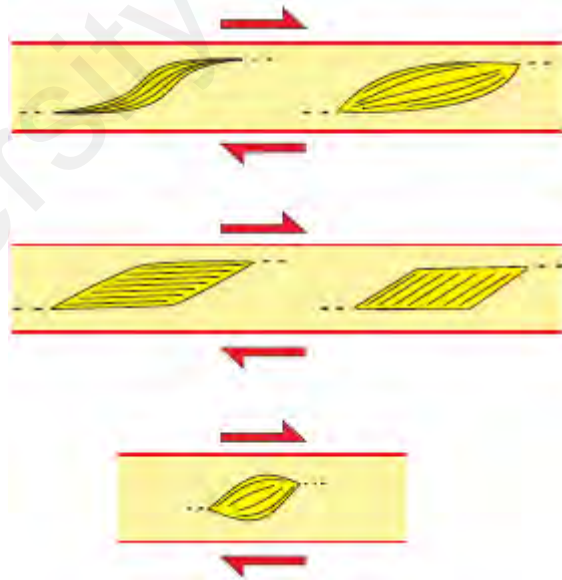


Figure 4.5: The mica fish types commonly found in the mylonite. After Trouw *et. al.*, (2010).

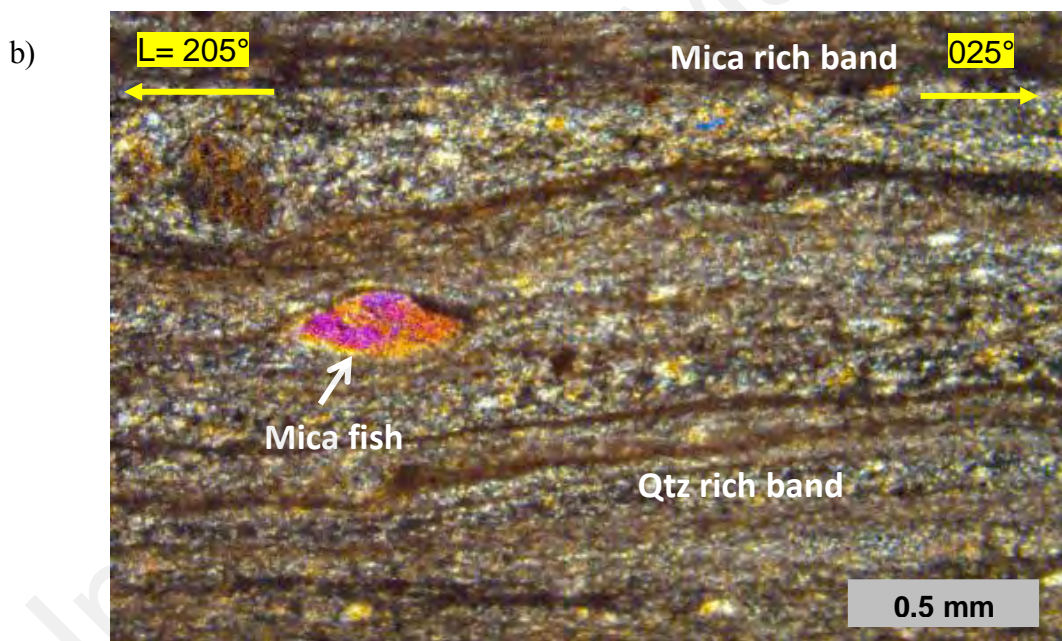
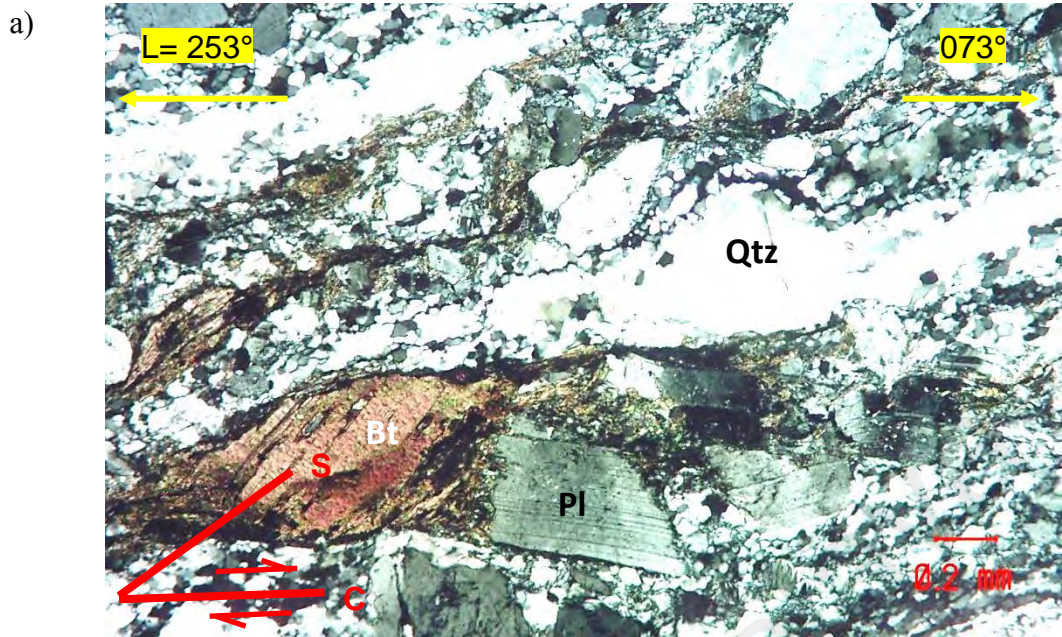


Plate 4.5: a) Biotite fish surrounded by quartz showing internal deformation and recrystallization along the rims. Note that the mineral cleavage is parallel to the side of the fish in protomylonite. b) A lens-shaped mica fish indicates dextral sense of shear by stair stepping and a weak oblique fabric in quartz in ultramylonite

Sample a: PM22

Sample b: UM7

4.3.5 Fragmented book-shaped porphyroclast

Elongate rigid porphyroclasts of feldspar grains fractured along cleavages can be separated into aggregates of fragments with a geometry shape similar to asymmetric boudins, sometimes separated by seams of matrix (Deubendorfer and Christensen, 1998; Babaie and LaTour, 1998). There are domino types (antithetic) and shear band type fragmented porphyroclasts (synthetic) (Figure 4.6). The geometry depends on the bulk shear sense and the initial orientation of microfaults in the clasts, which may be partly controlled by crystallographic directions in the porphyroclasts and by flow type. However domino type is more common than shear band type.

In the protomylonite and mesomylonite of Bukit Tinggi Fault Zone, feldspar porphyroclasts fractured and moved along the microshear are common. Most of them have microshear at high angle position relative to the compositional layering and form antithetic book-shaped fragments (Plate 4.6). The sense of slip of the book shaped feldspars is in agreement with the sense of shear obtained from S-C fabric, mica fish and oblique foliation.

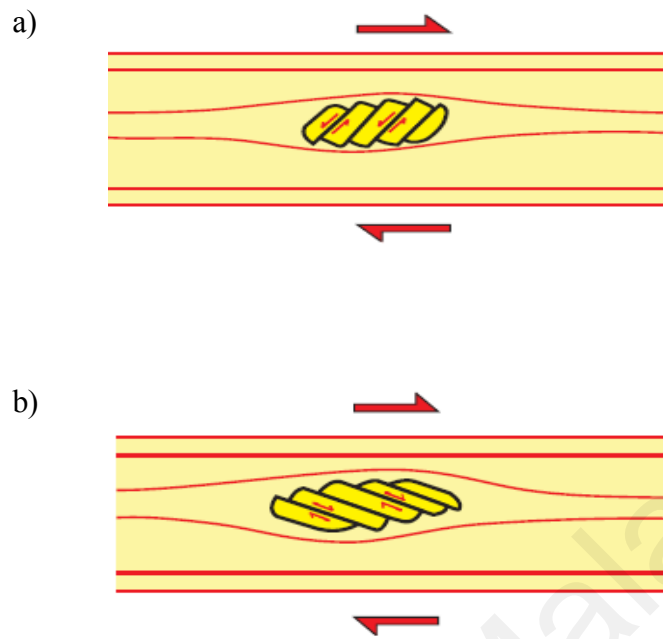


Figure 4.6: a) Domino type fragmented porphyroclast. Notice that the movement along the porphyroclast is antithetic to the sense of shear and the angle between these faults and the C-surface is usually larger than 45° . b) Shear band type fragmented porphyroclast. Notice the movement along the faults in the porphyroclast is synthetic with the sense of shear in the surrounding mylonite and the angle between the microfaults and the C-surface is smaller than 45° . After Trouw *et al.*, (2010).

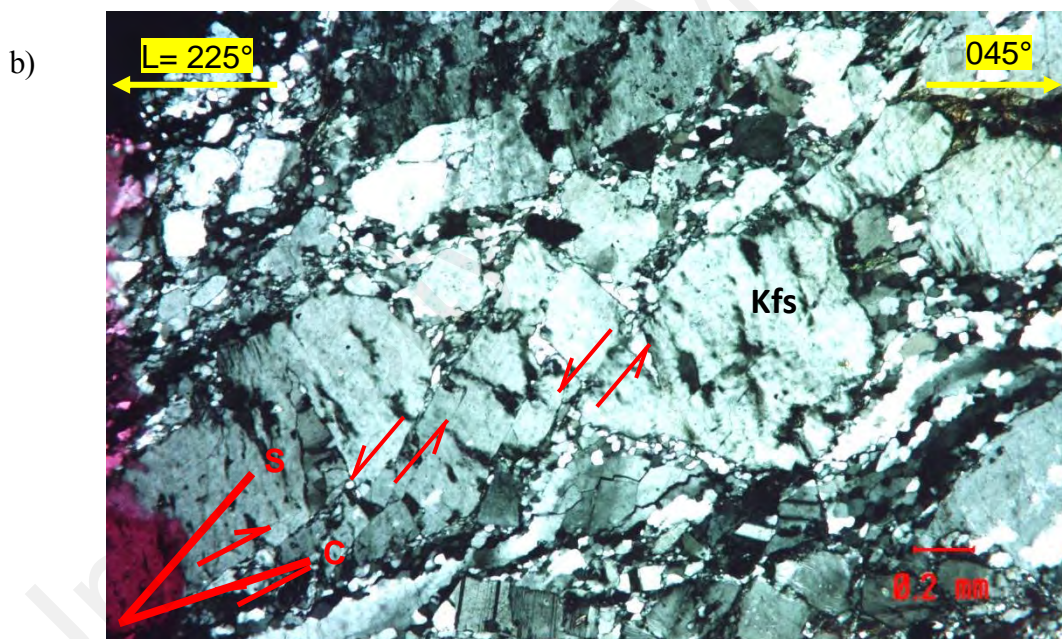
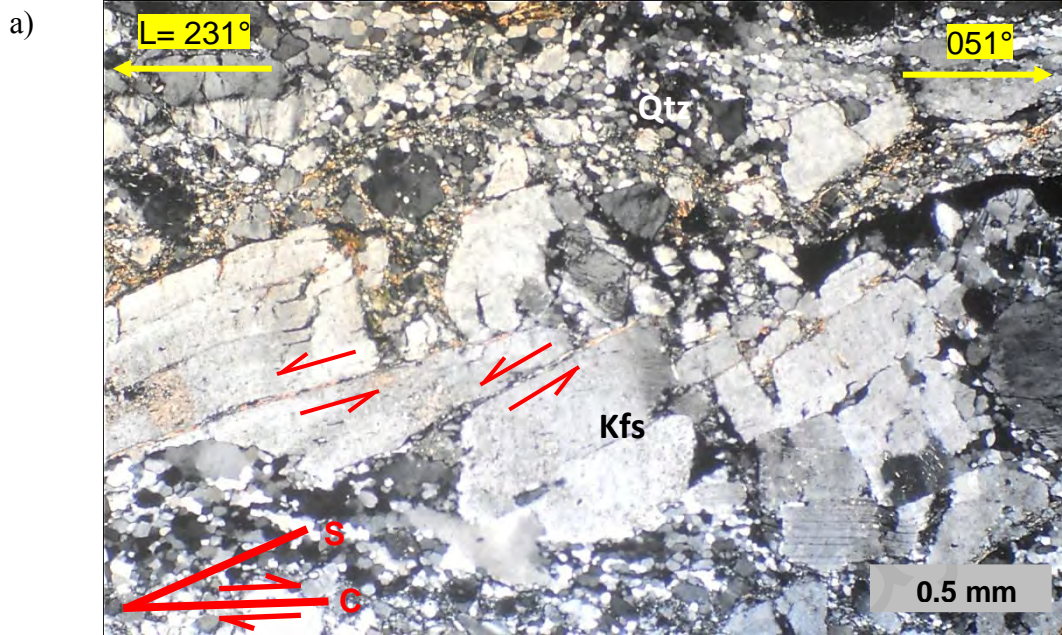


Plate 4.6: Photomicrographs show the fractures in K-feldspar porphyroclasts with apparent sinistral displacement along the microfaults that separate the three fragments. These domino type antithetic fragmented porphyroclasts indicate dextral sense of shear in the protomylonite.

Sample : PM21

4.4 Foliation

The mylonitic foliations recorded in the field and shown in the geological maps (Figures 3.4 to 3.6) and plotted in the stereonet (Figure 4.6) are C-surfaces. The C-surfaces are mainly striking at NW-SE, ranging from 100° to 170° and most are between 120° and 140° . The strikes of the C-surfaces are similar to the trend of Bukit Tinggi Fault Zone, confirming that the C-surfaces are parallel or sub-parallel to the fault zone. The C-surfaces are mainly dipping between 60° and vertical towards SW (Figure 4.7). There are also some measurements that dip towards the NE. The measurements taken are attached in Appendix C.

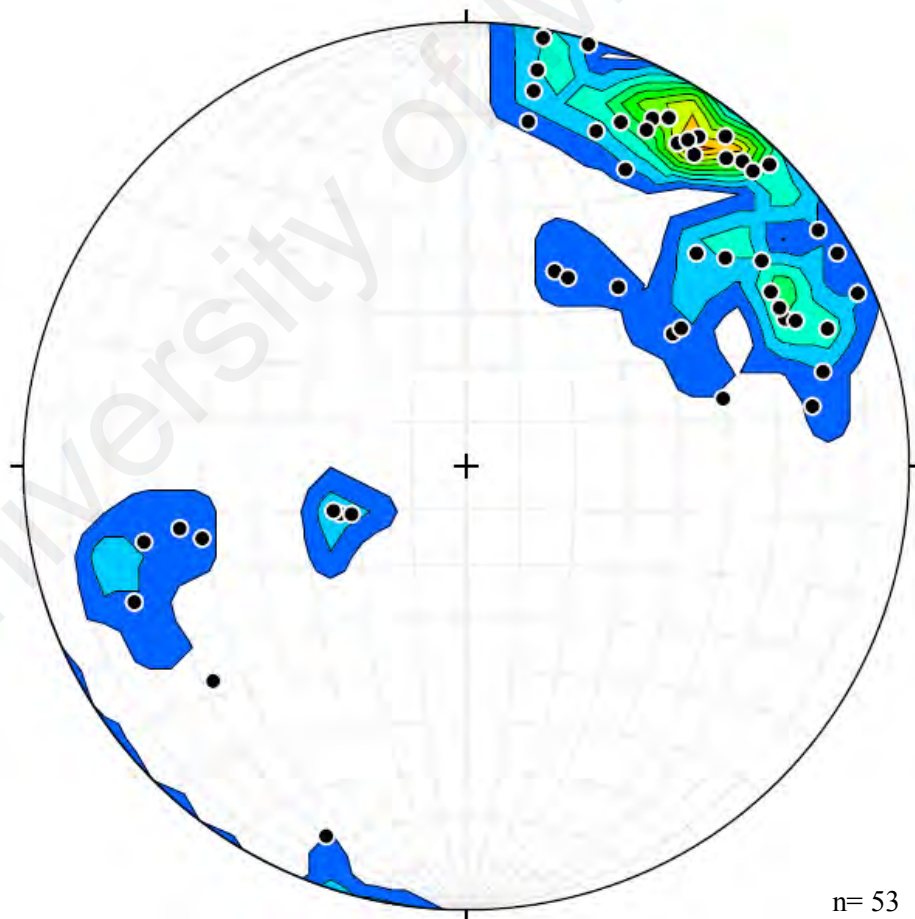


Figure 4.7: Equal area stereonet plot of pole to mylonitic foliations (C-surfaces) of the BTFZ.

4.5 Lineation

In the mylonite zone, stretching lineations are commonly observed (Figure 4.8). The lineations are made of elongated minerals rotated or grown in a preferred direction creating a grain or mineral lineation. Most lineations are parallel to the X direction of the finite strain ellipsoid (Passchier and Trouw, 2005). This lineation lies in a surface defined by preferred orientation of platy minerals and flattened grains (S-surface).

According to Passchier (1998), stretching lineations that represent the longest strain axis (X) can be used to identify the direction of tectonic transport (i.e. the direction that one rock mass had been displaced relative to another) if they form in ductile shear zones with shear flow.

The stretching lineations measured from the area are mainly plunge towards 190° to 254° with smaller group of readings plunging towards NE (Figure 4.9). The plunge angles of the lineation are variable, ranging from 26° to 88° and most are between 40° and 70° , indication the presence of significant dip-slip component.

From the combination of information from kinematic analysis and orientation of lineation, it is shown that all the SW dipping foliation shows reverse-dextral displacement with hanging wall moved towards the NE (Figure 4.8). A small group of readings with foliations dip towards the NE have normal-dextral displacement and the same top-to NE vergence. The measurements taken are attached in Appendix C.



Figure 4.8: The granite mylonite shows large stretched drawn-out cylindrical grains defining the stretching lineations (L). The grains are quartz and feldspar pointing to the NE. Bukit Tinggi, Pahang.

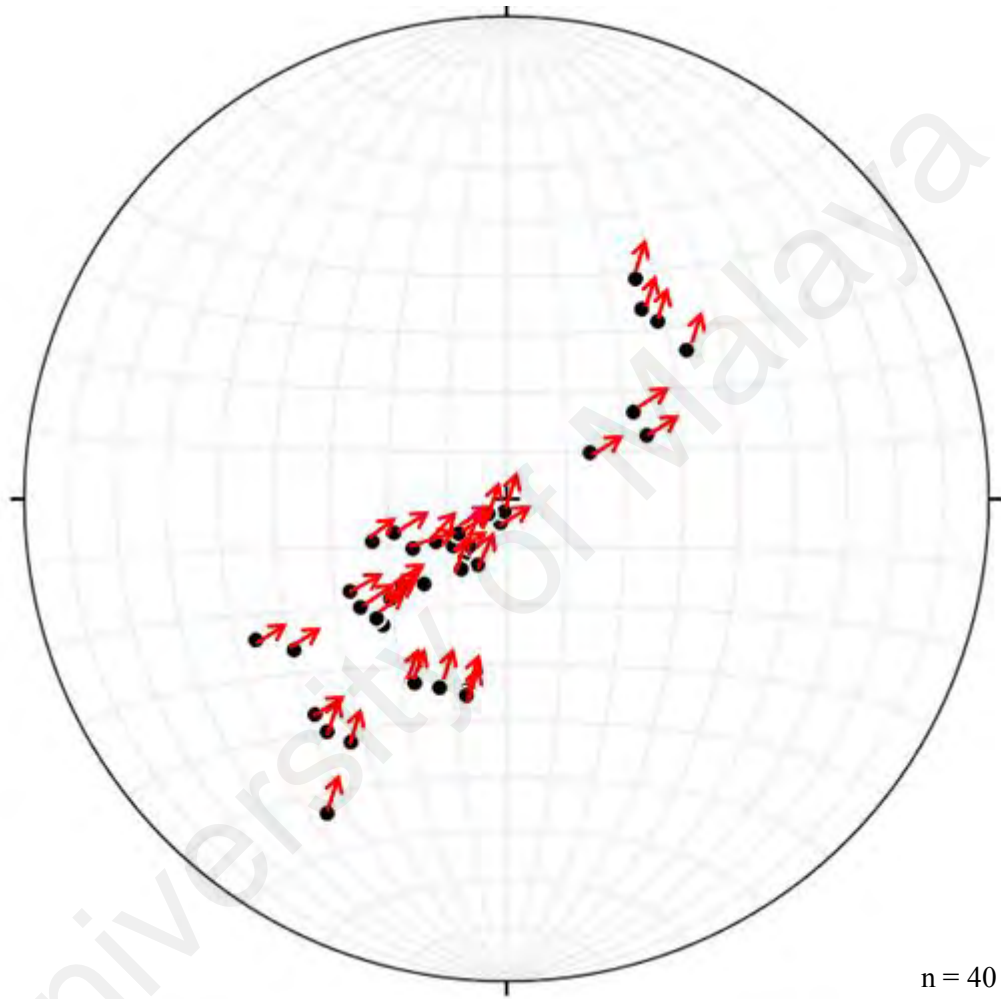


Figure 4.9: Equal area stereonet plot of lineations measurements with arrows indicating the movement of the hanging wall. (Note: point with no direction is due to uncertain movement direction).

4.6 Discussion

The only previous age determination of BTFZ was by Harun (2002) through K-Ar dating of flasered granite from Kajang-Kuala Klawang area which is located in Kuala Lumpur Fault Zone resulted in Late Cretaceous age (83.6 Ma). This study shows that the age of BTFZ using $^{40}\text{Ar}/^{39}\text{Ar}$ radiometric dating (92 Ma and 84 Ma) is closed to the age that recorded by Harun (2002).

Bignell and Snelling (1977) has recorded several similar age from granite samples from locations near the main BTFZ (Figure 2.2). They obtained K-Ar age of muscovite between 95 Ma and 143 Ma. Cottam *et al.* (2013) recorded age of granite east of Kuala Lumpur as Late Cretaceous (100 Ma) using biotite for $^{40}\text{Ar}/^{39}\text{Ar}$ dating. It was reported that in the K-Ar dating of granites of Peninsular Malaysia, the histogram of the data show maxima around 135 Ma and 85 Ma. The maximum ages are around upper Jurassic-lower Cretaceous were attributed by Bignell and Snelling (1977) to period of uplift, following the interpretation by Hutchison (1973a). However, it could also be caused by resetting of the age faulting events.

The mylonite zone exhibits many mesoscopic and microscopic features which can be used to determine the sense of shear during the brittle-ductile fault development. The stretching lineation records the preserved direction of maximum elongation that prevailed, at least, during the final stages of mylonitization.

The measured foliation surfaces of BTFZ are steeply dipping while the lineations are variable from steep plunge to nearly horizontal slip. This implies that the net slip of this subvertical fault zone is oblique. The strike-slip component is consistently dextral. However, both reverse and normal dip-slip components are recorded, with the former being dominant. The reverse-slip is recorded from SW dipping foliations, while normal-slip is related to NE dipping foliations. However, both reverse and normal slips give similar top-to the NE vergence. This indicates that the

BTFZ is a dextral top-to the E fault zone. The different dip-slip recorded is probably caused by change of dip direction of the steep fault zone, or due to the anatomosis of the broad fault zone (Figure 4.10).

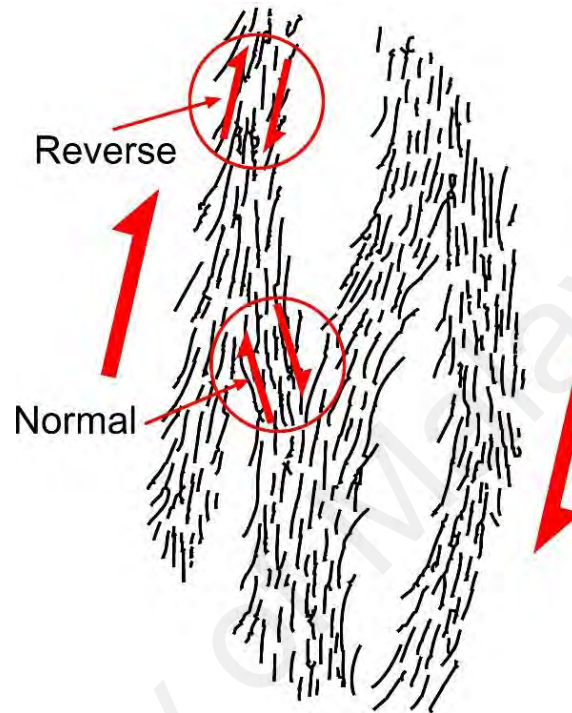


Figure 4.10: Schematic diagram of a steep reverse anatomosing shear zone. The dominant slip will be reversed but some normal-slip will also be present due to the change in dip direction. Both reverse and normal slip sections will have the similar vergence direction.

Moreover, the observations and thermochronological data also demonstrate that Peninsular Malaysia experienced several periods of exhumation during Late Cretaceous to early Paleogene and Eocene (Krahenbuhl, 1991; Cottam *et al.*, 2013). NNE-SSW strike-slip faults were formed during the same time (Mustaffa, 2000a), at the same time as intrusion of Kemahang Granite, Stong complex, Taku Schist and deformation of continental deposits (Shuib, 2009a). The study shows that BTFZ was formed during the Late Cretaceous. Recent studies in northern Peninsular Malaysia (Md Ali *et al.*, 2016, Francois *et al.*, in press) indicates 4 episodes of deformation (D1-D4), and the last top-to the SE deformation episode (D4) is believed to be a Late Cretaceous post-orogenic

detachment event. However, although the general vergence is similar, the BTFZ is steep and largely reverse, as opposed to the gentle extensional nature of the detachment, unless the BTFZ has been rotated by younger faults. The BTFZ may also be related to the ~ENE–WSW oriented contraction during renewed subduction along western Sunda margin (Hall *et al.*, 2011; Morley, 2012).

University of Malaya

CHAPTER 5: GEOCHEMICAL CHARACTERISATION OF THE MYLONITES

5.1 Introduction

Recent studies show that almost all major and many trace elements can be mobilized during mylonitization (Sinha *et al.*, 1986; Brewer and Atkin, 1989; O'Hara and Blackburn, 1989; Glazner and Bartley, 1991; Selverstone *et al.*, 1991; Condie and Sinha, 1996). The behavior of mobile and immobile elements is controlled by the types of metamorphic reactions involved within the shear zones and the nature of the fluid phase (Kerrick *et al.*, 1980; Marquer, 1989). Nevertheless, according to Vocke *et al.* (1987) and Dickin (1988), an experimental geochemical data may also permitted conflicting interpretations regarding element mobility within different metamorphic P-T conditions.

The purpose of this chapter is to document the chemical changes associated with the formation of retrograde fault zone, the Bukit Tinggi Fault Zone (BTFZ) in the Late Triassic granite exposed in the western part of the Main Range Granite (MRG).

5.2 XRF whole-rock element analysis

Table 5.1 and Table 5.2 present simplified raw elements data for protolith and granite mylonites of BTFZ. Chemical changes during deformation are investigated using X-Ray Fluorescence (XRF) analyses of major and trace elements in a representative suite of both protolith and mylonites samples. Data from whole rock chemical analyses only show relative changes in bulk rock chemical composition (Gresens, 1967). For example, if a fault rock experiences SiO₂ enrichment during silicification, it will show much lower concentrations of all other elements compared with its protolith (Streit and Cox, 1998). In order to eliminate this problem of 'relative abundance', the elemental concentrations in a fault rock have to be normalized to that

within the protolith (Jefferies, 2006). As protolith and mylonites in this study both contain high concentrations of SiO_2 and Al_2O_3 , variations in the concentrations of less abundant elements may not be apparent (Rollinson, 1993). Normalisation of mylonites samples to the protolith also addresses this problem since the amount of enrichment or depletion of each element in each mylonites can be calculated relative to the protolith. The full data is attached in Appendix B.

5.3 Major element composition of mylonites

Figure 5.1 presents mean raw data for protolith while Figure 5.2 shows mean raw data for mylonites. In the mylonites SiO_2 and Al_2O_3 dominate in all fault rocks reflecting the abundance of silicates such as quartz, feldspar and white mica. SiO_2 shows a marked wt% increase of close to 9% (from 68% in the protolith to 77% in mylonites). The mylonites have moderate Al_2O_3 content (11.4~14.6 wt%).

Table 5.1: Summary of concentration for major elements in protolith and mylonites.

Protolith													
Element	LOI	SiO ₂	Al ₂ O ₃	Fe ₂ O ₃	CaO	MgO	Na ₂ O	K ₂ O	MnO	TiO ₂	P ₂ O ₅	Cr ₂ O ₃	Ba
Range (wt %)	0.5-1.0	67.8-70.0	14.6-15.1	2.2-3.9	1.5-2.2	0.4-1.4	2.7-3.3	4.7-6.2	0.04-0.06	0.3-0.7	0.07-0.2	0.02-0.03	0.06-0.1
Average	0.8	68.9	14.9	3.1	1.9	1	2.9	5.2	0.05	0.5	0.2	0.02	0.08
SD	0.3	1	0.2	0.6	0.3	0.4	0.3	0.7	0.01	0.1	0.07	0.003	0.02
Protomylonite													
Element	LOI	SiO ₂	Al ₂ O ₃	Fe ₂ O ₃	CaO	MgO	Na ₂ O	K ₂ O	MnO	TiO ₂	P ₂ O ₅	Cr ₂ O ₃	Ba
Range (wt%)	0.4-0.9	69.6-77.3	11.6-14.6	1.1-2.8	0.4-2.0	0.1-0.6	2.8-3.5	4.7-6.3	0.02-0.05	0.1-0.5	0.02-0.1	0.02-0.03	0.01-0.07
Average	0.6	74.1	13	1.9	1	0.3	3.06	5.4	0.03	0.3	0.06	0.03	0.04
SD	0.12	2.2	0.9	0.4	0.4	0.1	0.2	0.5	0.01	0.09	0.02	0.005	0.02
Mesomylonite													
Element	LOI	SiO ₂	Al ₂ O ₃	Fe ₂ O ₃	CaO	MgO	Na ₂ O	K ₂ O	MnO	TiO ₂	P ₂ O ₅	Cr ₂ O ₃	Ba
Range (wt%)	0.8-0.9	74.1-76.3	11.5-13.2	2.0-2.2	0.5-1.0	0.2-0.2	2.4-3.1	5.1-5.5	0.03-0.04	0.2-0.3	0.05	0.02-0.04	0.03
Average	0.8	75.2	12.3	2.1	0.8	0.2	2.8	5.3	0.04	0.2	0.05	0.03	0.03
SD	0.02	1.6	1.2	0.2	0.4	0.007	0.5	0.3	0.007	0.05	0	0.01	0

Table 5.2: Summary of concentration for trace elements in protolith and mylonites.

	Protolith										
Element	Ga	Nb	Pb	Rb	Sr	Th	U	Y	Zn	Ba	Zr
Range (ppm)	17.6-22.0	13.3-18.0	9.5-23.8	269.5-552.4	87.5-130.7	25.0-61.0	7.1-16.5	30.4-51.3	40.0-64.0	556.0-1087.0	128.7-269.9
Average	20.2	15.6	15.1	378.3	112.1	36.2	12.7	36.2	54.8	742.3	198.3
SD	1.9	2	4.3	126	18.3	16.7	4	10.1	10.9	249.1	57.7
	Protomylonite										
Element	Ga	Nb	Pb	Rb	Sr	Th	U	Y	Zn	Ba	Zr
Range (ppm)	14.5-21.2	6.9-18.6	6.7-38.2	236.7-692.5	19.5-118.4	35.7-78.5	8.0-25.1	28.9-173.8	27.0-48.0	66.0-600.0	107.7-264.9
Average	17.4	12.7	19.9	380.4	62	56.5	15.2	54	34.7	304.2	198.4
SD	1.6	3.1	8.8	114.2	31.2	11	4.8	33.8	5.6	147	46.6
	Mesomylonite										
Element	Ga	Nb	Pb	Rb	Sr	Th	U	Y	Zn	Ba	Zr
Range (ppm)	15.0-16.7	13.2-18.4	7.8-12.8	373.7-425.5	35.2-52.6	55.8-80.2	16.3-20.9	24.0-58.8	27.0-38.0	196.0-259.0	186.3-226.1
Average	15.9	15.8	10.3	399.6	43.9	68	18.6	41.4	32.5	227.5	206.2
SD	1.2	3.7	3.5	36.6	12.3	17.3	3.3	24.6	7.8	44.5	28.1

A little variation of alkalis across the mylonite zones were shown by Na₂O ranges from 2.4~3.5 wt% and K₂O varies from 4.7~6.3 wt%. TiO₂ (0.1~0.5 wt%) and CaO (0.4~2.0 wt%) concentration are lower in mylonite than the protolith. The level of Fe₂O₃ (1.1~2.8 wt%) is low as well as MgO (0.1~0.6 wt%). Fe₂O₃ and MgO are fluctuated across the fault zone, with Fe₂O₃ present in higher proportions than MgO, but ratios of the two vary between each mylonites. Loss of ignition (LOI) is very low within 0.4-0.9 wt%. MnO, P₂O₅ and Cr₂O₃ concentration are very low (MnO is 0.02-0.05; P₂O₅ is 0.02-0.12; Cr₂O₃ is 0.02-0.036). Hence, their concentrations in all rocks are negligible. In general, these noteworthy changes in major oxide abundances are a reflection of the observed modal changes that are, in turn, a consequence of the mineralogical and textural changes attending the process of mylonitisation.

5.4 Trace element composition of mylonites

The raw data for both protolith and mylonites are given in Figures 5.3 and 5.4 respectively. All samples have higher concentration of Rb, Ba and Zr. Similarly, the trace element compositions exhibit significant variations, particularly in the case of Rb (236.7~692.5ppm), Ba (66-600ppm), Y (24~173.8ppm), Sr (19.5-118.4), high field-strength elements (HFSE) (Zr: 107.7~264.9ppm) and Pb (6.7-38.2 ppm). There are relatively low contents of Ga 14.5-21.2 ppm, Nb 6.9~18.6 ppm, Th 35.7-80.2 ppm, U 8-25.1 ppm and Zn 27-48 ppm.

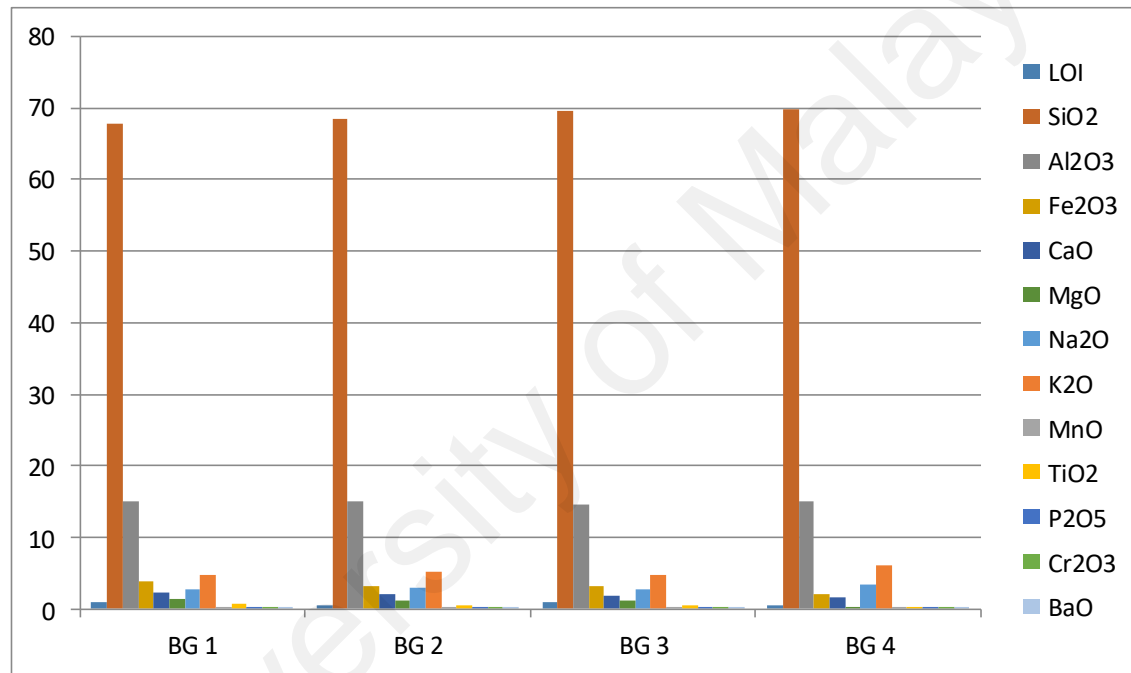


Figure 5.1: ICP-MS major element data in wt% unit for protolith. (BG= Biotite Granite).

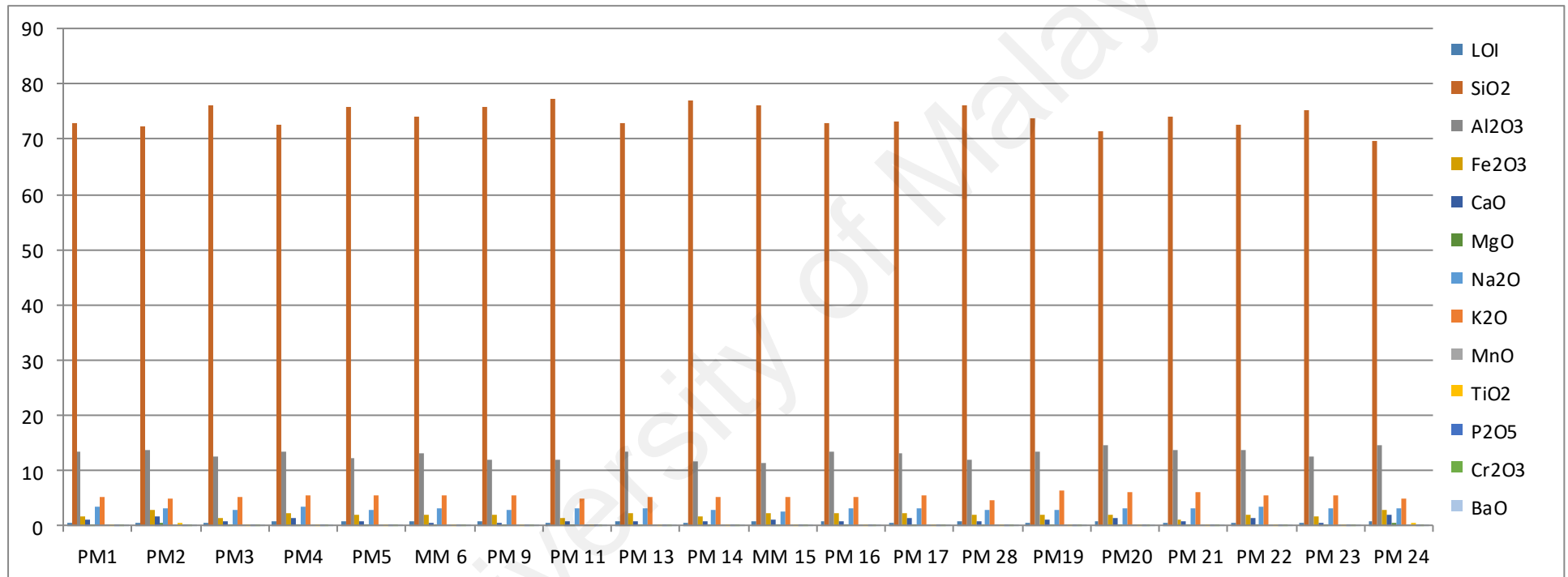


Figure 5.2: ICP-MS major element data in wt% unit for mylonites. (PM= Protomylonite, MM= Mesomylonite)

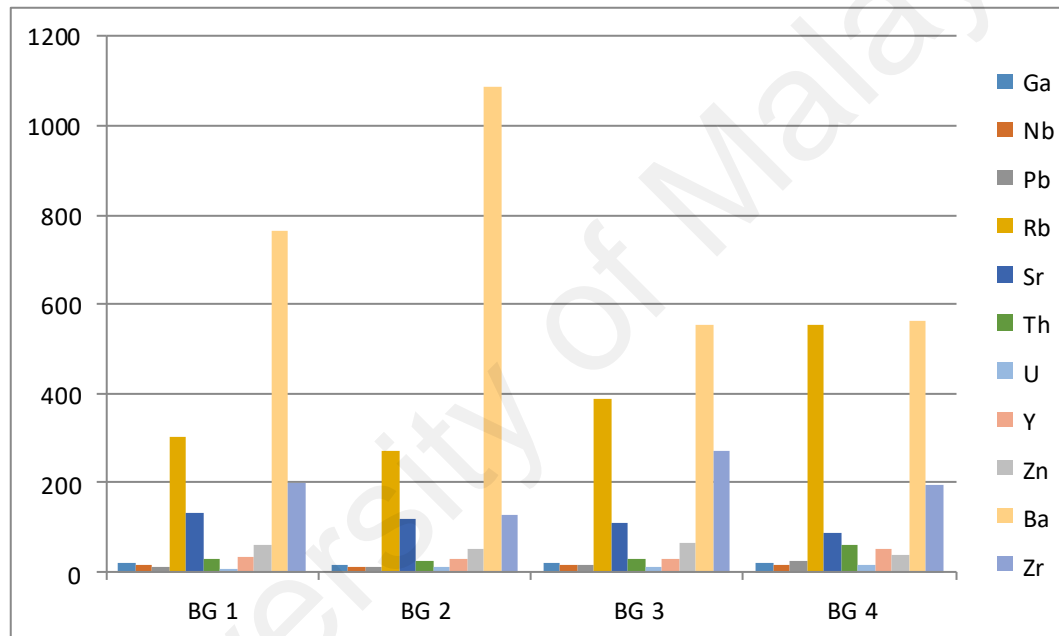


Figure 5.3: ICP-MS trace element data in ppm unit for protolith.

(BG= Biotite Granite).

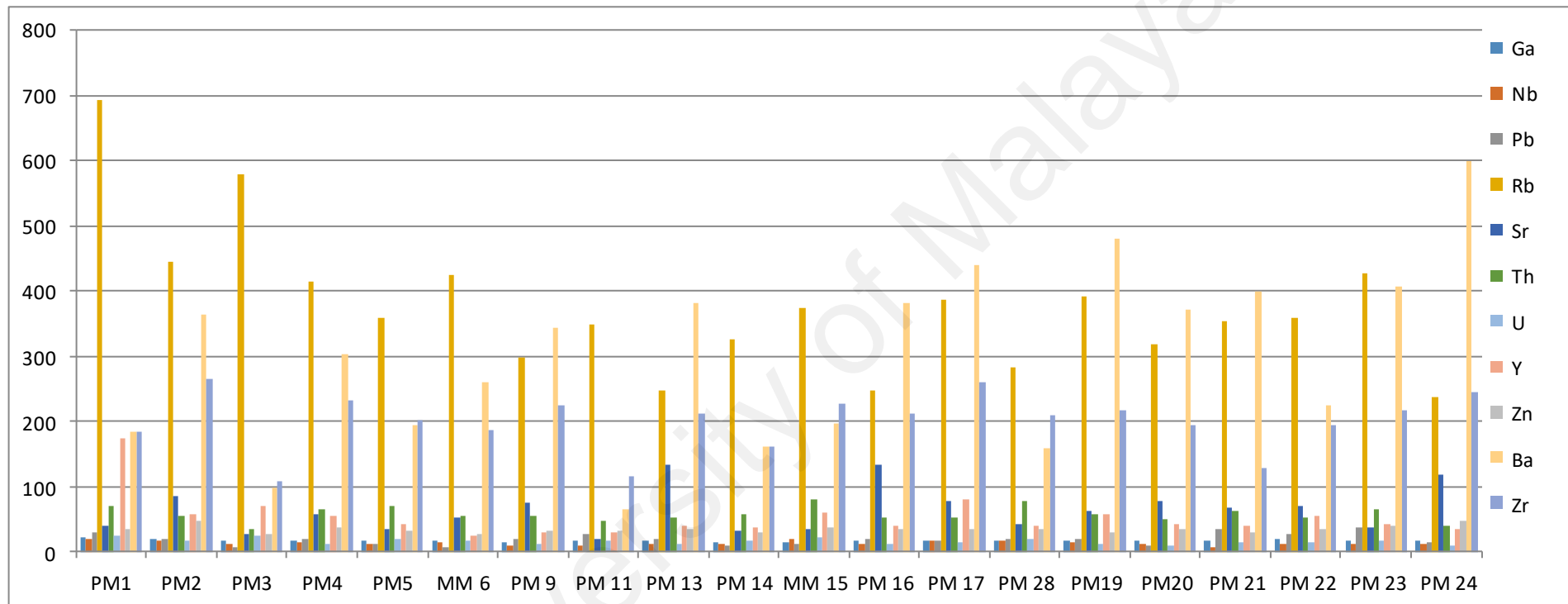


Figure 5.4: ICP-MS trace element data in ppm unit for mylonites.
 (PM = Protomylonite, MM = Mesomylonite)

5.5 Protolith-normalised major and trace element data

Major element distributions associated with the formation of mylonites in the Bukit Tinggi Fault zones are discussed below. For better visualization of enrichments and depletions of major elements, protolith-normalised major elements spider diagram graph were plotted in Figure 5.5.

From an inspection of the major element average values, the most significant change from granite to mylonite is that enrichment of SiO_2 . It shows a steady but consistent increase, suggesting that some silicification has taken place in the mylonite zone.

The Al_2O_3 remain nearly constant relative to the protolith with a slight depletion. As it remains nearly constant close to the protolith concentration, it suggests that Al_2O_3 behaved as an immobile element during deformation and alteration. According to Tobisch *et al.*, (1991), Al_2O_3 are useful for normalization because of their higher and more accurately determined concentrations.

Na_2O and K_2O , loss of ignition (LOI) and Cr_2O_3 concentration were erratic. For the most part, K_2O and Na_2O are leached during feldspar hydrolysis with Na decreasing more markedly than K_2O because of formation of muscovite/sericite.

TiO_2 and CaO concentration are lower and depleted in the mylonites from the protolith. The progressive depletion in CaO and noticeable fluctuation of Na_2O across mylonite zone are corroborated by the progressive disappearance of plagioclase with deformation. The depleted CaO in the mylonite relative to the protolith may also be due to recrystallization of oligoclase to albite (Bialek, 1999).

Fe_2O_3 and MgO are depleted across the fault zone, with Fe_2O_3 present in higher proportions than MgO, but ratios of the two vary between each sample. The reductions in MgO, Fe_2O_3 and CaO whilst increases in K_2O and Na_2O may reflect alteration of mafic-type minerals, such as biotite to chlorite coupled with breakdown of plagioclase

to white mica (Jefferies, 2006). Widespread alterations of biotite to chlorite as well as increasing of albite and white mica are observed. MnO and P₂O₅ concentration are also depleted, although not so significant with progressive strain.

Figure 5.6 presents whole rock trace element analyses for mylonite across the fault zone, presented in the same format as major element data in Figure 5.5. They show a greater divergence from protolith concentrations produce a saw-tooth pattern across the fault zone.

In the profile, Th shows enrichment. While Nb, Pb, Rb, Sr, U, Y and Zr elements were erratic. Zn, Ba and Ga are depleted relative to the protolith.

University of Malaya

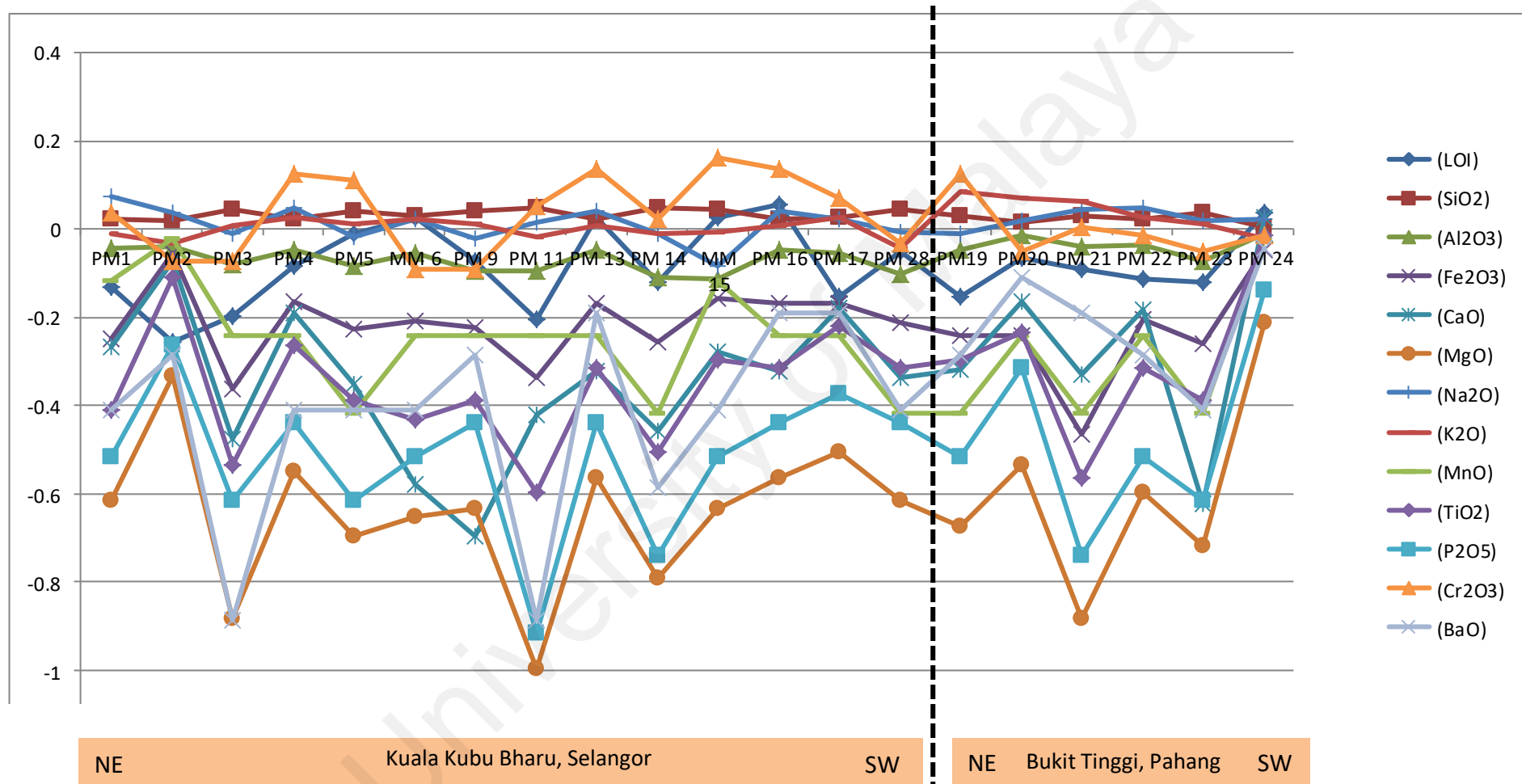


Figure 5.5: Protolith-normalised major element geochemical transects the BTFZ from NE to SW. (PM= Protomylonite, MM= Mesomylonite)

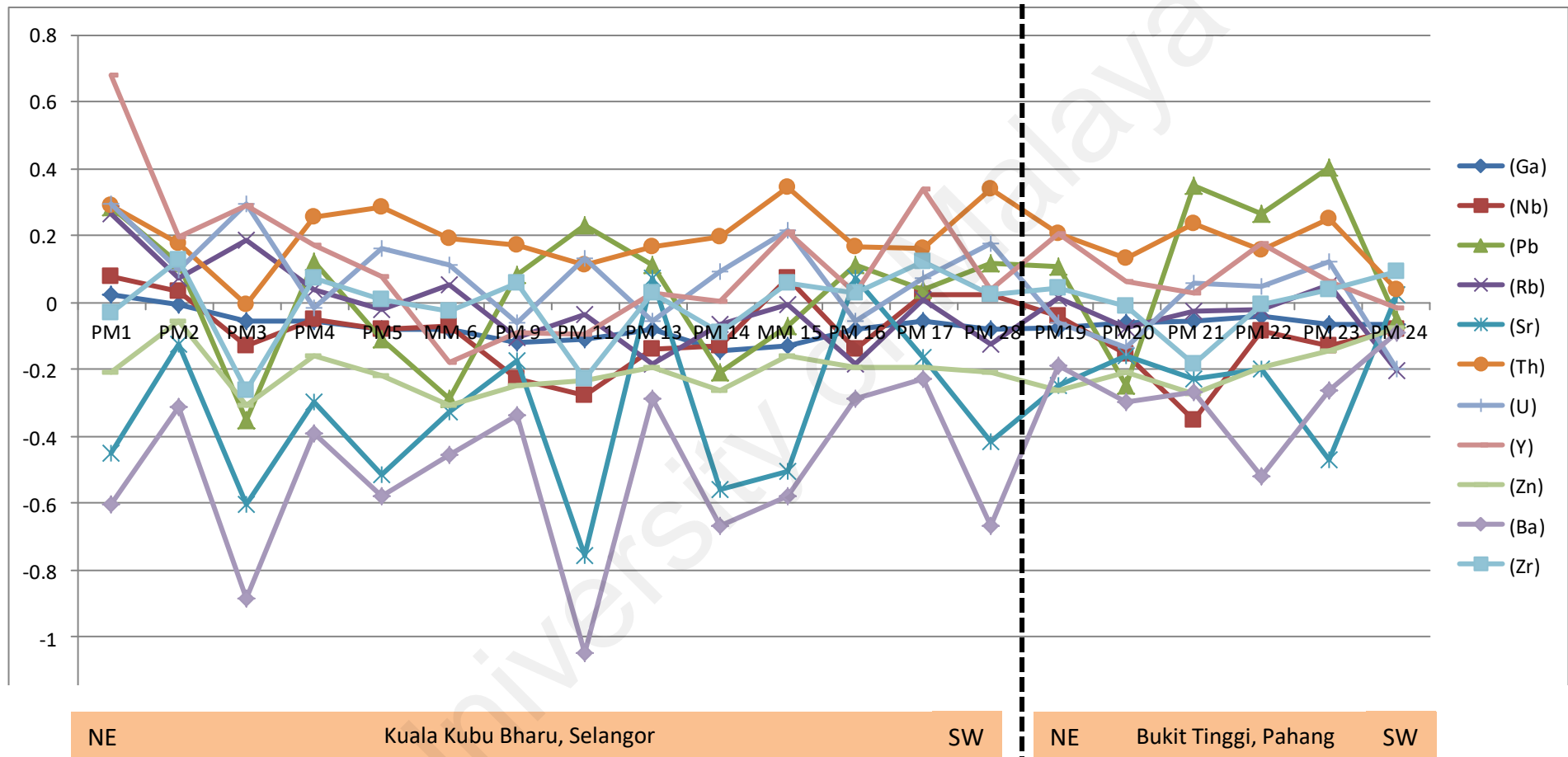


Figure 5.6: Protolith-normalised trace element geochemical transects the BTFZ from NE to SW.
 (PM= Protomylonite, MM= Mesomylonite)

The 'saw-tooth' spider diagram of normalized whole-rock trace elements suggest transverse migration of components has taken place across the fault zone (Hippertt, 1998), particularly applies to mobile elements such as Pb, Rb, Sr and U. However, as other trace elements are largely considered to be immobile, it may be that migration of major elements (Si, K, Na) between fault rocks produce a 'relative abundance' effect resulting in the observed profile (Hippert, 1998). Sr follows the geochemical behaviour of Ca and is depleted during plagioclase breakdown. The loss of Ba, Sr as well as Rb during deformation is mainly explained by the transformation of biotite into chlorite and also by observed K-feldspar and plagioclase breakdown and increase of white mica (Neiva *et al.*, 1987).

Noteworthy, the pattern of CaO, K₂O, Ba, Rb and Sr (fig 5.5 and 5.6) is irregular. This change is most probably due to the elements behaviour which is accompanied by change in the dominant deformation mechanisms operative in the mylonites and evidence for recrystallization by progressive misorientation of limited feldspar subgrains. Sericitization and chloritization indicated the fluid migration in the fault zone.

5.6 Discussion

The chemical changes noted from the whole-rock major and trace element data above are a reflection of the noticeable mineralogical and textural changes in mylonites. However, this is only reliable if one protolith is involved in fault zone deformation. A mixture of two different protoliths will give an average composition of both components and thus produce misleading results with regards to the degree of alteration.

Slight enrich in SiO₂ relative to the protolith may correspond to a zone of preferential silicification. Quartz veins have been identified in the mylonites, but are not widespread. The latter can be attributed to the local migration of in-situ SiO₂ rich fluids

that are derived from the breakdown of feldspars during mylonitization (Bryant, 1966; Dixon and Williams, 1983; O'Hara, 1988; O'Hara and Blackburn, 1989; Newman and Mitra, 1993) and the SiO₂ rich fluids derived from the dewatering of sedimentary/metasedimentary rocks (Newman and Mitra, 1993) nearby.

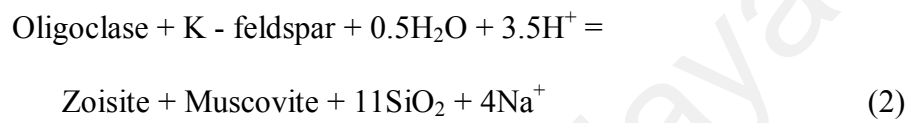
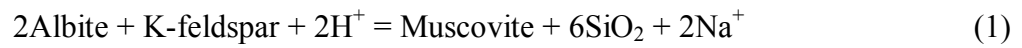
The data has highlighted the progressive breakdown of the stages in the protolith due to Na- and K-metasomatism (e.g. K-feldspar to albite) and growth of new, weaker mineral phases (e.g. white mica and chlorite) at different level during fault rock (in particular mylonites) development (Jefferies, 2006). Potassium fluctuates suggesting that more K-feldspars changed into muscovites during the entire mylonitization process (Kwon, 2009).

The depleted CaO in the mylonite relative to the protolith is probably due to recrystallization of oligoclase to albite (Bialek, 1999). The depletion of calcium can also be explained by exchange reaction during recrystallization of oligoclase or andesine to albite.

The large reductions in MgO, Fe₂O₃ and CaO whilst varies in K₂O and Na₂O may reflect alteration of mafic-type minerals, such as biotite, coupled with breakdown of Ca-rich feldspar to albite and white mica (Jefferies, 2006). Progressive alteration of biotite to chlorite and increasing of albite and white mica aided by the fracturing observed and fluid infiltration within the fractures in mylonites.

The 'saw-tooth' form and greater spread of normalized whole-rock trace elements suggest that transverse migration of components has taken place across the fault zone (Hippert, 1998), particularly applies to mobile elements such as Pb, Rb, Sr and U. However, as other trace elements are largely considered to be insoluble and therefore immobile it may be that migration of major elements (Si, K, Na) between fault rocks produce a 'relative abundance' effect resulting in the observed profile above (Hippert, 1998).

The marked loss of Ba, Sr as well as Rb during deformation is mainly explained by the transformation of biotite into chlorite and also by observed K-feldspar and plagioclase breakdown and increase of white mica (Neiva *et al.*, 1987). Feldspar breakdown could occur according to one or more of the following reactions (O'Hara & Blackburn, 1989):



University of Malaya

CHAPTER 6: SUMMARY AND CONCLUSION

6.1 Summary

6.1.1 Characteristics of the Bukit Tinggi Fault Zone (BTFZ)

The Bukit Tinggi Fault Zone is a major fault zone demarcated by sub-parallel NW-SE lineaments that transects the western flank of Main Range Granite, Peninsular Malaysia. It is sub-vertical and dipping to both the SW and NE.

The fault zone is characterized by strongly deformed granites, with mylonitic textures which has a thickness up to about 5 km wide to the east of Kuala Lumpur area. The strain distribution in this sheared zone is variable on a local scale, forming rocks ranging from protomylonite to ultramylonite.

The trend of foliations in the mylonites is NW-SE subparallel to the Bukit Tinggi Fault Zone orientation. The lineations are plunging at various angles towards 190° -254° for the SW dipping foliations with dextral-reverse slip and towards 030° - 065° for the NE dipping foliations with dextral-normal slip. The vergence, however is consistently towards the NE.

The result from the $^{40}\text{Ar}/^{39}\text{Ar}$ dating of the secondary/recrystallized biotite from the mylonites gives a plateau age of 92.4 ± 0.8 Ma and 84.3 ± 0.8 Ma respectively. This indicates that the ductile deformation episode of BTFZ happened during the Late Cretaceous (Santorian to Turonian).

6.1.2 Characteristics of the mylonites

The protolith here is known as Bukit Tinggi granite. It is a medium to coarse-grained biotite granite, with hypidiomorphic granular texture and tabular or oval K-feldspar megacrysts. The biotite granite deforms along the Bukit Tinggi Fault Zone

resulted in the formation of protomylonite, minor mesomylonite and rare bands of ultramylonite.

Protomylonite is medium to coarse-grained, porphyroclastic and shows two sets of foliations (C/S surfaces). The foliation is identified by preferred orientation of tabular to ellipsoidal feldspar porphyroclasts especially K-feldspar, elongated quartz grains and some mica strings. The feldspar clasts are fractured, has undulatory extinction and minor recrystallization. Quartz forms elongated grains with strong undulose extinction and elongated recrystallized aggregates. Biotite shows bending, recrystallization and are often chloritized.

The mesomylonite has distinct preferred orientation of small elongated porphyroclasts, particularly the K-feldspar porphyroclasts, enclosed by dark grey fine foliated matrix. The S-surfaces are demarcated by preferred orientation of porphyroclasts, elongated recrystallized quartz grains and elongated feldspar clasts. The C-surfaces generally form dark-coloured continuous shear bands that are rich in biotite, have finer grain size and more intensely recrystallized, that cut the S-surfaces.

Ultramylonite is dark grey to black in colour with scarce porphyroclasts appear as fine white and grey specks a few mm in diameter. The foliation is defined by alternating dark and light coloured bands and in the mesoscopic scale only one set of foliation is observed. Under the microscope, C-surfaces are defined by distinct compositional banding, while the S-surfaces by preferred orientation of elongated clasts and recrystallized quartz.

The degree of recrystallization of quartz increases from protomylonite to mesomylonite and ultramylonite. In the protomylonite and mesomylonite, relict quartz form elongated grains and ribbons with undulose extinction, deformation bands and subgrains. Recrystallization is mainly by subgrain rotation (SGR). Quartz in the

ultramylonite is complete recrystallized. The microstructures of quartz indicate a ductile behaviour.

There are many microcracks in the feldspars, which produce angular grain fragments, microfaults, and antithetic bookshelf fractures, often along cleavages. The main mechanism of reduction in size of feldspar is the comminution of feldspar grains by fracturing and microcracking. The dominance of these deformed microstructures to recrystallization reflects the largely brittle behaviour of K-feldspar. Recrystallization is limited in feldspars and characterized by lobate boundary and associated fine elongated feldspar neocrysts indicating bulging recrystallization (BLG) mechanism.

The existent of undulatory extinction, bending, and kinking of biotite and muscovite is common, and recrystallization is also observed. These deformation features reflect the ductile behaviour of mica.

The ductile behaviour of quartz and mica and largely brittle behaviour of feldspars indicate that the mylonites of the BTFZ were formed in the brittle-ductile transition zone. The deformation temperature is ranging from 300°C to a maximum temperature of about 500°C.

6.1.3 Kinematic analysis of the mylonites

Mesosopic and microscopic kinematic analysis was carried out to determine the tectonic mobility during the deformation of BTFZ. Observations are made parallel to the lineation and perpendicular to the foliation. The mesoscopic features include S-C fabrics and porphyroclasts. In the microscopic scale, S-C fabric, oblique foliation, σ -porphyroclast, mica fish, fragmented book-shaped porphyroclast are common kinematic indicators found in mylonites of BTFZ.

The measured foliation surfaces of BTFZ are steeply dipping while the lineations are variable from steep plunge to nearly horizontal slip. Results of kinematic

analysis show that the strike-slip component is dextral. However, both reverse and normal dip-slip components are recorded, with the former being dominant. The reverse-slip is recorded from SW dipping foliations, while normal-slip is related to NE dipping foliations. However, both reverse and normal slips give similar top-to-NE vergence. This indicates that the BTFZ is a dextral top-to-NE fault zone. The different dip-slip recorded is probably caused by change of dip direction of the steep fault zone, or due to the anatomosis of the broad fault zone with different fault branches having different dip directions.

6.1.4 Deformation related chemical changes

The most significant change for major elements from granite to mylonite is the slight enrichment of SiO_2 in the mylonites. The Al_2O_3 remain nearly constant relative to the protolith with a slight depletion. Na_2O and K_2O , loss of ignition (LOI) and Cr_2O_3 concentration were erratic. For the most part, K_2O and Na_2O are leached during feldspar hydrolysis with Na decreasing more markedly than K_2O .

TiO_2 and CaO concentration are lower and depleted in the mylonites from the protolith. Fe_2O_3 and MgO are depleted across the fault zone, with Fe_2O_3 present in higher proportions than MgO, but ratios of the two vary between each sample. MnO and P_2O_5 concentration are also depleted, although not so significant with progressive strain.

The trace elements show a greater divergence from protolith concentrations produce a saw-tooth pattern across the fault zone. The element Th shows enrichment while Zn, Ba and Ga are depleted relative to the protolith. Trends of Nb, Pb, Rb, Sr, U, Y and Zr elements are erratic.

The enrichment of SiO_2 may be caused by preferential silicification from in-situ SiO_2 rich fluids derived from the breakdown of feldspars during mylonitization or the

SiO₂ rich fluids derived from the dewatering of sedimentary/metasedimentary rocks nearby.

Fault has slightly affected the geochemical content in granite as shown by the mylonites. The reductions in MgO, Fe₂O₃ and CaO and variable K₂O and Na₂O trends reflect alteration of mafic-type minerals, such as biotite, coupled with breakdown of Ca-rich feldspar to albite and white mica. The reduction of Ba, Sr and Rb is mainly explained by the transformation of biotite into chlorite and breakdown of K-feldspar and plagioclase to white mica.

6.2 Conclusion

The Bukit Tinggi Fault Zone is a steeply dipping and NW-SE trending fault zone that cut the Main Range Granite from Kuala Kubu Bharu, Selangor through Bukit Tinggi, Pahang down to Kuala Kelawang, Negeri Sembilan. Biotite granite of the Bukit Tinggi pluton is sheared into a broad zone of granite mylonites along the fault zone, consisting of mainly protomylonite, minor mesomylonite and rare ultramylonite. Late Cretaceous ages (84.3 Ma and 92.4 Ma) of deformation were obtained from ⁴⁰Ar/³⁹Ar dating.

Microscopic studies indicate that quartz and mica behave in a ductile manner, while feldspars are largely brittle during deformation. The mylonites are thus formed in the brittle-ductile transition zone. The microstructures of the minerals also indicate that the deformation occurred between 300°C and 500°C. Taking the average geothermal gradient of 30°/km, this corresponds to a depth of about 10 km to 17 km.

The foliations and lineations attitude shows that the BTFZ is an oblique slip fault. Abundant mesoscopic and microscopic kinematic indicators are present in the mylonite, including S-C fabric, σ -porphyroclast, oblique foliation, mica fish and offset

fractured clasts. The strike-slip component is dextral. Both reverse and normal dip-slip components are recorded, but the vergence is towards approximately the East.

Mylonitisation has affected the major element concentrations of the fault rocks relative to the protolith. Slight enrichment of SiO_2 may be caused by preferential silicification of mylonites by SiO_2 rich fluids from in-situ or nearby sources. SiO_2 can be derived from the breakdown of feldspars during mylonitization. TiO_2 , CaO , Fe_2O_3 , MgO , MnO and P_2O_5 are reduced relative to the protolith, while the trends of K_2O and Na_2O are inconsistent, and Al_2O_3 remain nearly constant. The reduction is probably due to alteration biotite coupled with breakdown of Ca-rich feldspar to albite and white mica.

University of Malaya

REFERENCES

- Abdullah, I. (1996). Struktur Geologi Konglomerat Murau. *Geological Society of Malaysia Warta Geologi*, 22, 186.
- Abdullah, I., Jasin, B., Jantan, A., Samsudin, A. R. & Said, U. (1989). The Semanggol Formation post Semanggol structures and their significance to regional geology. *Geological Society of Malaysia Warta Geologi*, 15, 28-29.
- Alexander, J. B., & Procter, W. D. (1955). *Investigations upon a proposed dam-site at Klang Gates, Federation of Malaya (5)*. Malaysia: Overseas geology and mineral resources.
- Alexander, J. B., & Procter, W. D. (1965). *Geological map of Peninsular Malaya, 6th edition (Diamond Jubilee), 1,500,000*. West Malaysia: Geological Survey Department.
- Almashoor, S. S., & Tjia, H. D. (1987). A prominent fault across the Malaysia - Thai boundary; preliminary report. *Geological Society of Malaysia Warta Geologi*, 13, 35-37.
- Aw, P. C. (1990). *Geology and mineral resources of the Sungai Aring area, Kelantan Darul Naim*. Kelantan: Geological Survey of Malaysia District Memoir.
- Babaie, H. A., & LaTour, T. E. (1998). *Semi-brittle deformation and cataclastic flow of hornblende-quartz rock in a ductile shear zone. Fault related rocks—a photographic atlas*. New Jersey: Princeton University Press.
- Bell, I. A., Wilson, C. J. L., McLaren, A. C., & Etheridge, M. A. (1986b). Kinks in mica, role of dislocations and (001) cleavage. *Tectonophysics*, 127, 49–65.
- Bell, T. H. (1998). *Recrystallisation of biotite by subgrain rotation*. In, Snoke A, Tullis J, Todd VR (eds) *Fault related rocks – a photographic atlas*. New Jersey: Princeton University Press.
- Berthé, D., Choukroune, P., & Jegouzo, P. (1979a). Orthogneiss, mylonite and non-coaxial deformation of granites, the example of the South Armorican Shear Zone. *Journal of Structural Geology*, 1, 31-42.
- Bialek, D. (1999). Chemical changes associated with deformation of granites under greenschist facies conditions, the example of the Zawidow Granodiorite (SE Lusation Granodiorite Complex, Poland). *Tectonophysics*, 303, 251-261.
- Bignell, J., & Snelling, N. J. (1977). K–Ar ages on some basic igneous rocks from peninsular Malaysia and Thailand. *Geological Society of Malaysia Bulletin*, 8, 89-93.
- Boullier, A. M. (1980). A preliminary study on the behavior of brittle minerals in a ductile matrix, example of zircons and feldspars. *Journal of Structural Geology*, 2, 211-217.

- Brewer, T. S., & Atkin, B. P. (1989). Elemental mobilities produced by low-grade metamorphic events. A case study from the Proterozoic supracrustals of southern Norway. *Precambrian Research*, 45, 143–158.
- Brodie, K. H., & Rutter, E. H. (1985). On the relationship between deformation and metamorphism with special reference to the behaviour of basic rocks. In Thompson, A. B., & Rubie, D.C.. *Advances in Physical Geochemistry (2)* (pp. 138-179). New York Berlin Heidelberg Tokyo: Springer-Verlag.
- Brodie, K., Fettes, D., Harte, B., & Schmid, R. (2007). Structural terms including fault rock terms. In Fettes, D. J., Desmons, J., & Arkai, P. *Metamorphic rocks: a classification and glossary of terms: recommendations of the International Union of Geological Sciences Subcommission on the Systematics of Metamorphic Rocks* (pp 1-14). Edinburgh: Cambridge University Press.
- Bryant, B. (1966). Formation of phyllonites in the Grandfather mountain area, northeast North Carolina. *U.S. Geological Survey Professional Paper*, 550-D, 1444150.
- Burley, A. J. & Othman, J. (1990). A gravity survey of Perlis, Kedah and Penang. *Geological Society of Malaysia Bulletin*, 26, 13-20.
- Burton, C. K. (1965). Wrench faulting in Malaya. *The Journal of Geology*, 73, 781-798.
- Cobbing, E. J., & Mallick, D. I. J. (1987). *South-East Asia granite project. Field report for Peninsular Malaysia*. Keyworth: British Geological Survey.
- Cobbing, E. J., Pitfields, P. E. J., Darbyshire, D. P. F., & Mallick, D. I. J. (1992). *The granites of the South-East Asian tin belt (10)*. London: Overseas Memoir of the British Geological Survey.
- Condie, K. C., & Sinha, A. K. (1996). Rare earth and other trace element mobility during mylonitization, a comparison of the Brevard and Hope Valley shear zones in the Appalachian Mountains, USA. *Journal of Metamorphic Geology*, 14, 213-226.
- Cottam, M., Hall, R., & Ghani, A. A. (2013). Late Cretaceous and Cenozoic tectonics of the Malay Peninsula constrained by thermochronology. *Journal of Asian Earth Sciences*, 76, 241-257.
- Dickin, A. P. (1988). Evidence for limited REE leaching from the Roffna Gneiss, Switzerland - a discussion of the paper by Vocke *et al.* (1987) (CMP95, 145–154). *Contributions to Mineralogy and Petrology*, 99, 273–275.
- Dixon, J., & Williams, G. (1983). Reaction softening in mylonites from the Arnaboll thrust Sutherland. *Scottish Journal of Geology*, 19, 157-168.
- Drury, M. R., & Urai, J.L. (1990). Deformation-related recrystallization process. *Tectonophysics* 172, 235–253.

- Duebendorfer, E. M., & Christensen, C. H. (1998). *Plastic-to-brittle deformation of microcline during deformation and cooling of a granitic pluton. Fault-Related Rocks A Photographic Atlas*. Princeton, Princeton University Press.
- Etheridge, M. A., & Wilkie, J. C. (1979). Grainsize reduction, grain boundary sliding and the flow strength of mylonites. *Tectonophysics*, 58, 159–178.
- Faleiros, F. M., da Cruz Campanha, G. A., da Silveira Bello, R. M., & Fuzikawa, K. (2010). Quartz recrystallization regimes, c-axis texture transitions and fluid inclusion reequilibration in a prograde greenschist to amphibolite facies mylonite zone (Ribeira Shear Zone, SE Brazil). *Tectonophysics*, 485(1), 193–214.
- Francois, T., Md Ali, M. A., Matenco, L., Willingshofer, E., Ng, T. F., Taib, N. I., & Shuib, M. K. (in press) Late Cretaceous extension and exhumation of the Stong Complex and Taku Schist, NE Peninsular Malaysia, *Journal of Asian Earth Sciences*.
- Gates, A. E., & Glover, L. (1989). Alleghanian tectono-thermal evolution of the dextral transcurrent hylas zone, Virginia Piedmont, USA. *Journal of Structural Geology*, 11, 407–419.
- Ghani, A. A., Searle, M. P., Robb, L., & Chung, S. L. (2013). Transitional I S type characteristic in the Main Range Granite, Peninsular Malaysia. *Journal of Asian Earth Sciences*, 76, 225–240.
- Glazner, A. F., & Bartley, J. M. (1991). Volume loss, fluid flow and state of strain in the extensional mylonites from the central Mojave Desert, California. *Journal of Structural Geology*, 5, 587–594.
- Gobbett, D. J. (1965a). The Lower Palaeozoic rocks of Kuala Lumpur, Malaysia. *Federation Museums Journal*, 9, 67–79.
- Gottstein, G., & Mecking, H. (1985). *Recrystallization*. In, Wenk HR (ed) *Preferred orientation in deformed metals and rocks – an introduction to modern texture analysis*. New York, Academic Press.
- Gresens, R. L. (1967). Composition-volume relationships of metasomatism. *Chemical Geology*, 2, 47–65.
- Gundersen, L. C. S., & Gates, A. E. (1995). Mechanical response, chemical variation, and volume change in the Brookneal and Hylas shear zones, Virginia. *Journal of Geodynamics*. 19, 231–252.
- Hadizadeh, J., & Tullis, J. (1992). Cataclastic flow and semi-brittle deformation of anorthosite. *Journal of Structural Geology*, 14(1), 57–63.
- Hall, R. (2011). Australia–SE Asia collision, plate tectonics and crustal flow. *Geological Society London Special Publications* 355, 75–109.
- Hanmer, S., & Passchier, C. W. (1991). Shear sense indicators, a review. *Geological Survey of Canada Paper*, 90, 1–71.

- Harun, Z. (1994). Zon Sesar Alur Lebey (The Alur Lebey Fault Zone). *Geological Society of Malaysia Warta Geologi*, 20, 219-220.
- Harun, Z. (2002). Late Mesozoic Early Tertiary Faults of Peninsular Malaysia. *Geological Society Malaysia Bulletin*, 45, 117-120.
- Hippertt, J. (1998). Breakdown of feldspar, volume gain and lateral mass transfer during mylonitization of granitoid in a low metamorphic grade shear zone. *Journal of Structural Geology*, 20(2), 175-193.
- Hippertt, J. F., & Hongn, F. D. (1998). Deformation mechanisms in the mylonite/ultramylonite transition. *Journal of Structural Geology*, 20, 1435–1448.
- Hobbs, B. E., Means, W. D., & Williams, P. F. (1976). *An outline of structural geology*. New York, Wiley.
- Hongn, F. D., & Hippertt, J. F. M. (2001). Quartz crystallographic and morphologic fabrics during folding/transposition in mylonites. *Journal of Structural Geology* 23, 81–92.
- Hutchison, C.S. (1973a). *Volcanic activity*. In, Gobbett, D.J. & Hutchison, C.S. (eds). *Geology of the malay Peninsula*. New York, Wiley Interscience.
- Ingamells, C.O., & Engels, J.C. (1976). Preparation, analysis and sampling constants for a biotite. *National Bureau of Standards Special Publication*, 422, 401–419.
- Jaroslow, G. E., Hirth, G., & Dick, H. J. B. (1996). Abyssal peridotite mylonites, implications for grain-size sensitive flow and strain localization in the oceanic lithosphere. *Tectonophysics*, 256, 17-37.
- Jefferies, S. P. (2006). *Microstructural and geochemical processes in long-lived reactivated crustal-scale fault zones, A case study from the Median Tectonic Line, SW Japan*. Durham: Durham University.
- Ji, S. (1998a). Deformation microstructure of natural plagioclase. In, Snoke A, Tullis J, Todd VR (eds). *Fault related rocks – a photographic atlas*. New Jersey: Princeton University Press.
- Ji, S. (1998b). *Kink bands and recrystallization in plagioclase*. In, Snoke A, Tullis J, Todd VR (eds) *Fault related rocks – a photographic atlas*. New Jersey, Princeton University Press.
- Kerrich, R., Allison, I., Barnett, R. L., Moss, S., & Starkey, J. (1980). Microstructural and chemical transformations accompanying deformation of granite in a shear zone at Mieville, Switzerland; with implications for stress corrosion cracking and superplastic flow. *Contributions to Mineralogy and Petrology*, 73(3), 221-242.
- Krahenbuhl, A. (1991). Magmatism, tin mineralization and tectonics of the Main Range. *Geological Society of Malaysia Bulletin*, 29, 1-100.

- Kronenberg, A. K. (1994). Hydrogen speciation and chemical weakening of quartz. In, Heaney PJ, Prewitt CT, Gibbs GV (eds) *Silica, physical behavior, geochemistry, and materials applications. Mineralogical Society of America Reviews in Mineralogy*, 29,123–176.
- Kruhl, J. L. (1986). Textures and C-axis orientations of deformed quartz crystals from porphyritic dykes of the Alpine Root Zone (Western Alps). *International Journal of Earth Sciences*, 75, 601-623.
- Kwon, S., Park, Y., Park, C., & Kim, H. S. (2009). Mass-balance analysis of bulk-rock chemical changes during mylonitization of a megacryst-bearing granitoid, Cheongsan shear zone, Korea. *Journal of Asian Earth Sciences*, 35(6), 489-501.
- Lee, A. K. (1990). *The Geology and mineral resources of the Hulu Lepar area, Pahang*. Malaysia: Geological Survey of Malaysia District Memoir.
- Lee, C. P. (2004). Part 1 Paleozoic. In, Lee, C.P., Leman, M.S., Hassan, K., Nasib, B.M. & Karim, R. (eds). *Stratigraphic Lexicon of Malaysia*. Malaysia: Geological Society of Malaysia.
- Liew, T. C. (1983). *Petrogenesis of the Peninsular Malaysian Granitoid Batholiths*. (Unpublished Doctoral of Philosophy Thesis). Canberra: Australian National University.
- Liew, T., & Page, R. (1985). U-Pb zircon dating of granitoid plutons from the West Coast Province of Peninsular Malaysia. *Journal of the Geological Society*, 142(3), 515-526.
- Lister G. S., & Snoke, A. W. (1984). S-C Mylonites. *Journal of Structural Geology*. 6(6), 617-638.
- Lloyd, G. E., & Freeman, B. (1994). Dynamic recrystallisation of quartz and quartzites. *Journal of Structural Geology*, 16, 867–881.
- Luan, F. C., & Paterson, M. S. (1992). Preparation and deformation of synthetic aggregates of quartz. *Journal of Geophysical Research*, 97, 301–320.
- M.R., De Bresser, J.H.P., Pennock, G.M. (Eds.), Deformation Mechanisms, Rheology and Tectonics, Current Status and Future Perspectives. *Geological Society of London Special Publication*, 200, 171–190.
- Macdonald, S. (1968). *The geology and Mineral resources of north Kelantan and north Terengganu (10)*. West Malaysia: Geological Survey West Malaysia District Memoir.
- Mahendran, G., Shuib, M. K., & Raj, J. K. (1991). The stratigraphy of the Batu Arang area [abstract], *Geological Society of Malaysia Warta Geologi*, 17, 166.
- Mares, V. M., & Kronenberg, A. (1993). Experimental deformation of muscovite. *Journal of Structural Geology*, 15(9), 1061-1075.

- Mares, V. M., & Kronenberg, A. K. (1993). Experimental deformation of muscovite. *Journal of Structural Geology*, 15(9-10), 1061-1075.
- Marquer, D. (1989). Transfert de matie`re et de`formation des granitoides - aspects me`thodologiques. *Swiss Bulletin of Mineralogy and Petrology*, 69, 13-33.
- Md Ali, M. A., Willingshofer, E., Matenco, L., Francois, T., Daanen, T. P., Ng, T. F., Taib, N. I., & Shuib, M. K. (2016). Kinematics of post-orogenic extension and exhumation of the Taku Schist, NE Peninsular Malaysia. *Journal of Asian Earth Sciences*, 127, 63-75.
- Means, W. D. (1981). The concept of steady-state foliation. *Tectonophysics*, 8, 179-199.
- Metcalf, I. (2000). The Bentong-Raub Suture Zone. *Journal of Asian Earth Sciences*, 18, 691-712.
- Metcalf, I. (2013). Tectonic evolution of the Malay Peninsula. *Journal of Asian Earth Sciences*, 76, 195-213.
- Miranda, R., Valadares, V., Terrinha, P., Mata, J., do Rosario Azevedo, M., Gaspar, M., Kullberg, J. C., & Ribeiro, C. (2009). Age constraints on the Late Cretaceous alkaline magmatism on the West Iberian Margin. *Cretaceous Research*, 30(3), 575-586.
- Morley, C. K. (2012). Late Cretaceous-Early Paleogene tectonic development of SE Asia. *Earth-Science Reviews*, 115, 37-75.
- Neiva, A. M. R., Neiva, J. M. C., & Parry, S. J. (1987). Geochemistry of the granitic rocks and their minerals from Serra da Estrela, Central Portugal. *Geochimica et Cosmochimica Acta*, 51, 439-454.
- Newman, J., & Mitra, G. (1993). Lateral variations in mylonite zone thickness as influenced by fluid-rock interactions, Linville Falls fault, North Carolina. *Journal of Structural Geology*, 15, 849-863.
- Ng, S. W. P., Chung, S. L., Robb, L. J., Searle, M. P., Ghani, A. A., Whitehouse, M. J., Oliver, G. J. H., Sone, M., Gardiner, N. J., & Roselee, M. H. (2015). Petrogenesis of Malaysian granitoids in the Southeast Asian tin belt, Part 1. Geochemical and Sr-Nd isotopic characteristics. *Geological Society of America Bulletin*, 127, 1209-1237.
- Ng, T. F. (1992). *Petrography, structure and geotechnical studies of the Kuala Lumpur granite, eastern part of Kuala Lumpur, Peninsular Malaysia*. (Unpublished Master of Philosophy Dissertation). Kuala Lumpur, University of Malaya.
- Ng, T. F. (1994). Microstructures of the deformed granites of eastern Kuala Lumpur-Implications for mechanisms and temperatures conditions of deformation. *Geological Society of Malaysia Bulletin*, 35, 47-59.

- Nishikawa, O., & Takeshita, T. (1999). Dynamic analysis and two types of kink bands in quartz veins deformed under subgreenschist conditions. *Tectonophysics*, 301(1), 21-34.
- Nishikawa, O., & Takeshita, T. (2000). Progressive lattice misorientation and microstructural development in quartz veins deformed under subgreenschist conditions. *Journal of Structural Geology*, 22(2), 259-276.
- O'Hara, K. & Blackburn, W.H. (1989). Volume-loss model for trace-element enrichments in mylonites. *Geology*, 17, 524-527.
- O'Hara, K. (1988). Fluid flow and volume loss during mylonitization, an origin for phyllonite in an overthrust setting, North Carolina, USA. *Tectonophysics* 156, 21-36.
- Odin, G.S. *et al.* (35 collaborators). (1982). Interlaboratory Standards for Dating Purposes. Numerical Dating in Stratigraphy. Chichester: Wiley and Sons.
- Passchier, C. W. (1985). Water-deficient mylonite zones- an example from the Pyrenees. *Lithos*, 18, 115-127.
- Passchier, C. W., & Trouw, R. A. J. (2005). *Microtectonics*. Berlin, Springer Verlag.
- Passchier, C., & Simpson, C. (1986). Porphyroclast systems as kinematic indicators. *Journal of Structural Geology*, 8(8), 831-843.
- Passchier, C.W. (1998). Monoclinic model shear zones. *Journal of Structural Geology*, 20, 1121-1137.
- Poirier, J. P. (1985). *Creep of crystals, high-temperature deformation processes in metals, ceramics and minerals* (21). Cambridge: Cambridge University Press.
- Post, A., & Tullis, J. (1998). The rate of water penetration in experimentally deformed quartzite, Implications for hydrolytic weakening. *Tectonophysics*, 295, 117-137.
- Pryer, L. L., & Robin, P. Y. (1995). Retrograde metamorphic reactions in deforming granites and the origin of flame perthite. *Journal of Metamorphic Geology*, 13(6), 645-658.
- Pryer, L. L. (1993). Microstructures in feldspars from a major crustal thrust zone, the Grenville Front, Ontario, Canada. *Journal of Structural Geology*, 15(1), 21-36.
- Pryer, L.L., Robin, P. Y. F. (1996). Differential stress control on the growth and orientation of flame perthite, a palaeostress-direction indicator. *Journal of Structural Geology*, 18, 1151-1166.
- Raj, J. K. (1982c). A reappraisal of the Bok Bak Fault. *Geological Society of Malaysia Warta Geologi*, 8, 35-41.
- Raj, J. K., Abd. Rahman, A. H. & Shuib, M. K. (1998). Tertiary basins of inland Peninsular Malaysia, review and tectonic evolution. *Geological Society of Malaysia Bulletin*, 42, 211-226.

- Ramsay, J. G. (1980a). Shear zone geometry, a review. *Journal of Structural Geology*, 2, 83–101.
- Ramsay, J. G., & Graham, R. H. (1970). Strain variation in shear belts. *Canadian Journal of Earth Sciences*, 7, 786–813.
- Roberts, D., & Nissen, A. L. (2006). Geochemical changes accompanying mylonitization of granite at the base of the Helgeland Nappe Complex, Nord-Trøndelag, Central Norway. *Norges Geologiske Undersøkelse Bulletin*, 446, 35-41.
- Rollinson, H. (1993). *Using geochemical data, evolution, presentation, interpretation*. United Kingdom: Longman Scientific & Technical.
- Rubie DC (eds) Metamorphic reactions, kinetics, textures, and deformation. *Advances in Physical Geochemistry*, 4, 138–179.
- Schmid, S., Paterson, M., & Boland, J. (1980). High temperature flow and dynamic recrystallization in Carrara marble. *Tectonophysics*, 65(3), 245-280.
- Searle, M. P, Whitehouse, M. J., Robb, L. J., Ghani, A. A., Hutchison, C. S., Sone, M., Ng, S.W. P., Roselee, M. H., Chung, S. L., & Oliver G. J. H. (2012). Tectonic evolution of the Sibumasu–Indochina terrane collision zone in Thailand and Malaysia, constraints from new U–Pb zircon chronology of SE Asian tin granitoids. *Journal of the Geological Society*, 169(4), 489-500.
- Selverstone, J., Morteani, G., Staude, J. M. (1991). Fluid channelling during ductile shearing, transformation of Granodiorite into aluminous schist in the Tauern Window, Eastern Alps. *Journal of Metamorphic Geology*, 9, 419-431.
- Shu, Y. K. (1969). Some north-west trending faults in the Kuala Lumpur and other areas. *Newletter Geological Society Malaysia*, 17, 1-5.
- Shu, Y. K. (1989). *The geology and mineral resources of the Kuala Kelawang area, Jelebu, Negeri Sembilan (20)*. Malaysia: Geological Survey Malaysia District Memoir.
- Shuib, M. K. (2000a). The Mesozoic Tectonics of Peninsular Malaysia - An overview. In GSM Dynamic stratigraphy & Tectonics of Peninsular Malaysia - Seminar III. The Mesozoic of Peninsular Malaysia. *Geological Society of Malaysia Warta Geologi*, 26, 5.
- Shuib, M. K. (2003). Transpression in the strata of Pulau Kapas, Terengganu. *Geological Society of Malaysia Bulletin*, 46, 299-306.
- Shuib, M. K. (2004). Synsedimentary deformation of the Kapas Conglomerate, Pulau kapas, Terengganu. *Geological Society of Malaysia Bulletin*, 48, 103-109.
- Shuib, M. K. (2009a). Major Fault. In C.S. Hutchison & D.N.K Tan (Eds). *Geology of Peninsular Malaysia* (pp. 250-269). Kuala Lumpur: University of Malaya and Geological Society of Malaysia.

- Shuib, M. K., & Abd. Rahman, A. H. (1999). A Five-fold stratigraphic and tectonic subdivision of the Malay peninsula and the implication on its tectonic evolutionary history. *Geological Society of Malaysia Warta Geologi*, 25, 65-66.
- Shuib, M. K., & Jamaluddin, T. J. (1999). *Multiple deformations in the Upper Paleozoic Mersing Beds of the Tg. Balau and Tg. Lompat, Desaru, Johore – A field Guide Book (27)*. Malaysia: Geological Society of Malaysia.
- Shuib, M. K., Manap, M. A., Tongkul, F., Rahim, I. A., Jamaludin, T. A., Surip, N., Bakar, R. A., Abas, M. R. C., Musa, R. C. & Ahmad, Z. (2017). Active Faults in Peninsular Malaysia with emphasis on active geomorphic features of Bukit Tinggi Region. *Malaysian Journal of Geosciences*, 1, 13-26.
- Sibson, R.H. (1977). Fault rocks and fault mechanisms. *Geological Society London*, 133, 191-213.
- Simpson, C., & Schmid, S. M. (1983). An evaluation of criteria to determine the sense of movement in sheared rocks. *Geological Society of America Bulletin*, 94, 1281-1288.
- Singh, D.S. (1985). *Geological map of Peninsula Malaysia (8)*. Kuala Lumpur: Geological Survey of Malaysia.
- Sinha, A. K., Hewitt, D. A., & Rimstidt, J. D. (1986). Fluid interaction and element mobility in the development of ultramylonites. *Geology*, 14, 883-886.
- Snelling, N. J., Bignell, J. D., & Harding, R. R. (1968). Ages of Malayan granites. *Geologie en Mijnbouw*, 47, 358-359.
- Stauffer, P. H. (1968). The Kuala Lumpur fault zone, a proposed major strike-slip fault across Malaya. *Newsletter Geological Society Malaysia*, 15, 2-4.
- Stauffer, P. H. (1969). Tin mineralization and faults in the Kuala Lumpur region. *Newsletter Geological Society Malaysia*, 20, 5-6.
- Stesky, R. (1978). Mechanisms of high temperature frictional sliding in Westerly granite. *Canadian Journal of Earth Sciences*, 15(3), 361-375.
- Stipp, M., Stuenitz, H., Heilbronner, R., & Schmid, S. M. (2002a). The eastern Tonale fault zone, a 'natural laboratory' for crystal plastic deformation of quartz over a temperature range from 250 to 700°C. *Journal of Structural Geology*, 24(12), 1861-1884.
- Stipp, M., Stünitz, H., Heilbronner, R., & Schmid, S.M. (2002b). Dynamic recrystallization of quartz, correlation between natural and experimental conditions. In, De Meer, S., Drury, M. R., De Bresser, J. H. P. & Pennock, G.M. (eds). *Deformation Mechanisms, Rheology and Tectonics: Current status and future prospectives* (pp. 171-190). United Kingdom: Geological Society of London.

- Streit, J. E., Cox, S. F. (1998). Fluid infiltration and volume change during mid-crustal mylonitisation of Proterozoic granite, King Island, Tasmania. *Journal of Metamorphic Geology* 16, 197-212.
- Stünitz, H., Fitz Gerald, J. D., & Tullis, J. (2003). Dislocation generation, slip systems, and dynamic recrystallization in experimentally deformed plagioclase single crystals. *Tectonophysics*, 372(3-4), 215-233.
- Stünitz, H., Fitz Gerald, J. D., & Tullis, J. (2003). Dislocation generation, slip systems, and dynamic recrystallization in experimentally deformed plagioclase single crystals. *Tectonophysics*, 372, 215–233.
- Surip, N., & Taylor, G. (2000). *StereoSAR DEM for mapping of geological structures in Selangor, Malaysia*. Penang: Geological Society of Malaysia Annual Conference.
- Tate, R. B., Tan, D. N. K., & Ng, T. F. (2009). *Geological Map of Peninsular Malaysia*. In, Hutchison, C. S., Tan, D. N. K. (Eds.), *Geology of Peninsular Malaysia*. Kuala Lumpur, University of Malaya/Geological Society of Malaysia.
- Tjia, H. D. (1972). *Strike-slip faults in West Malaysia (24)*. Montreal: International Geological Congress.
- Tjia, H. D. (1975a). Western extension of the Kuala Lumpur Fault Zone. *Geological Society of Malaysia Newsletter*, 1(2), 30-33.
- Tjia, H. D. (1978). *Structural geology of Peninsular Malaysia*. In, Nutalaya, P. (ed) *Proceedings of the third regional conference of geology and mineral resources of S.E.Asia*. Bangkok: Asian Institute of Technology.
- Tjia, H.D. (1969). Regional implication of Lebir fault zone. *Geological Society of Malaysia Newsletter*, 19, 6-7.
- Tjia, H.D. (1989a). Tectonic history of the Bentong-Bengkalis suture. *Geologi Indonesia*, 12, 89-111.
- Tjia, H.D. (1989c). Superimposed structures in Upper Paleozoic metasediments, Eastern Johor (abstract). *Geological Society of Malaysia Warta Geologi*, 15, 33.
- Tjia, H.D. (1993). The Kisap Thrust in the Kampung Kilim area, Pulau Langkawi. *Geological Society of Malaysia Warta Geologi*, 19, 247-250.
- Tjia, H.D. (1996). Tectonics of deformed and underformed Jurassic-Cretaceous strata of Peninsular Malaysia. *Geological Society of Malaysia Bulletin*, 39, 131-156.
- Tjia, H.D. (1997). The Kuala Lumpur Fault Zone revisited. *Geological Society of Malaysia Warta Geologi*, 23, 225-230.
- Tobisch, O. T., Barton, M. D., Vernon, R. H. & Paterson, S. R. (1991). Fluid enhanced deformation, transformation of granitoids to banded mylonites, western Sierra Nevada, California, and southeastern Australia. *Journal of Structural Geology* 13, 1137-1156.

- Trouw, R. A. J., Passchier, C.W., & Wiersma, D. J. (2010). *Atlas of Mylonites and related microstructures*. London New York: Springer- Heidelberg Dordrecht.
- Tullis, J. (1978). *Mylonites-natural and experimental; Processes and conditions of mylonite formation as inferred from experimental deformation studies*. Boston, Massachusetts: Geological Society of America Short Course Notes.
- Tullis, J., & Yund, R. (1992). The brittle-ductile transition in feldspar aggregates, An experimental study. *International Geophysics*, 51, 89-117.
- Tullis, J., & Yund, R. A. (1980). Hydrolitic weakening of experimentally deformed Westerly granite and Hale albite rock. *Journal of Structural Geology*, 2, 439-451.
- Tullis, J., & Yund, R.A. (1991). Diffusion creep in feldspar aggregates, experimental evidences. *Journal of Structural Geology*, 13, 987-1000.
- Tullis, J., Dell'Angelo, L., & Yund, R. A. (1990). Ductile shear zones from brittle precursors in feldspathic rocks, the role of dynamic recrystallization. In, Hobbs BE, Heard HC (eds) Mineral and rock deformation, laboratory studies. *AGU, Geophysical Monograph Series 56*, 67-81.
- Twiss, R. J. (1977). Theory and applicability of a recrystallized grain size paleopiezometer. *Pure and Applied Geophysics*, 115, 227-244.
- Vernon, R., Williams, V., & D'arcy, W. (1983). Grain-size reduction and foliation development in a deformed granitoid batholith. *Tectonophysics*, 92(1), 123-145.
- Vocke, R. D., Hanson, G. N., Grunenfelder, M. (1987). Rare earth element mobility in the Roffna-Gneiss. *Contributions to Mineralogy and Petrology*, 95, 145-154.
- Warren, J. M., & Hirth, G. (2006). Grain size sensitive deformation mechanisms in naturally deformed peridotites. *Earth and Planetary Science Letters*, 248, 438-450.
- White, S. (1975). Tectonic deformation and recrystallization of oligoclase. *Contributions to Mineralogy and Petrology*, 50, 287-304.
- White, S. H., Burrows, S. E., Carreras, J., Shaw, N. D., & Humphreys, F. J. (1980). On mylonites in ductile shear zones. *Journal of Structural Geology*, 2, 175-187.
- Wu, S., & Groshong Jr, R. H. (1991a). Low temperature deformation of sandstone, southern Appalachian fold-thrust belt. *Geological Society of America Bulletin*, 103, 861-875.

LIST OF PUBLICATION AND PAPER PRESENTED

ISI PAPER SUBMITTED:

Saaid, N., Ng, T. F., Ghani, A.A. (2017). Microstructures of mylonitic granites in a brittle-ductile shear zone – An example from the Bukit Tinggi Fault Zone, Peninsular Malaysia. *Current Science*.

(<http://www.currentscience.ac.in/csajs/index.php/cs/author/submission/26122>)

PAPERS PRESENTED:

1. Norsafawati bt. Saaid, Ng Tham Fatt & Azman A. Ghani: Deformation microstructures of mylonites along the Bukit Tinggi Fault Zone, Peninsular Malaysia. National Geoscience Conference. 23-24 June 2012, Pullman Hotel, Kuching, Sarawak, p.137-138.

2. Norsafawati Saaid, Ng Tham Fatt & Azman A. Ghani: Textural and geochemical transformation of granite along Bukit Tinggi Fault Zone, Peninsular Malaysia. National Geoscience Conference. 13-14 June 2014, Grand Continental Hotel, Kuala Terengganu, Terengganu, p. 74-75.

University of Malaysia

APPENDIX A : Detail of major faults in Peninsular Malaysia

Name of fault	Orientation	Type of fault	Location	Characteristics
Lebir Fault Zone	NNW-SSE	Sinistral normal fault.	<ul style="list-style-type: none"> • Along Sungai Lebir near Manek Urai (Kelantan). 	<ul style="list-style-type: none"> • It is a 10 km wide curvilinear lineament that spans the gap between Sungai Lebir and the eastern margin of Taku Schist near Kuala Krai. • Rocks were deformed into brecciated metasediments, flasered granites and mylonites. • Tjia (1969), Singh (1985), Aw (1990) and Shuib (2009) indicate the fault as sinistral movement. • The fault however might have been initiated as a dextral strike slip terrane boulding fault shown by the eastern belt granite batholith that terminated to the fault zone. • Tjia (1989c) estimated about 200 km of left-lateral displacement along the fault, based on the distribution of the Upper Paleozoic metasediments on the north and south side of the fault. • Passes through the Jurassic-Cretaceous basins containing the Tembeling, Gagau and Koh Formation. • The informations were used by Tjia (1996) and Shuib (2000a) to indicate that the latest Triassic to Jurassic-Cretaceous basins were formed and deformed by strike-slip movements along this fault zone.

Kisap Thrust	NW-SE, NE-SW	Thrust fault	<ul style="list-style-type: none"> • From southern part of Langkawi (tip of Pulau Dayang Bunting), through the main island up to Pulau Dangli at the northernmost tip. 	<ul style="list-style-type: none"> • The largest thrust in the Peninsular Malaysia has been well described. • Distinct curvilinear lineaments cut by NE-SW dextral faults. • On the geological map and cross section, the fault trace is separated the Setul Formation from the Singa and Cuping Formation. • The thrust appears to occur within the Setul Formation at both Pulau Dayang Bunting and Hosna Quarry, Kilim. • The drag folds associated with the fault indicated that tectonic transport was to the west with smaller back-thrusting directed to the east (Tjia, 1993). • The thrust is displaced by a NE-SW dextral strike-slip fault. The strike-slip faults, post-dated the granite intrusion, displaced the Kisap thrust during the Late Triassic and rotated the earlier structures.
Balau-Murau Fault Zone	NNW-SSE	Dextral strike slip fault.	<ul style="list-style-type: none"> • From Batu Layar northwards to the Balau Fault Zone (Shuib and Jamaluddin, 1999). • Through Tanjong Leman, Tanjong Murau and Mersing. 	<ul style="list-style-type: none"> • It is a distinct magnetic anomaly associated with NNW-SSE trending lineaments near Mersing suggests that the zone is a major basement fault. • The fault zone separated the Murau Formation to the east from the Carboniferous Mersing beds on the west. • The Murau-Bukit Keluang Fault segments at Tanjong Murau was interpreted as a normal fault (Abdullah, 1996). • The fault is interpreted as dextral strike-slip by Shuib and Jamaluddin (1999). • The fault zone is linked to the dextral strike-slip Balau Fault Zone.
Bukit	NNW-SSE	Dextral strike-slip	<ul style="list-style-type: none"> • Terengganu 	<ul style="list-style-type: none"> • Represent the Balau-Murau Fault in Terengganu.

Keluang Fault		fault.		<ul style="list-style-type: none"> • Separate the Upper Permian Bukit Keluang Conglomerate from Carboniferous metasediments.
Kapas Fault	N-S	Dextral transpression fault.	<ul style="list-style-type: none"> • Pulau Kapas (Terengganu). 	<ul style="list-style-type: none"> • A 100 m wide fault that forms the western boundary of a continental deposit of probable Permian age (Shuib, 2003, 2004). • Carboniferous metasediments within the fault zone show refolding suggesting repeated movement. Drag features and associated small-scale structures suggest dextral transpression (Shuib, 2003, 2004). • Soft-sediment deformational structures within the Kapas Conglomerate suggest that the first episode of faulting was syn-depositional initiated during Permian time. • Drag refolding features along the faults suggest that a later, possibly Upper Triassic, dextral strike-slip movement reactivated the faults. • The Kapas Conglomerate is cut by NW-SE striking sinistral strike-slip faults and the fault also shows evidence of sinistral reactivation believed to have taken place in the Late Cretaceous (Shuib, 2003, 2004). • The faults of Terengganu are pre-Early Permian to Middle-Late Permian, reactivated several times until the Tertiary.
Kuala Lumpur Fault Zone (KLFZ)	NW-SE	Sinistral fault	<ul style="list-style-type: none"> • Cut across the Kuala Lumpur. 	<ul style="list-style-type: none"> • A major NW-SE fault zone that transects across KL area (Stauffer, 1968; Shu, 1969). • It is indistinct, broad and diffused (Surip and Taylor, 2000). • The fault zone is made of five main strands: <ul style="list-style-type: none"> i) The major Ampang Fault coincides with the Klang Gates Quartz Reef. ii)Kongkoi Fault joins the Klang Gates Quartz Reef westward. iii)Bukit Tajoh forms splay to the Kongkoi fault.

				<p>iv)Ulu Kelang forms splay to the Kongkoi fault.</p> <p>v)Farther south, the Ulu Langat Fault coincides with the Tekali Quartz Reef that continues eastward into the Jelebu Fault.</p> <ul style="list-style-type: none"> • Five sets of steep mesoscopic brittle faults and shear zone define each strand of the fault zone. • Displacement total length up to 20 km. • According to Tjia (1989a), the fault zone can be traced westward up to Pulau Jemur. The radar imagery shows that KLFZ may be traced eastward into the broad Mersing Fault Zone. • It passes through the Batu Arang Tertiary Basin. This basin is situated on overlapping segments of right-stepping en-echelon splays of the KLFZ. Transtensional stress at the overlapping segments gave rise to the fault-controlled Batu Arang Basin (Mahendran <i>et al.</i>, 1991; Raj <i>et al.</i>, 1998; Shuib and Abd. Rahman, 1999). • It is believed that the fault zone was active until the Eocene to (?) Late Miocene.
Bukit Tinggi Fault Zone (BTFZ)	NW-SE	Sinistral strike-slip fault.	<ul style="list-style-type: none"> • North of the KLFZ. • Trace north to Kuala Kubu Bharu until south to Kuala Kelawang (Shu, 1969). 	<ul style="list-style-type: none"> • The curve is distinct and strongly expressed for a distance of at least 120 km and strongly expressed by fault rock zones. • Mylonites are common. They have a distinct foliation and stretching lineation. • The sub-vertical to moderately inclined stretching lineations along the fault zone shows that the fault is a dip-slip component. • Microscopic and field studies on mylonite show that the early ductile microstructures were superimposed by later brittle-ductile and brittle structures. • Fault kinematic studies show that the early ductile movement had a dextral sense of shear (Ng, 1994), but at Kuala Kelawang and along the Karak Highway (Harun, 2002) showed that the

				<p>movement was sinistral, attributed to a later reactivation.</p> <ul style="list-style-type: none"> • A zone of protomylonite at KM 32 at the Karak Highway, exhibits only plastic microstructures, indicating that deformation at 450°C probably occurred shortly after the emplacement of the granite, before complete cooling (Ng, 1994).
Seremban Fault Zone	NW-SE	Sinistral strike-slip fault.	<ul style="list-style-type: none"> • Trace from NW of Gunong Ledang, northwestward into the Main Range Granite at Bahau and passing through Seremban. 	<ul style="list-style-type: none"> • It is similar and parallel to the KLFZ. • Like KLFZ, the western extension of this fault splays into 3 to 4 curvilinear strands that displace the Paleozoic metasediments. • Within the granite mass, the fault is broad, but distinctly expressed as steep scarps. Its trace is very distinct, where it cuts the enveloping metasedimentary rocks. • The northernmost strand of the fault zone joins the Pertang Fault to link with its northern neighbour, the KLFZ. • This fault zone is cut by a distinct N-S trending lineament. • Mylonites, sheared granites and wide breccia zones characterize the fault zone within the granite.
Bok Bak Fault Zone	NNW-SSE and NNE-SSW.	Sinistral strike-slip (NNW-SSE), Dextral strike-slip (NNE-SSW).	<ul style="list-style-type: none"> • Transects the Main Range Granite at the Western part of the Peninsular Malaysia from southwest Kelantan, passing through central Perak, Bukit Perak (Kedah) and ends near Pokok Sena (Kedah). • Extended southward 	<ul style="list-style-type: none"> • The fault is broad, indistinct and not well expressed within the granite body, but its trace is very distinct when it cuts the enveloping metasedimentary rocks. • The surface trace is very distinct in the Baling area where it is defined by remarkably straight valleys and rivers. • The trace is not continuous but forms en-echelon segments. • Burton (1965) estimated the displacement was 55 km while Raj (1982c) estimated the displacement to be 20 km. Abdullah (1989) estimated the displacement to be 25 km. Burley and Othman (1990) estimated the displacement to be 30 km. • The fault zone wide is 10 km. It is defined by a broad zone of sub-

			to central Perak and southwest Kelantan based on LANDSAT lineament study (Raj, 1982c).	parallel faults exhibiting intense fracturing.
Ruok Fault Zone	NNW-SSE	Sinistral strike-slip, reactivated as normal faulting.	<ul style="list-style-type: none"> From the Pattani river (Thailand) into Malaysia along Sungai Kenerong, then along the Temenggor lake before ending just north of the Bok Bak Fault Zone. 	<ul style="list-style-type: none"> It is a 4 km wide zone of topographic negative lineaments and distinct on RADARSAT imagery. It trends 165° and parallel to the Bok Bak, Galas and Lebir Fault Zones. Passes through the East-West highway at KM 184 from Ipoh. Represented in schist that contains numerous sigmoid quartz veins (Almashoor and Tjia, 1987).
Galas Fault Zone	NNW-SSE	Oblique sinistral reverse fault.	<ul style="list-style-type: none"> Extend across the Thailand border, near Bukit Saiong (Kedah) to the Tembeling area. 	<ul style="list-style-type: none"> Tjia (1989a) recognized these faults on LANDSAT imagery and labeled them “fault zone 4”. Slightly displaced dextrally by a series of N-S trending fault zones including the Tomo Fault and the Bentong-Raub Suture Zone. Along the East-West Highway near Batu Melintang, the fault zone can be seen as a more than 100 m wide zone of sheared granite and gneiss with distinct foliation trending NNW-SSE. Kinematic indicators, such as mica and feldspar augen within the sheared granites, show a sinistral reverse sense of movement. The fault zone is expressed as a wide zone of sheared granite forming the western margin of the Upper Cretaceous Kemahang granite. At the contact with the Taku schist, granitic apophyses of the

				<p>Kemahang granite commonly occur as closely-spaced veins parallel to the foliation, forming a lit-par-lit injection gneiss (Macdonald, 1968).</p> <ul style="list-style-type: none"> • Along the East-West Highway past Jeli, the granite shows a distinct steeply-dipping foliation trending NNW-SSE, defined by preferred orientation of ellipsoidal K-feldspar phenocrysts and flattened quartz and biotite aggregates. Both S and C fabrics can be recognized. • Within the shear zone, coarse grained granite has been recrystallised to augen gneiss containing narrow zones of mylonite. • The shear zone foliation strikes approximately 340°, dips 47°-70° to the NE, and contains a roughly oblique down-dip stretching lineation.
Lepar Fault Zone	NW-SE	Sinistral strike-slip fault.	<ul style="list-style-type: none"> • Parallel to Sungai Lepar (Pahang). 	<ul style="list-style-type: none"> • Can be seen apparently on the RADARSAT imagery as a series of straight lineaments parallel to Sungai Lepar, accentuated by linear sub-parallel ridges. • Consists of a series of several NW-SE striking fault strands. • At the broadest, the fault zone measures 18 km across and it can be traced for at least 45 km along the length of Sungai Lepar. • The fault zone marks the boundaries between the granites and the metasediments (Lee, 1990). • Granites along the fault zone have undergone brittle-shearing marked by zones of brecciation. • The metasediments along the fault zone have been sheared into phyllonites that shows sub-horizontal to horizontal striations indicating strike-slip movement. • The fault zone seems to truncate the Lebir Fault Zone. It is cut by N-S striking faults that bound and cut the Jurassic-Cretaceous

				<p>Bertangga Sandstone.</p> <ul style="list-style-type: none"> • Based on cross-cutting relationships, it is believed that the fault zone was initiated in the Late Cretaceous and was reactivated during the Tertiary.
Mersing-Endau Fault Zone	WNW-ESE	Sinistral strike slip	<ul style="list-style-type: none"> • From Endau (north) to Kota Tinggi (south), through Layang-layang and Segamat (west). 	<ul style="list-style-type: none"> • Occurs as an 80 km wide zone which is parallel to and along strike with the KLFZ. • On the RADARSAT imagery, these faults cut and displaced a set of sub-parallel less distinct NNW-SSE trending lineaments.

APPENDIX B: Description of samples used in the study

Name of sample	Type of sample	Location
BG1	Biotite granite	KKB-Fraser Hill road
BG2	Biotite granite	KKB-Fraser Hill road
BG3	Biotite granite	KKB-Fraser Hill road
BG4	Biotite granite	KKB-Fraser Hill road
PM1	Protomylonite	KKB-Fraser Hill road
PM2	Protomylonite	KKB-Fraser Hill road
PM3	Protomylonite	KKB-Fraser Hill road
PM4	Protomylonite	KKB-Fraser Hill road
MCS	Mica-chlorite Schist	KKB-Fraser Hill road
PM5	Protomylonite	Main outcrop opposite Selangor Dam, KKB
MM6	Mesomylonite	Main outcrop opposite Selangor Dam, KKB
UM7	Ultramylonite	Main outcrop opposite Selangor Dam, KKB
MM8	Mesomylonite	Main outcrop opposite Selangor Dam, KKB
PM9	Protomylonite	Main outcrop opposite Selangor Dam, KKB
UM10	Ultramylonite	Main outcrop opposite Selangor Dam, KKB
PM11	Protomylonite	Main outcrop opposite Selangor Dam, KKB
UM12	Ultramylonite	Main outcrop opposite Selangor Dam, KKB
Dyke	Microgranite	Main outcrop opposite Selangor Dam, KKB
Dyke	Microgranite	Main outcrop opposite Selangor Dam, KKB
PM13	Protomylonite	Main outcrop opposite Selangor Dam, KKB
PM14	Protomylonite	Main outcrop opposite Selangor Dam, KKB
MM15	Mesomylonite	Main outcrop opposite Selangor Dam, KKB
PM16	Protomylonite	Main outcrop opposite Selangor Dam, KKB
PM17	Protomylonite	Main outcrop opposite Selangor Dam, KKB
PM28	Protomylonite	Main outcrop opposite Selangor Dam, KKB
PM18	Protomylonite	KM 52.3, Karak Highway
PM19	Protomylonite	Hutan Lentang, Bukit Tinggi.
PM20	Protomylonite	KM 50, Karak Highway
PM21	Protomylonite	KM 47.2, Karak Highway
PM22	Protomylonite	Sg. Tanglir, Bukit Tinggi.
PM 23	Protomylonite	KM 46.5, Karak Highway
PM 24	Protomylonite	KM 45.5, Karak Highway
MM25	Mesomylonite	Kuala Kelawang
CSS	Calc-Silicate Schist	Kuala Kelawang
PM26	Protomylonite	Kuala Kelawang
PM27	Protomylonite	Kuala Kelawang
PG	Pyroxene bearing granite	Penjara Jelebu, Kuala Kelawang
JS	Jelebu Schist	Kg. Telekong, Kuala Kelawang
KKG	K. Kelawang Granite	Kg. Telekong, Kuala Kelawang
CAT	Cataclasite	Jeram Gading, Kuala Kelawang

University of Malaya

APPENDIX C: Measurements of the samples

Sample code	X	Y	Lithology	Sample Types	S Surface (°)	S Dip	C Surface (°)	C Dip	Lineation Direction (°)	Lineation Plunge (°)	Top to	Displacement
BG1	3.71911	101.75614	Biotite granite	E	No	No	No	No	No	No	No	No
BG2	3.72145	101.75479	Biotite granite	E	No	No	No	No	No	No	No	No
BG3	3.72204	101.75314	Biotite granite	E	No	No	No	No	No	No	No	No
BG4	3.68992	101.74896	Biotite granite	E	No	No	No	No	No	No	No	No
PM1	3.68307	101.74827	Protomylonite	E	No	No	No	No	No	No	No	No
PM2	3.67105	101.74867	Protomylonite	E	No	No	No	No	No	No	No	No
PM3	3.64868	101.74121	Protomylonite	E	No	No	No	No	No	No	No	No
PM4	3.5683	101.71642	Protomylonite	E	No	No	100	75SW	No	No	No	No
MCS	3.56798	101.71463	Mica-chlorite Schist	B	No	No	100	80SW	190	68	No	No
PM5	3.56996	101.70447	Protomylonite	E	126	80NE	132	82SW	217	78	No	No
							128	84SW	225	70	No	No
							126	76SW	220	80	No	No
MM6	3.56996	101.70448	Mesomylonite	E	No	No	123	76SW	No	No	No	No
UM7	3.56998	101.70445	Ultramylonite	C	No	No	125	80SW	205	78	NE	Dextral Reverse
MM8	3.56999	101.70444	Mesomylonite	C	No	No	125	80SW	230	78	NE	Dextral Reverse
							118	78SW	240	76	NE	Dextral Reverse
							124	78SW	214	76	NE	Dextral Reverse
PM9	3.56998	101.70442	Protomylonite	E	No	No	100	68SW	No	No	No	No
UM10	3.57001	101.70423	Ultramylonite	C	No	No	100	88SW	195	86	NE	Dextral Reverse
							100	88SW	198	86	NE	Dextral Reverse
							106	89SW	197	88	NE	Dextral Reverse

Sample code	X	Y	Lithology	Sample Types	S Surface (°)	S Dip	C Surface (°)	C Dip	Lineation Direction (°)	Lineation Plunge (°)	Top to	Displacement
PM11	3.57006	101.70382	Protomylonite	F	No	No	118	65SW	No	No	No	No
UM12	3.57003	101.70352	Ultramylonite	C	No	No	130	44SW	222	40	NE	Dextral Reverse
							147	46SW	235	45	NE	Dextral Reverse
							147	48SW	213	40	NE	Dextral Reverse
Dyke	3.56984	101.70304	Microgranite	A	108	82NE	No	No	No	No	No	No
Dyke	3.56982	101.70303	Microgranite	A	102	89NE	No	No	No	No	No	No
PM13	3.56981	101.70304	Protomylonite	E	No	No	111	70SW	No	No	No	No
PM14	3.56971	101.70287	Protomylonite	E	No	No	114	74SW	No	No	No	No
MM15	3.56971	101.70287	Mesomylonite	C	No	No	108	75SW	No	No	No	No
PM16	3.56971	101.70287	Protomylonite	E	No	No	110	80SW	No	No	No	No
PM17	3.57011	101.69402	Protomylonite	E	No	No	110	80SW	No	No	No	No
PM28	3.56346	101.6744	Protomylonite	E	No	No	110	80SW	No	No	No	No
PM18	3.39433	101.8894	Protomylonite	C	120	60SW	165	50SW	210	26	NE	Dextral Reverse
							114	40SW	241	40	NE	Dextral Reverse
							118	40SW	218	39	NE	Dextral Reverse
PM19	3.39065	101.88657	Protomylonite	E	No	No	No	No	No	No	No	No
PM20	3.38584	101.88387	Protomylonite	E	No	No	No	No	No	No	No	No
PM21	3.37006	101.85691	Protomylonite	F	285	84NE	291	78NE	030	46	NE	Dextral Normal

Sample code	X	Y	Lithology	Sample Types	S Surface (°)	S Dip	C Surface (°)	C Dip	Lineation Direction (°)	Lineation Plunge (°)	Top to	Displacement
					332	84NE	338	70NE	035	50	NE	Dextral Normal
					336	86NE	338	70NE	040	50	NE	Dextral Normal
PM22	3.36793	101.84926	Protomylonite	E	158	74SW	150	68SW	243	72	NE	Dextral Reverse
					160	77SW	155	68SW	253	66	NE	Dextral Reverse
					162	86SW	159	76SW	235	86	NE	Dextral Reverse
					162	84SW	156	70SW	236	80	NE	Dextral Reverse
					356	80NE	347	64NE	065	64	NE	Dextral Normal
					345	77NE	320	64NE	55	64	NE	Dextral Normal
					347	74NE	345	52NE	060	74	NE	Dextral Normal
					350	78NE	348	56NE	050	50	NE	Dextral Normal
PM 23	3.36685	101.85164	Protomylonite	E	165	70NE	170	68SW	No	No	No	Dextral Normal
PM 24	3.36107	101.84648	Protomylonite	E	135	75NE	141	64SW	230	64	NE	Dextral Reverse
							165	72SW	225	60	NE	Dextral Reverse
							153	68SW	231	67	NE	Dextral Reverse

Sample code	X	Y	Lithology	Sample Types	S Surface (°)	S Dip	C Surface (°)	C Dip	Lineation Direction (°)	Lineation Plunge (°)	Top to	Displacement
MM25	3.12861	101.91333	Mesomylonite	A	No	No	340	25NE	No	No	No	No
							338	23NE	No	No	No	No
							342	26NE	No	No	No	No
CSS	3.11725	101.95962	Calc-Silicate Schist	C	No	No	No	No	No	No	No	No
PM26	3.09279	102.03252	Protomylonite	E	No	No	156	86SW	228	60	NE	Dextral Reverse
							146	85SW	234	59	NE	Dextral Reverse
							150	86SW	240	59	NE	Dextral Reverse
PM27	3.07405	102.04861	Protomylonite	E	No	No	137	60 SW	192	57	NE	Dextral Reverse
							145	70SW	254	70	NE	Dextral Reverse
							137	60SW	192	56	NE	Dextral Reverse
							134	82SW	208	55	NE	Dextral Reverse
							135	86SW	200	56	NE	Dextral Reverse
							130	80SW	207	55	NE	Dextral Reverse
PG	3.04137	102.09497	Pyroxene bearing granite	E	No	No	No	No	No	No	No	No
JS	3.04267	102.11038	Jebebu Schist	A	No	No	No	No	No	No	No	No

Sample code	X	Y	Lithology	Sample Types	S Surface (°)	S Dip	C Surface (°)	C Dip	Lineation Direction (°)	Lineation Plunge (°)	Top to	Displacement
KKG	3.09333	102.06667	K.Klawang Granite	E	No	No	No	No	No	No	No	No
CAT	3.09423	102.05345	Cataclasite	A	No	No	No	No	No	No	No	No

Sample types

A : None

B : Sample

C : Sample + Thin Section

D : Sample + Geochem

E : Sample + Thin Section + Geochem

F : Sample + Thin Section + Geochem + Ar/Ar dating

APPENDIX D: Detail geochemical data for the samples.

Sample	PROTOLITH				MYLONITES				
	BG 1	BG 2	BG 3	BG 4	PM1	PM2	PM3	PM4	PM5
SiO ₂ (wt%)	67.8	68.5	69.5	69.9	72.8	72.2	76.3	72.7	75.8
Al ₂ O ₃	14.95	15.02	14.6	15.14	13.46	13.59	12.41	13.34	12.28
Fe ₂ O ₃	3.9	3.28	3.26	2.17	1.78	2.79	1.37	2.15	1.87
CaO	2.2	1.97	1.9	1.51	1.02	1.6	0.63	1.22	0.84
MgO	1.4	1.11	1.08	0.38	0.24	0.46	0.13	0.28	0.2
Na ₂ O	2.71	2.98	2.72	3.31	3.47	3.18	2.86	3.28	2.82
K ₂ O	4.7	5.12	4.77	6.17	5.07	4.82	5.3	5.49	5.34
MnO	0.06	0.05	0.06	0.04	0.04	0.05	0.03	0.03	0.02
TiO ₂	0.66	0.56	0.51	0.33	0.2	0.4	0.15	0.28	0.21
P ₂ O ₅	0.22	0.18	0.19	0.07	0.05	0.09	0.04	0.06	0.04
Cr ₂ O ₃	0.027	0.027	0.025	0.02	0.027	0.021	0.021	0.033	0.032
BaO	0.08	0.11	0.06	0.06	0.03	0.04	0.01	0.03	0.03
LOI	1	0.56	0.97	0.49	0.56	0.42	0.48	0.62	0.74
Total	99.707	99.467	99.645	99.59	98.747	99.661	99.731	99.513	100.222
Ga(ppm)	20.9	17.6	20.4	22	21.2	19.9	17.7	17.8	16.7
Nb	18	13.3	14.8	16.2	18.6	16.7	11.6	13.8	12.9
Pb	9.5	10.1	17.2	23.8	29.2	19.9	6.7	20.1	11.7
Rb	304.8	269.5	386.6	552.4	692.5	445.8	578.3	414.8	359.4
Sr	130.7	119.3	111	87.5	39.7	84.4	27.9	56.6	34.3
Th	30.9	25	27.8	61	70.2	54.1	35.7	65.2	69.4
U	7.1	13.5	13.6	16.5	25.1	15.9	24.9	12.2	18.3
Y	32.6	30.5	30.4	51.3	173.8	56.7	70.1	53.9	43.3
Zn	62	53	64	40	34	48	27	38	33
Ba	763	1087	556	563	184	363	97	302	195
Zr	198	128.7	269.9	196.6	185	264.9	107.7	233.3	202.1
La	44.9	35.1	41.8	70.5	71.2	47.8	33.3	54.7	52.6
Ce	93.1	72.3	83	142.6	158.7	96.3	74.3	111.2	109.1
Pr	10.75	8.57	9.48	16.14	18.08	11.1	8.7	12.94	12.73
Nd	39.1	31.3	35.5	53.5	64.6	43.2	28.7	40.9	37.8
Sm	7.39	6.31	7.02	10.52	14.29	8.46	7.06	8.75	7.47
Eu	1.09	1	0.89	0.71	0.32	0.66	0.25	0.5	0.39
Gd	6.95	5.94	6.44	8.94	15.36	8.58	7.66	8.21	6.31
Tb	1.04	0.87	0.94	1.44	3.08	1.41	1.5	1.29	1.01
Dy	5.83	5.36	5.47	8.82	22.75	9.63	11.13	8.16	6.36
Ho	1.06	0.95	1.06	1.67	5.17	1.8	2.34	1.67	1.21
Er	2.98	3.01	2.64	4.66	17.52	5.49	7.3	5.18	3.95
Tm	0.42	0.4	0.4	0.72	3.12	0.86	1.1	0.78	0.59
Yb	2.94	2.46	2.58	4.71	22.72	5.31	7.35	5.11	3.61
Lu	0.38	0.38	0.41	0.65	3.4	0.8	1.06	0.75	0.52

MYLONITES

	MM 6	PM 9	PM 11	PM 13	PM 14	MM 15	PM 16	PM 17	PM 28
SiO ₂ (wt%)	74.1	76	77.3	72.8	77.1	76.3	72.8	73.2	76.3
Al ₂ O ₃	13.19	12.02	11.97	13.44	11.64	11.46	13.44	13.2	11.79
Fe ₂ O ₃	1.95	1.89	1.45	2.14	1.74	2.19	2.14	2.14	1.94
CaO	0.5	0.38	0.72	0.9	0.66	1	0.9	1.25	0.87
MgO	0.22	0.23	0.1	0.27	0.16	0.23	0.27	0.31	0.24
Na ₂ O	3.08	2.78	3.04	3.21	2.85	2.42	3.21	3.09	2.88
K ₂ O	5.46	5.34	4.98	5.28	5.07	5.11	5.28	5.52	4.68
MnO	0.03	0.03	0.03	0.03	0.02	0.04	0.03	0.03	0.02
TiO ₂	0.19	0.21	0.13	0.25	0.16	0.26	0.25	0.31	0.25
P ₂ O ₅	0.05	0.06	0.02	0.06	0.03	0.05	0.06	0.07	0.06
Cr ₂ O ₃	0.02	0.02	0.028	0.034	0.026	0.036	0.034	0.029	0.023
BaO	0.03	0.04	0.01	0.05	0.02	0.03	0.05	0.05	0.03
LOI	0.8	0.64	0.47	0.86	0.57	0.83	0.86	0.53	0.67
Total	99.62	99.64	100.248	99.324	100.046	99.956	99.324	99.729	99.753
Ga(ppm)	16.7	15.3	15.7	16.7	14.5	15	16.7	17.8	16.7
Nb	13.2	9.2	8.2	11.3	11.6	18.4	11.3	16.4	16.5
Pb	7.8	18.3	25.8	19.7	9.4	12.8	19.7	16.6	19.8
Rb	425.5	296.7	349.6	247.7	326.5	373.7	247.7	386.2	282.4
Sr	52.6	74.6	19.5	132.7	30.9	35.2	132.7	76.9	43.1
Th	55.8	53.8	47	53.1	56.8	80.2	53.1	52.5	78.5
U	16.3	11	17.2	11.1	15.7	20.9	11.1	15	18.9
Y	24	29.3	28.9	38.5	36.3	58.8	38.5	79	39.6
Zn	27	31	32	35	30	38	35	35	34
Ba	259	343	66	381	160	196	381	439	159
Zr	186.3	225.6	116.7	210.7	160.7	226.1	210.7	261	209.7
La	17.3	41	24	58.7	34.9	55.3	62.3	45	47.2
Ce	37.5	82.3	51.5	116.7	71.6	115	123.2	93.5	98.2
Pr	4.44	9.61	6.48	13.73	8.33	13.32	13.89	11.38	11.93
Nd	14.6	30.8	24.3	46.1	26.1	45	45.1	40.1	37.9
Sm	2.98	5.36	4.58	8.72	5.13	8.62	7.93	9.03	6.84
Eu	0.15	0.47	0.18	0.56	0.25	0.4	0.61	0.67	0.38
Gd	2.82	4.86	4.4	7.43	4.77	8.45	6.73	9.33	6.01
Tb	0.52	0.76	0.71	1.23	0.8	1.34	1.03	1.68	0.97
Dy	3.36	4.51	4.37	7.4	5.61	8.35	6.92	11.19	6.18
Ho	0.78	0.87	0.92	1.49	1.1	1.82	1.21	2.34	1.27
Er	2.57	2.79	2.77	4.25	3.41	5.66	3.64	7.78	3.89
Tm	0.4	0.4	0.41	0.61	0.51	0.8	0.51	1.17	0.59
Yb	2.93	2.83	2.63	4.09	3.13	5.27	3.1	7.44	3.88
Lu	0.44	0.4	0.38	0.6	0.43	0.74	0.45	0.96	0.58

MYLONITES

	PM19	PM20	PM 21	PM 22	PM 23	PM 24
SiO ₂ (wt%)	73.7	71.4	74	72.7	75.2	69.6
Al ₂ O ₃	13.42	14.5	13.65	13.7	12.64	14.58
Fe ₂ O ₃	1.8	1.81	1.08	1.96	1.73	2.84
CaO	0.91	1.3	0.89	1.24	0.45	2.01
MgO	0.21	0.29	0.13	0.25	0.19	0.61
Na ₂ O	2.85	3.05	3.25	3.28	3.07	3.08
K ₂ O	6.32	6.09	6.02	5.49	5.33	4.95
MnO	0.02	0.03	0.02	0.03	0.02	0.05
TiO ₂	0.26	0.3	0.14	0.25	0.21	0.5
P ₂ O ₅	0.05	0.08	0.03	0.05	0.04	0.12
Cr ₂ O ₃	0.033	0.022	0.025	0.024	0.022	0.024
BaO	0.04	0.06	0.05	0.04	0.03	0.07
LOI	0.53	0.65	0.61	0.58	0.57	0.82
Total	100.143	99.582	99.895	99.594	99.502	99.254
Ga(ppm)	16.9	17.6	17.7	18.4	17.3	17.3
Nb	14.1	10.9	6.9	12.8	11.5	12.9
Pb	19.3	8.5	33.7	27.8	38.2	13.5
Rb	390.5	317.7	354.2	359.4	428.3	236.7
Sr	63.3	77.5	66.2	70.6	37.8	118.4
Th	57.8	49.1	62.1	51.8	64.2	39.5
U	11	9.3	14.4	14.1	16.7	8
Y	57.9	41.7	38.5	54	41.6	35
Zn	30	34	29	35	39	46
Ba	481	372	399	225	406	600
Zr	217.8	193.1	129.4	194.7	215.6	245.2
La	61.3	60	57.7	42.1	51.3	52.5
Ce	119.2	124.4	104.3	86	102.9	104.6
Pr	14.21	14.28	11.76	9.84	11.77	12.48
Nd	50.3	48.1	39	31.3	40.9	39.9
Sm	9.59	9	6.79	6.22	7.87	7.49
Eu	0.67	0.63	0.54	0.22	0.61	0.96
Gd	9.32	8.03	5.87	5.58	7.64	6.68
Tb	1.47	1.25	0.9	0.94	1.25	1.04
Dy	9.3	7.16	5.41	6.08	8.06	6.37
Ho	1.84	1.4	1.19	1.22	1.56	1.16
Er	5.28	4.22	3.72	4.27	5.22	3.53
Tm	0.86	0.58	0.54	0.65	0.77	0.47
Yb	4.88	3.53	3.56	4.03	4.98	3.32
Lu	0.67	0.49	0.5	0.62	0.73	0.42